Development of a Cold Gas Propulsion System for the TALARIS Hopper

by

Sarah L. Nothnagel

B.S. Astronautical Engineering

University of Southern California, 2009

Submitted to the Department of Aeronautics and Astronautics

in Partial Fulfillment of the Requirements for the Degree of

Master of Science in Aeronautics and Astronautics

at the

Massachusetts Institute of Technology

June 2011

Signature of Author: _____

Department of Aeronautics and Astronautics
May 16, 2011

Certified by: _____

Jeffrey A. Hoffman
Professor of the Practice of Aerospace Engineering
Thesis Supervisor

Certified by: _____

Brett J. Streetman
Senior Member of the Technical Staff, Draper Laboratory
Thesis Supervisor

Accepted by: _____

Eytan H. Modiano
Associate Professor of Aeronautics and Astronautics
Chair, Graduate Program Committee

Development of a Cold Gas Propulsion System for the TALARIS Hopper

by

Sarah L. Nothnagel

Submitted to the Department of Aeronautics and Astronautics

on May 16, 2011, in Partial Fulfillment of the

Requirements for the Degree of Master of Science in

Aeronautics and Astronautics

Abstract

The TALARIS (Terrestrial Artificial Lunar And Reduced gravIty Simulator) hopper is a small prototype flying vehicle developed as an Earth-based testbed for guidance, navigation, and control algorithms that will be used for robotic exploration of lunar and other planetary surfaces. It has two propulsion systems: (1) a system of four electric ducted fans to offset a fraction of Earth's gravity (e.g. 5/6 for lunar simulations), and (2) a cold gas propulsion system which uses compressed nitrogen propellant to provide impulsive rocket propulsion, flying in an environment dynamically similar to that of the Moon or other target body. This thesis focuses on the second of these propulsion systems. It details the practical development of the cold gas spacecraft emulator (CGSE) system, including initial conception, requirements definition, computer design and analysis methods, and component selection and evaluation. System construction and testing are also covered, as are design modifications resulting from these activities. Details of the system's integration into the broader TALARIS project are also presented. Finally, ongoing and future work as well as lessons learned from the development of the CGSE are briefly discussed.

Thesis Supervisor: Jeffrey A. Hoffman

Title: Professor of the Practice of Aerospace Engineering

Thesis Supervisor: Brett J. Streetman

Title: Senior Member of the Technical Staff, Draper Laboratory

Acknowledgments

It feels pretty incredible to sit here looking at something the size of a book with my name on it, but I never could have written this thesis without the support of many other people. I'm glad to have the opportunity here to express my appreciation for them.

My advisors, Professor Jeff Hoffman at MIT and Brett Streetman at Draper, have both been wonderful. They kept me on track throughout my research and provided excellent feedback as I wrote it all up. Thank you both for your guidance.

I am also indebted to many staff members at both MIT and Draper. Everybody I've met in the MIT AeroAstro Department has been helpful and friendly to me, but I especially want to thank Paul Bauer, who seems to know something about everything. No matter whether I was working on design or testing, electronics or fluid flow, I knew I could take my questions to him and get solid technical advice. Over at Draper, Mike Johnson connected me to the world of controls, and he helped me understand exactly what the CGSE had to do beyond producing a lot of thrust to be a useful system. And I'm far from being able to call myself an electrical engineer, but Steve Finberg and Keith Baldwin greatly increased my knowledge and skills in that field, at least as it applied to the work I did for this thesis.

Thanking students on the TALARIS team by name is a bit of a dangerous proposition, since there have been so many of us; I could run on for pages and pages and still manage to forget someone. But still, I would like to call out a few individuals for their particular assistance. Senior Ph.D. students first: Phillip Cunio really helped me find my place in the TALARIS project (and taught me the ways of the tyrannosaurus to boot), while Bobby Cohanim helped me navigate Draper and gave me a sense of perspective reaching beyond grad school. I know that both of you have done a lot of heavy lifting, organizational and otherwise, to keep the project going, and I appreciate it. As for technical assistance, I owe special thanks to several students. Zach Bailey worked side-by-side with me during my first year on TALARIS; he provided continuity from the previous work done in the design classes, and he was instrumental in helping me develop the CGSE design and early testing procedures. And I am especially grateful to Joe Morrow, who has driven me to re-examine my assumptions and go deeper in my analysis of the CGSE. He also picked up a whole lot of slack in the lab for me over the last couple months, allowing me to focus on getting this beast written. I'd also like to thank Alessandro Golkar for taking the time to sit down with me to explain his model and suggest ways to improve my own model. And Eph Lanford answered all my annoying questions about the TALARIS structure and CAD model, wrestled with

the tube bender, and was generally ready and willing to help no matter what I asked. On a more personal note, I'd like to thank Farah Alibay for helping me maintain some form of a social life, and with it, my sanity. And Chris Han, though I may jokingly call you a terrible influence, the truth is you've been a good friend, and I'm glad to have taken this grad school journey along with you. There are many more students I could thank, but I feel like I should probably start wrapping this up. Please know that it's been a joy to work with all of you, and I'm especially grateful to everybody who ever worked on the Black Ops team.

Last but most certainly not least, I'd like to thank my family, especially my parents and my brother. Mom, Dad, and Alex, your unconditional love and support form the foundation on which I've been able to build all my accomplishments. I love you dearly, and I hope I can continue to make you proud.

This thesis was prepared at Draper Laboratory under Internal Research and Development funds.

_____

Sarah L. Nothnagel May 16, 2011

Table of Contents

List of Figures

List of Tables

Notation

Acronyms and Abbreviations

ACAT	Advanced Concept Architecture Test
ACS	Attitude Control System
ALHAT	Autonomous Landing and Hazard Avoidance Technology
CGSE	Cold Gas Spacecraft Emulator
CGTA	Cold Gas Test Article
CNC	Computer Numerical Control
COTS	Commercial Off-The-Shelf
DAQ	Data Acquisition (device or system)
DOF	Degree(s) Of Freedom
EDF	Electric Ducted Fan
EDL	Entry, Descent, and Landing
GLXP	Google Lunar X PRIZE
GNC	Guidance, Navigation, and Control
HTV	Hover Test Vehicle
ID	Inner Diameter
ILN	International Lunar Network
IMU	Inertial Measurement Unit
ISRU	In-Situ Resource Utilization
KKV	Kinetic Kill Vehicle
LAN	Local Area Network
LEAP	Lightweight Exo-Atmospheric Projectile
LEAPFROG	Lunar Entry and Approach Platform For Research On Ground
LED	Light-Emitting Diode
LLRV	Lunar Landing Research Vehicle
LLTV	Lunar Landing Training Vehicle
MIT	Massachusetts Institute of Technology
MMH	Monomethylhydrazine
MOSFET	Metal-Oxide-Semiconductor Field-Effect Transistor
NASA	National Aeronautics and Space Administration

NI	National Instruments
NIST	National Institute of Standards and Technology
NPT	National Pipe Thread
NTO	Nitrogen Tetroxide
OD	Outer Diameter
PVC	Polyvinyl Chloride
PWM	Pulse-Width Modulation
RIO	Reconfigurable Input/Output (device)
SCBA	Self-Contained Breathing Apparatus
SPHERES	Synchronized Position Hold Engage Reorient Experimental Satellites
TALARIS	Terrestrial Artificial Lunar And Reduced gravIty Simulator
USB	Universal Serial Bus
USC	University of Southern California
WGTA	Warm Gas Test Article
1D	One-Dimensional
2D	Two-Dimensional

Units

A	ampere
bar	bar (10^5 Pa)
Hz	hertz
in.	inch
J	joule
K	kelvin
kg	kilogram
kΩ	kilohm
lb	pound
m	meter
mA	milliampere
mol	mole
MPa	megapascal
ms	millisecond

N	newton
Pa	pascal
psi	pounds per square inch
psia	pounds per square inch absolute
psig	pounds per square inch gauge (relative to surrounding atmosphere)
RPM	revolutions per minute
s	second
SCFM	standard cubic feet per minute (standard conditions of 60°F and 14.7 psia)
V	volt
Vdc	volts of direct current
W	watt
°	degree (angular measurement)
°C	degrees Celsius
°F	degrees Fahrenheit
Ω	ohm

Variables and Constants

a	constant used in the Redlich-Kwong real gas equation of state
A_e	nozzle exit area
A_t	nozzle throat area
b	constant used in the Redlich-Kwong real gas equation of state
C_V	flow coefficient
F_γ	specific heat ratio factor, $\gamma/1.40$
g	acceleration due to gravity at Earth's surface, 9.81 m/s^2
F_P	piping geometry correction factor
F_{Th}	thrust
H	enthalpy
h	specific enthalpy
I_{sp}	specific impulse
M	molar mass
M_e	Mach number at nozzle exit
m	mass

$\dot{m}$	mass flow
P_a	ambient pressure
P_c	chamber pressure
P_{crit}	critical pressure (pressure at vapor-liquid critical point of a substance)
P_e	nozzle exit pressure
P_1	inlet pressure
P_2	outlet pressure
ΔP	differential pressure
q_g	volumetric flow rate
$\dot{Q}$	heat flow
R	ideal gas constant, 8.314 J/(mol K)
R_{sp}	specific gas constant, R/M
SG_g	specific gravity of gas relative to air at standard conditions of 60°F and 14.7 psia
T_c	chamber temperature
T_{crit}	critical temperature (temperature at vapor-liquid critical point of a substance)
T_1	inlet temperature
T_2	outlet temperature
T/W	thrust-to-weight ratio
u	specific internal energy
u_e	exhaust velocity
u_{eq}	equivalent exhaust velocity
V	volume
V_m	molar volume, M/ρ
x_T	terminal pressure drop ratio (valve or regulator alone)
x_{TP}	terminal pressure drop ratio for entire assembly of valve or regulator and fittings
Y	expansion factor
Z	compressibility factor
α	conical half-angle
γ	ratio of specific heats
ε	nozzle expansion ratio
λ	nozzle correction factor
$\mu_{J\,T}$	Joule-Thomson coefficient

1 Introduction

The TALARIS (Terrestrial Artificial Lunar And Reduced gravIty Simulator) hopper is a small prototype flying vehicle designed to serve as an Earth-based testbed for guidance, navigation, and control (GNC) algorithms that will be used to explore lunar and other planetary surfaces. To date, nearly all robotic exploration on the surface of the Moon and other planets has been done by stationary landers or wheeled rovers. Hoppers would open up new modes of exploration with their alternate form of mobility. However, because they are a new technology without the long heritage of landers and rovers, there is a greater need for testing to reduce the risk associated with hoppers. The TALARIS testbed provides the opportunity to develop and mature hopper-based GNC algorithms on Earth, which allows for a more controlled environment and easier human access for modifications, upgrades, and repairs if necessary.

A hop consists of three main phases: propulsive ascent, traverse flight, and soft landing. A commanded maneuver of this type has been performed off the Earth once, by the Surveyor 6 spacecraft on the Moon. On November 17, 1967, after Surveyor 6 had been sitting on the lunar surface for a week, the spacecraft's three liquid-fueled vernier rocket engines were reignited and fired for 2.5 s [1]. The control system was set such that the spacecraft would tilt 7° to the west upon liftoff, and the thrust generated was sufficient to cause the spacecraft to rise to an altitude of about 3.5 m and to land 2.4 m away from its starting point. This allowed Surveyor 6 to send back images of the surface disturbances at its initial landing site, providing information on mechanical properties of the lunar surface as well as the effects of firing rocket engines near the surface. Furthermore, the displacement of the spacecraft provided a baseline for stereoscopic viewing and photogrammetric mapping of the surrounding lunar terrain [1]. However, the Surveyor 6 hop is merely the tip of the iceberg in terms of the potential value that could be gained from exploring with hoppers.

Hoppers could improve planetary exploration from both the science and engineering perspectives. Hoppers can travel more quickly than rovers, and they can also cover a greater diversity of terrain. Hoppers could fly over large obstacles and traverse steep inclines, possibly even hopping into or out of craters. They might also provide unique opportunities for science during a hop, such as low-altitude aerial observations or examinations of cliff faces or canyon walls at various heights. For more in-depth analysis of the ways in which hoppers might contribute to planetary exploration objectives, see [2] and [3]. Hoppers have certain advantages from an engineering perspective as well. For a rover, initial landing and travel over the surface involve two dissimilar types of propulsion; by contrast, a hopper can be

designed to use the same propulsion system for both purposes, which may allow for a simpler design. Furthermore, hoppers enable a concept known as ultra-precision landing. A traditional lander must perform high-precision GNC activities during the entry, descent, and landing (EDL) phase to ensure that it arrives at its intended landing site; however, precision can be limited by other events that may be going on during EDL, such as jettisoning insertion stages, deploying parachutes or other braking equipment, etc. A rover might be allowed a somewhat larger landing footprint, since it could potentially cover any remaining distance to the target after landing, but this would be dependent upon the rover being able to traverse the terrain between the landing site and the final destination. A hopper, however, could cover rougher or steeper terrain and travel more swiftly than most rovers, increasing the probability of success for this tactic as well as allowing greater flexibility in selection of landing sites. Thus, hoppers provide the best chance of achieving ultra-precise final positioning with lower risk and cost than performing precise GNC all the way from orbit [4]. This concept is illustrated in Figure 1-1.

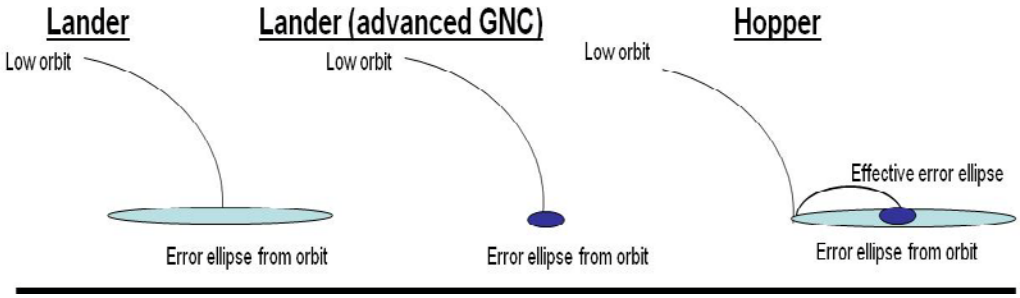

Figure 1-1. Ultra-precision landing [3].

The benefits of hoppers do come with some costs. A hopper's ultimate range is limited by the amount of propellant it can carry (though in-situ resource utilization, or ISRU, might allow for replenishment of propellant to mitigate this issue), and a flying trajectory creates a more difficult GNC problem and a higher degree of risk than traveling along the ground. Still, hoppers could be used in certain situations to expand planetary exploration capabilities as a complement to traditional landers and rovers.

While one of the long-term goals of TALARIS is to serve as a flexible testbed for a wide range of hopping applications, it is also designed for a specific, immediate purpose: participation in the Google Lunar X PRIZE (GLXP), a $30 million competition for privately-funded teams to send a robot to the Moon, travel 500 m over the surface, and transmit images and other data back to Earth [5]. The TALARIS project began early in 2008, when a small group of MIT students and faculty met with engineers from Draper Laboratory and Aurora Flight Sciences to consider entry into the GLXP competition. As part of this entry,

the idea of hopping was born, and it was determined that a terrestrial prototype would be needed. Draper and MIT embarked on the development of a full GNC testbed: TALARIS. Draper is slated to develop hopping GNC, and the role of the MIT TALARIS team is to support this development by providing an Earth-based testbed for Draper's algorithms as well as some of the GNC sensors that will be used on the actual spaceflight vehicle.

This interaction between MIT and Draper gives rise to another purpose for TALARIS: demonstration of Draper's GNC expertise and MIT's contributions to research for space exploration. As a flying vehicle, TALARIS can show off the work done by MIT and Draper in an exciting and easily comprehensible way. This could increase interest in the GLXP competition and the potential for using hoppers for planetary explanation, and it could also contribute positively to the overall reputations of MIT and Draper for developing innovative space technology, which might in turn lead to future opportunities in terms of funding or contracts for research and development.

The dual role of TALARIS as a testbed and a demonstrator creates a unique set of design considerations and constraints. To maximize effectiveness as a demonstrator, TALARIS should be able to safely operate with people in relatively close proximity. TALARIS could also deliver extra value by being able to travel and execute demonstrations at multiple locations. This would be easiest to achieve if TALARIS did not require an extensive infrastructure (e.g. a large support frame or safety catch net) or the use of hazardous materials (including many rocket propellants). At the same time, TALARIS must meet specific performance requirements to function as an effective testbed. The interactions between these two drivers greatly affected the design of TALARIS, particularly in terms of propulsion.

The TALARIS hopper as built has two propulsion systems: (1) a system of four electric ducted fans to offset a fraction of Earth's gravity (e.g. 5/6 for lunar simulation), and (2) a cold gas propulsion system which uses compressed nitrogen propellant to provide impulsive rocket propulsion, flying in an environment dynamically similar to that of the Moon or other target body. This thesis focuses on the second of these propulsion systems, called the cold gas spacecraft emulator (CGSE). While cold gas propulsion is a relatively mature and well-understood technology, the particular conditions of the TALARIS project shaped the process of designing, building, and testing the CGSE to make it a uniquely customized system. That process is described in depth in this thesis, partly as a detailed record of this portion of the TALARIS project, but also in hopes of illuminating some ideas of broader significance. While the CGSE is the result of a singular set of requirements, there are some lessons to be learned from its development which can be applied to the general practice of space systems engineering.

2 Propulsion System Architecture

Although most major architecture decisions for TALARIS were made before the work described in this thesis began, it is useful to discuss other approaches for the propulsion of prototype or simulator landers and exploration vehicles. For one thing, a brief review of the spacecraft emulator propulsion system was conducted before detailed design work began, to ensure that the decisions made for the original concept were still valid even though the TALARIS design had evolved in other areas. Furthermore, understanding the strengths and weaknesses of cold gas propulsion compared to the other options that might have been selected provides insight into the design decisions made.

2.1 Vehicles Other Than TALARIS

Since hopping is not a common method of exploring planetary surfaces, there is little precedent for prototype or testbed vehicles built for this purpose. The closest analogues to TALARIS are Earth-based lunar lander testing vehicles. Several different concepts have been developed for vehicles of this type, but they all face the problem of predicting lunar performance from tests performed on Earth. From a propulsion perspective, the major difference between Earth and the Moon is gravity; about six times more force is needed to lift an object on the Earth as compared to lifting an object of equal mass on the Moon. The atmosphere on Earth also introduces forces that are not present on the Moon, but the effects of wind can be mitigated by operating on calm days or even indoors, and drag forces for most vehicles are small compared to the forces needed to overcome gravity and to accelerate the vehicle for horizontal transit.

One approach to testing a lunar vehicle on the Earth is to simply operate the system as designed for the Moon, as long as it is powerful enough to operate in the higher gravity of Earth. Mission profiles may be scaled in terms of distance or time such that they use an equivalent amount of delta-V for a scaled flight on Earth as they would for actual operations on the Moon. This was the approach taken for the Northrop Grumman Lunar Lander Challenge, for which the goal was to simulate a descent from lunar orbit, refueling, and return to lunar orbit [7]. An equivalent task for demonstration on Earth was designed to involve taking off from a concrete pad, ascending to an altitude of approximately 50 m, flying 50 m horizontally, and landing on a second concrete pad, with refueling and a return flight within two hours and fifteen minutes. The vehicle had to remain aloft for at least 90 s on each flight for the first level of competition and 180 s on each flight for the second level [8]. The benefit of this method is that it allows for testing of both hardware and software exactly as they will be used in the real lunar mission.

However, as stated before, this does require that the flight vehicle be robust enough to operate on Earth. In practice, this generally means that the vehicle must be large, with a high total impulse capacity. This was true of the two vehicles that completed the Northrop Grumman Lunar Lander Challenge, which are shown in Figure 2-1 below. The Armadillo Aerospace Scorpius vehicle weighed 1900 lb (862 kg) when fully loaded with ethanol and liquid oxygen propellant [6], while the Masten Space Systems Xoie vehicle weighed 850 lb (386 kg) and used isopropyl alcohol and liquid oxygen for propellant [7].

(a) (b)

Figure 2-1. Prototype vehicles competing in the Northrop Grumman Lunar Lander Challenge. (a) Armadillo Aerospace Scorpius [6], (b) Masten Space Systems Xoie [7].

As can be seen by the settings of the photographs in Figure 2-1, test flights for both the Armadillo and Masten vehicles occurred in remote areas. This is due to the size of these vehicles, as well as the hazardous nature of their propellants, which required exceptional precautions to minimize risk to bystanders. This method of operation would not be practical for TALARIS, since TALARIS is designed to be operated by students in the urban setting of MIT and to perform in-person demonstrations for nearby observers. Also, as mentioned previously, the role of TALARIS is not only to contribute to efforts to win the GLXP, but also to serve as a platform for testing and demonstrating hopping planetary exploration in general. Thus, building TALARIS with full spaceflight hardware optimized for the Moon would not only be difficult and expensive, but it might actually decrease the overall usefulness of TALARIS as a testbed by making it less suitable to investigate operations under a wide range of conditions.

A second approach to Earth-based testing of lander vehicles is to create some sort of separation between counteracting the higher gravity of Earth and performing GNC tasks. In this case, there are two main architecture decisions to be made. The first major decision is the degree of division, or how

propulsion tasks will be grouped and defined. There are two basic methods of doing this. One way is to separate lift (i.e. support of the vehicle's weight) from attitude control. The other is to devote some lift to fractional weight relief, so that the effect of Earth's gravity on the testbed is effectively reduced to that of the Moon (or other target body), and to combine the remaining lift with attitude control to simulate the entire propulsion system that will be used on the actual lander. The second major decision is whether the two tasks will be performed by entirely separate propulsion systems, or whether there will be a single propulsion system with two separately-controlled sets of actuators.

Lunar lander testbeds have been built and flown with all four possible combinations of these divided propulsion architecture options. In fact, TALARIS took inspiration for its architecture from the Apollo program's Lunar Landing Research Vehicle (LLRV, Figure 2-2) and its successor, the Lunar Landing Training Vehicle (LLTV). These vehicles used a gimbaled turbofan jet engine for 5/6 weight cancellation and a system of hydrogen peroxide rockets to simulate the Lunar Module propulsion, which they did with great success; Neil Armstrong credited his successful lunar landing, as well as those of his fellow Apollo astronauts, in large part to extensive training on the LLRV and LLTV [9]. However, because they were designed to carry a human pilot, the LLRV and LLTV were much larger than TALARIS. Several more recent robotic lander simulation vehicles provide a closer comparison to TALARIS.

Figure 2-2. Lunar Landing Research Vehicle (LLRV) in flight, 1964 [8].

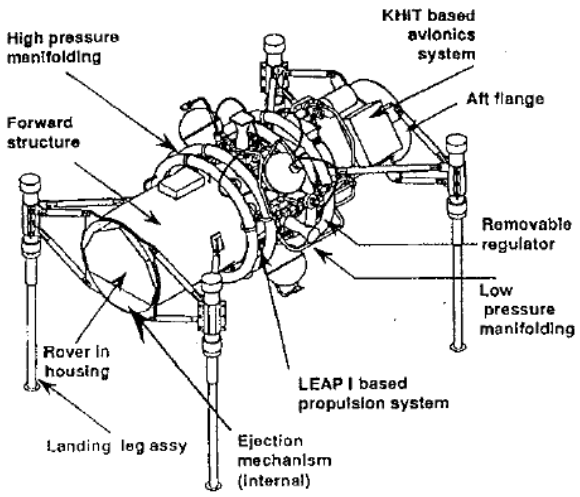

Figure 2-3. Diagram of ACAT lander prototype [10].

A relatively early vehicle comparable to TALARIS was built for the Advanced Concept Architecture Test (ACAT) demonstration in 1994 [10]. A small planetary lander prototype was constructed using surplus hardware from the Lightweight Exo-Atmospheric Projectile (LEAP) program for the development of kinetic kill vehicle (KKV) technology, or "hit-to-kill" ballistic missile interceptors designed for use in space. The ACAT lander (Figure 2-3), like the LLRV and LLTV, used two separate propulsion systems, but it handled the division of tasks differently. Rather than attempting to simulate a partial gravity environment, the ACAT lander used a modified version of a KKV divert propulsion system consisting of three bipropellant monomethylhydrazine/nitrogen tetroxide (MMH/NTO) thrusters for lift and a separate attitude control system (ACS) of eight cold gas nitrogen thrusters. The ACAT lander was successfully demonstrated in a test conducted in the National Hover Test Facility at Edwards Air Force Base in California, a facility built specifically for testing for LEAP and similar programs [10]. The TALARIS project does not have such a dedicated testing facility, though, and the dangers in handling rocket fuels such as MMH and NTO as well as operating a rocket engine performing combustion would likely require one. Thus, only limited aspects of the propulsion design of the ACAT lander can be applied to TALARIS.

Using a cold gas system which operates on compressed gas is an alternate method of propulsion that generally cannot provide as much impulse as a system using combustible propellants but also avoids many of the safety hazards inherent in such a system. Two recent NASA robotic lander test vehicles (shown in Figure 2-4 below) were designed, built, and tested, each using a single cold gas propulsion system with two sets of actuators, but with different approaches to the division of propulsion tasks.

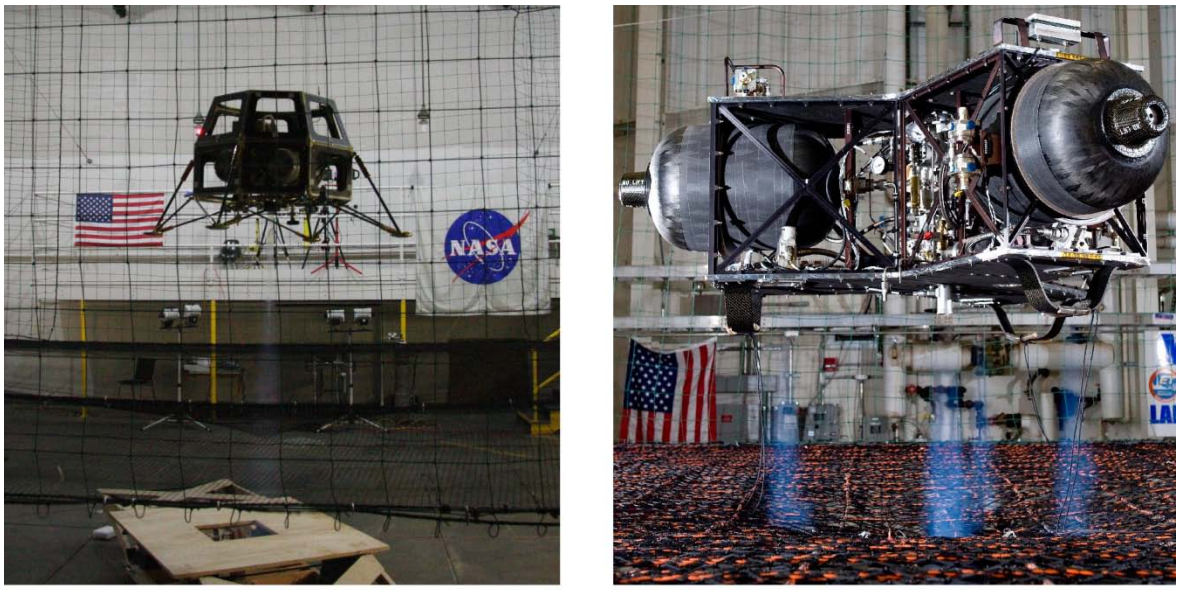

Figure 2-4. NASA robotic lunar lander testbeds using cold gas propulsion.
(a) NASA Ames Hover Test Vehicle (HTV) [11], (b) NASA Marshall Cold Gas Test Article (CGTA) [12].

The vehicle shown at left in Figure 2-4 is the Hover Test Vehicle (HTV), built at NASA Ames Research Center as an initial prototype of the Modular Common Bus, a low-cost spacecraft designed to be able to carry any science instrument fitting predefined mass and power budgets. The HTV was designed to hover at a stable altitude and position in order to test GNC algorithms; it accomplished this with one main lift and six ACS thrusters, all fed from the same pair of scuba tanks [13]. A different vehicle was developed at NASA Marshall Space Flight Center to simulate lunar landings as a risk reduction activity for robotic lunar lander flight projects, including the International Lunar Network (ILN) [14]. This Cold Gas Test Article (CGTA), shown at right in Figure 2-4 above, had one large central thruster to cancel 5/6 of Earth's gravity and a set of smaller thrusters to lift the last 1/6 of the weight and perform attitude control, but again all were fed from a common source of compressed air [12]. Both the NASA Ames HTV and the NASA Marshall CGTA had the same problem, inherent to relying only on cold gas propulsion: short flight times. In fact, because the CGTA was limited to flights of 10 seconds or less, the NASA Marshall team built a second-generation vehicle with the same architecture but a monopropellant hydrogen peroxide propulsion system in place of the cold gas system [14]. This Warm Gas Test Article (WGTA) is expected to have flight times as long as 60 seconds [15], which will allow for longer-duration GNC testing, but the hydrogen peroxide again introduces more difficult handling and operational safety issues. The evolution of the NASA Marshall robotic lunar lander program illustrates the difficulty in finding a middle ground between high performance and a safely operable and accessible system.

An alternate approach to resolving this dilemma was taken by a student group at the University of Southern California (USC) for a lunar lander testbed called LEAPFROG (Lunar Entry and Approach Platform For Research On Ground) [16], shown in Figure 2-5 below.

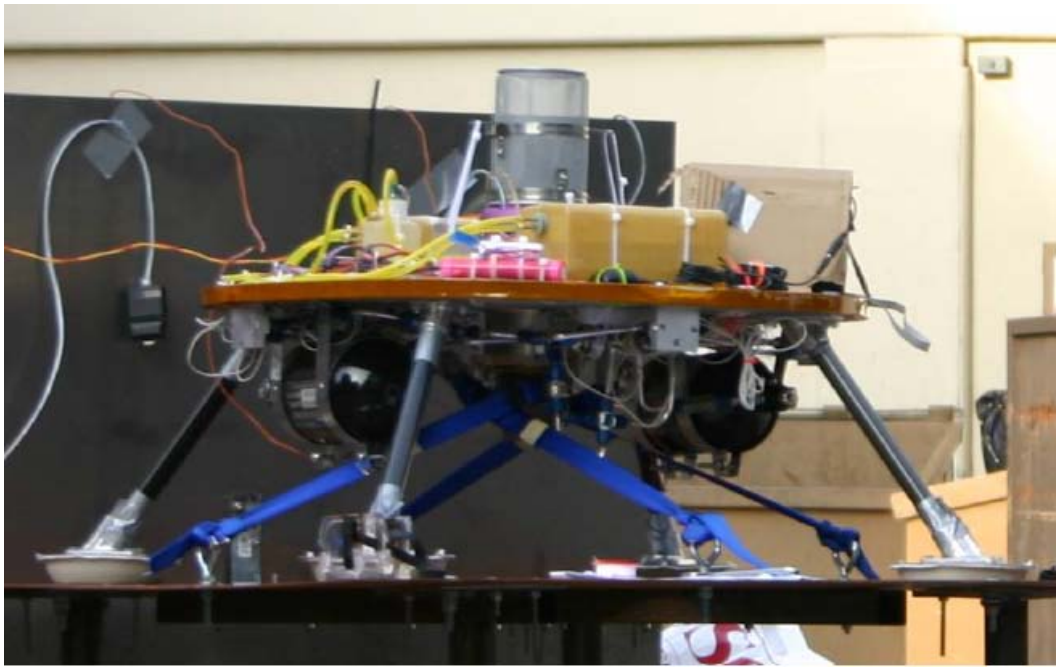

Figure 2-5. USC LEAPFROG lunar lander testbed [16].

The architecture for LEAPFROG separated the lift and attitude control functions and performed each with a different propulsion system. A small jet engine, designed for hobby aircraft, was used to provide lift for hover and descent flight, while the ACS was composed of 12 cold gas thrusters using nitrogen propellant [16]. Because LEAPFROG, like TALARIS, was a student-run project, many of the same safety constraints and desires for simplicity of development and operation applied. Given these conditions, the architecture chosen for LEAPFROG was a good option in terms of flight time; it was designed for flights of up to three minutes [16]. However, the impulsive rocket propulsion used by an actual lunar lander creates vehicle dynamics that can be substantially different from those provided by the continuous propulsion of an air-breathing jet engine. Since the jet engine in LEAPFROG supplied essentially all the lift an actual lunar lander would require, the long flight time came at a cost of lost simulation fidelity.

To sum up the various approaches taken for the design of propulsion systems for lunar lander testbeds, it is evident that there are many different architecture choices that can be made, but every design has its drawbacks. The following Table 2-1 presents a brief review of the projects using a divided propulsion architecture that were discussed in this section.

Table 2-1. Lunar lander testbed vehicles using divided propulsion architecture.

		Task Separation	
		Lift & ACS	Partial weight relief & simulated lander propulsion
System	One system, two sets of actuators	NASA Ames HTV (t)	NASA Marshall CGTA (t) NASA Marshall WGTA (p)
	Two separate systems	LEAP/ACAT (p) USC LEAPFROG (d)	Apollo LLRV and LLTV (p) ***TALARIS***

Key to main limitations: p = hazardous propellants
d = dynamics less similar to actual lander
t = short flight time

None of the three main limitations identified for lander testbed vehicles in Table 2-1 are desirable for the TALARIS project, but it is evident that some compromises must be made to achieve a successful flight vehicle design. With this in mind, a two-pronged approach was taken to optimize the propulsion architecture for TALARIS. Firstly, a unique combination of propulsion systems was selected to mitigate some of the difficulties encountered by other lander testbeds. Secondly, careful consideration was made of all the factors surrounding the TALARIS project, such that the design space was defined as fully as possible. In other words, some of the potential issues that could arise from particular propulsion system designs (such as serious safety hazards) were hard boundaries that the project could not cross, whereas others (such as imperfect dynamic similarity and short flight times) were simply undesirable attributes which should be minimized but could be areas in which to relax requirements if necessary.

2.2 Review of TALARIS Propulsion Architecture

As mentioned before, most of the major architecture decisions for TALARIS were made before the work described in this thesis began. The initial group from MIT, Draper, and Aurora made a preliminary study of GLXP vehicle concepts during January 2008 and handed their results off to the 16.89 graduate Space Systems Engineering design class at MIT in spring of that year. This class settled on a hopping mode of travel for the exploration vehicle and proposed that an Earth-based testbed vehicle be built to develop the concept further. A special graduate design class (16.898) was held in fall 2008, in which a basic architecture of dual propulsion systems was devised. As shown by the placement of TALARIS in Table 2-1, this architecture called for two separate propulsion systems, divided into the tasks of weight relief and simulation of lunar propulsion. It was believed that this architecture would provide the most

accurate conditions for testing GNC algorithms, and it had proven remarkably successful in the past with the LLRV and LLTV. Furthermore, keeping the simulated lunar propulsion entirely separate from weight relief meant that theoretically, software written for the TALARIS testbed could be moved directly over to control the actual GLXP hopper. Overall, the selected architecture was deemed to make TALARIS the most effective possible testbed for the GLXP hopper and a robust demonstrator of hopping in general.

In the 16.898 class, electric ducted fans (EDFs) were selected for the weight relief propulsion system, required to lift 5/6 of the vehicle's Earth weight at all times [17]. This decision clarifies some of the priorities of the TALARIS project. For instance, another option for weight relief might have been to devise some system of pulleys and counterweights from which to suspend the hopper. This would have had the benefit of little to no reliance on expendable propellant, thus allowing for longer flight times. However, it also would have had the drawbacks of restricting the flight range of the vehicle, introducing dynamics from the suspension tethers, and requiring a large amount of infrastructure to be moved with the vehicle for tests or demonstrations at a different site. The decision to make TALARIS a free-flying vehicle reveals that simulation fidelity and flexibility in operations are more important to the project than maximizing flight times at all costs. At the same time, it is important that flight times not be so short as to preclude the collection of useful data or make it difficult to demonstrate all the phases of a hop. The selection of a weight-relief propulsion system for TALARIS that makes use of the air through which it flies was made to maximize efficiency and flight times as much as possible, creating a propulsion architecture more similar to that of the USC LEAPFROG testbed with its flight times of several minutes as opposed to the NASA cold gas vehicles limited to flights of just seconds. Finally, the choice of the EDFs over other aerodynamic propulsion methods (such as rotors or small jet engines like the JetCat used by LEAPFROG) illustrates that beyond performance metrics such as propellant usage, thrust output, and system mass, other factors such as cost, safety, and ease of implementation were also considered.

The 16.898 class also selected cold gas propulsion to emulate the actual GLXP spacecraft propulsion system while operating in an artificial lunar gravity environment created by the constant weight offset from the EDFs. After the 16.898 class concluded in fall 2008, the 16.83/89 Space Systems Engineering class held in spring 2009 developed the design of the TALARIS testbed further, but due to limited resources they were only able to focus on one of the propulsion systems. They chose to work on the EDFs, and by the end of the semester they had built a first-generation vehicle that flew in a test stand constraining it to linear vertical motion only [17]. However, the cold gas propulsion system remained at the conceptual design stage when the work described in this thesis began.

2.3 Confirming the Decision to Use Cold Gas Propulsion

In summer 2009, detailed design work for the TALARIS spacecraft emulator propulsion system began. One of the first tasks undertaken was a review of the decision to use a cold gas propulsion system for this purpose. While a good deal of thought had been put into this decision in earlier stages of the TALARIS project, it was deemed necessary to revisit the question in light of the progress that had been made over time. This process not only confirmed that cold gas propulsion was the optimal choice for the spacecraft emulator propulsion system, but it also highlighted strengths and weaknesses that shaped the design of the cold gas propulsion system for TALARIS.

2.3.1 General Hopper Propulsion Design Considerations

One major design driver for the TALARIS spacecraft emulator propulsion system was hop trajectory. Two types of trajectories were considered. The first is the ballistic hop, in which the hopper's propulsion system provides an initial acceleration to the vehicle at launch and, if necessary, a deceleration at the end of flight for a softer landing. The majority of a ballistic hop is an unpowered coasting phase. For example, as discussed in Chapter 1, the Surveyor 6 probe performed a ballistic hop on the Moon; the accelerations involved were small enough that a braking phase was not required. The second type of trajectory is called the hover hop. In a hover hop, the vehicle ascends to a given height above the surface, translates horizontally while maintaining constant altitude and attitude, and descends vertically to a soft touchdown. Both the ballistic and hover hop trajectories are illustrated in Figure 2-6.

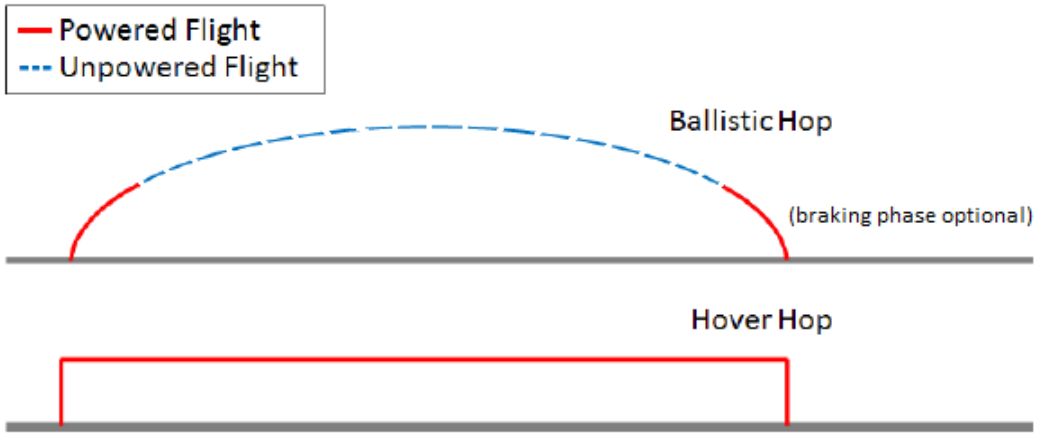

Figure 2-6. Comparison of ballistic and hover hop trajectories [18].

Ballistic hops tend to use less propellant than hover hops, since the duration of powered flight is shorter, but performing precision hops with a ballistic trajectory may be more difficult because of the narrow window of time available to make powered maneuvers. By contrast, hover hops tend to consume more propellant because the entire trajectory is powered, but this also allows the hopper to perform attitude control and course corrections mid-hop. A detailed analysis of the tradeoffs between these two types of hops is available in [18].

Selection of a hop trajectory influences the propulsion options available to a hopper. For example, designs have been proposed for hoppers using mechanical methods such as springs or pistons to exert a reaction force on a surface; see for instance [19,20,21,22]. However, mechanical hopping can only be ballistic, while the current concept of operations for the GLXP lunar hop calls for covering the mandated 500 m distance by hover hopping [18]. Furthermore, as described in Chapter 1, there are potential benefits to using the same propulsion system for initial landing on a planetary surface and later hopping travel. A mechanical method of hopping would not be very useful for an initial landing; rocket engines are much more appropriate for this purpose. Additionally, an impulsive rocket propulsion system capable of performing a hover hop could also be used to perform a ballistic hop if desired by simply firing the rockets only at the beginning and end of the flight. Thus, the TALARIS vehicle is designed to use rocket propulsion, in order to provide the most accurate simulation of the planned GLXP trajectory as well as to allow TALARIS to be a testbed for the greatest possible range of hopping applications.

There are many types of rocket propulsion systems, but not all are appropriate for hoppers. Because the propulsion system for a hover hop is required to perform attitude control as well as to provide acceleration to make the vehicle travel, it must be able to stop, restart, and deliver small impulse bits. Even ballistic hoppers, if they are designed to make multiple hops, require stop and restart capability for their propulsion systems. This rules out solid rockets. Hybrid rockets are a theoretical possibility, but they have much less flight heritage, and hybrid rocket development has generally been focused on high-thrust applications like launch vehicles and orbit insertion stages [23]. The remaining feasible options, for both the GLXP and TALARIS hoppers, are cold gas, monopropellant, and bipropellant propulsion.

Cold gas, monopropellant, and bipropellant systems all have extensive flight heritage. Of the three, cold gas systems are the least complex and costly, but they generally have the lowest thrust and specific impulse; bipropellant systems have the highest complexity and cost, but also the highest thrust and specific impulse; and monopropellant systems fall between the other two [24]. Higher complexity means that more hardware is necessary, and the additional hardware mass outweighs the performance gains

from the higher specific impulse when total impulse requirements are low. Figure 2-7 illustrates this relationship between system mass and total impulse.

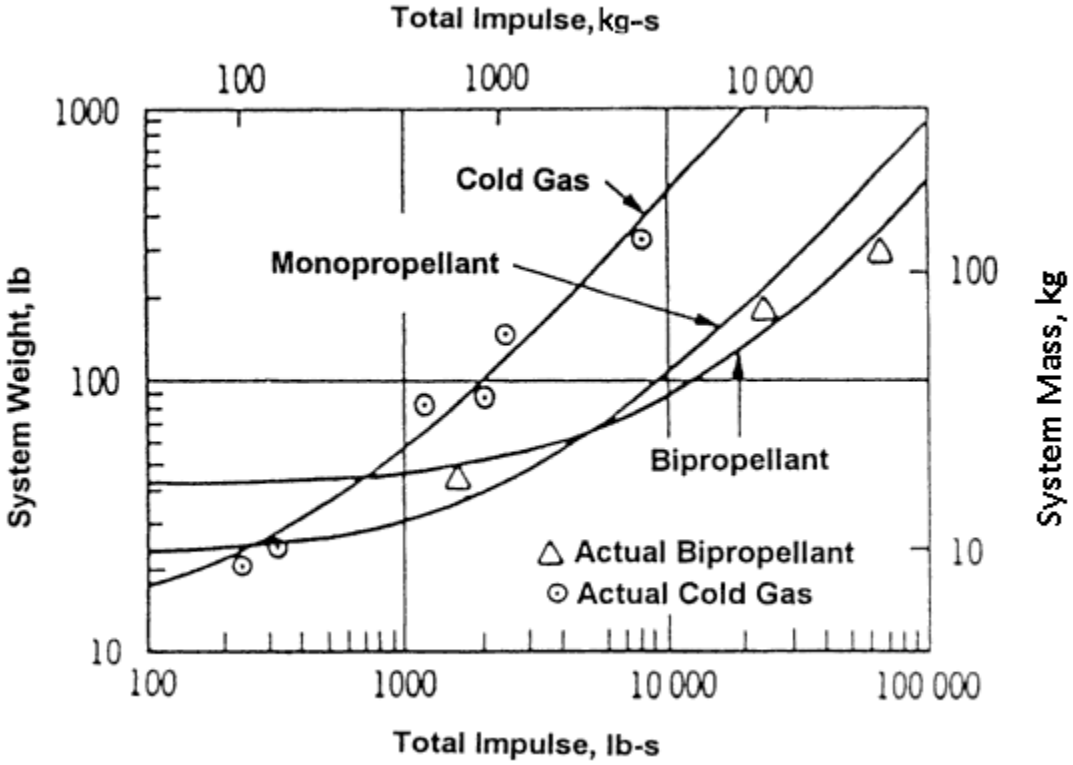

Figure 2-7. Weight/mass of propulsion systems vs. total impulse delivered [24].

The relationship illustrated in Figure 2-7 is reinforced by consideration of the lander testbeds discussed in section 2.1. The large vehicles that competed in the Northrop Grumman Lunar Lander Challenge used bipropellant propulsion because those systems can deliver the large amount of impulse needed with the lowest mass possible. By contrast, the smaller vehicles like the ACAT lander and the NASA test vehicles used monopropellant and cold gas propulsion, since those systems have better performance in the lighter weight range.

The design of the GLXP hopper, including size and impulse requirements, has not yet been finalized, although monopropellant hydrazine has been suggested for its propulsion system [17]. But all three types of propulsion systems under consideration behave similarly – they all control thrust by varying propellant flow, and all can be designed to have a pulsed operation mode for attitude control – so the TALARIS hopper should be able to provide an accurate simulation of the GLXP hopper regardless of the particular rocket propulsion system chosen for each vehicle.

2.3.2 Comparison of Cold Gas and Monopropellant Systems

Mass was used as an initial guide for propulsion system type selection for the TALARIS hopper. As mentioned earlier, the 16.898 class in fall 2008 developed an initial conceptual design for a spacecraft emulator propulsion system using nitrogen cold gas propellant; the estimated mass of this system was 17 to 20 kg (37.5 to 44.1 lbs) [25]. However, after evolving the design of the rest of the TALARIS vehicle, the 16.83/89 class in spring 2009 recommended reducing the mass of the cold gas system to 10 kg (22.0 lbs) [26]. As shown in Figure 2-7, these masses are in the range where the most efficient propulsion system type in terms of highest total impulse for lowest system mass begins to transition from cold gas to monopropellant. Thus, it was decided to examine in depth whether a monopropellant system might be a better choice than cold gas for the TALARIS spacecraft emulator propulsion system.

Monopropellant systems can offer a significant improvement in specific impulse (I_{sp}) over cold gas systems. Most cold gas propellants have an I_{sp} of less than 100 s (though helium gas can provide an I_{sp} of about 180 s)[1], while hydrazine, the most commonly used monopropellant, has an I_{sp} of approximately 230 s [27]. However, hydrazine is toxic and carcinogenic, and products of its decomposition include ammonia gas, which can also pose health hazards [28]. Thus, an alternative monopropellant was considered for the TALARIS hopper: hydrogen peroxide. It has an I_{sp} of about 150 s [27], which is not as good as hydrazine but still better than most cold gas propellants. More importantly, while hydrogen peroxide still requires careful handling, it is not as hazardous as hydrazine, and the products of its decomposition are oxygen gas and water, which are not harmful to humans [29]. Hydrogen peroxide was believed to be the monopropellant most likely to work within the safety constraints of the TALARIS project.

The concept of a hydrogen peroxide monopropellant system was compared to cold gas propulsion in the following aspects:

Impulse

As mentioned above, hydrogen peroxide has a better specific impulse than most cold gas propellants. However, it is also important to note that hydrogen peroxide is a liquid propellant and thus far denser than cold gas propellants. Therefore, hydrogen peroxide provides more impulse not only on a per-mass

[1] When used as a cold gas propellant, hydrogen (H_2) has a very high I_{sp} at almost 300 s, but it is almost never used this way because it is more efficient to burn it as fuel in a bipropellant system [27].

but also on a per-volume basis. This is important because propellant volume is limited on the TALARIS hopper; tanks must have certain dimensions to fit on the structure with the many components of the other subsystems of the vehicle. But regardless of whether mass or volume were the limiting factor on how much propellant TALARIS could carry, hydrogen peroxide would be able to provide more total impulse than most candidate cold gas propellants.

System components

A cold gas propulsion system is composed of relatively few types of components: propellant tanks, valves for filling the system and relieving excess pressure, plumbing (feed line tubes and possibly filters), a pressure regulator (though this is not used in a blowdown system), and thrusters with control valves and nozzles. A monopropellant hydrogen peroxide system can be built from these same types of components, with a few additions. The main addition would be catalyst beds, to start the exothermic decomposition of hydrogen peroxide to water and oxygen. These may be made relatively simply from stacked screens of silver wire mesh [29]. A separate pressurant tank and regulator might also be added if a regulated system were desired, but the effects of maintaining a constant thruster inlet pressure are substantially less noticeable for a monopropellant system than for a cold gas system, since the exothermic decomposition of a monopropellant generally has a much greater effect on the thruster chamber pressure than the initial pressure of the propellant. As a result, regulated monopropellant systems are generally thought to have unnecessary complexity and cost, and blowdown monopropellant systems are far more common [24]. Overall, a blowdown hydrogen peroxide system would not require many more components than a cold gas propulsion system, though size, mass, materials, etc. of analogous components would likely vary between the two types of systems.

Phase of propellant

Though the liquid phase of hydrogen peroxide has certain benefits as discussed in the Impulse section, it also has drawbacks. One challenge is ensuring proper propellant flow; since TALARIS is designed to operate on Earth, it could have a gravity-fed system, but this would require that the propellant tank be located above the thrusters, which would add additional constraints to the already difficult problem of placing all required components on the vehicle. Also, liquid hydrogen peroxide would be subject to slosh, which could not only complicate tank drainage but also add undesirable dynamics to the entire TALARIS vehicle. These effects could be mitigated with an appropriate propellant tank, perhaps including baffles or a diaphragm, but this would add complexity to the system design.

Handling propellant

There are several aspects to consider in regards to propellant handling. One is materials compatibility. This is especially critical in the case of hydrogen peroxide, because incompatible materials or impurities in an otherwise compatible material could not only lead to corrosion or other damage to components but also possibly catalyze the exothermic decomposition reaction before the propellant reaches the thrust chamber, causing extensive damage or injuries to personnel. The primary compatible materials recommended for a hydrogen peroxide system are certain alloys of aluminum and stainless steel, passivated with a chemical solution to form a protective layer of oxide on the surface of the metal before use, though various polymers are acceptable for use with lower concentrations of hydrogen peroxide and/or on a short-term basis [30]. This constraint would limit the materials available for use in the TALARIS propulsion system, and it would require additional care and procedures to be taken during construction, but it would likely not be an insurmountable obstacle. As for a cold gas system, materials compatibility depends on the propellant chosen, but many of the leading candidates (such as nitrogen and helium) are inert gases, which have few restrictions on the materials with which they can be used.

Another aspect of propellant handling is personal protective equipment. When using high-concentration hydrogen peroxide, splash protection is required, including a face shield and chemical safety goggles, a PVC or rubber suit, and chemical-resistant boots [29,30]. This would not be quite as expensive or cumbersome as the equipment required to handle a more hazardous chemical like hydrazine, which requires a self-contained breathing apparatus [29]. Still, personal protection against hydrogen peroxide is a good deal more involved than the precautions recommended for work with most compressed gases, which may be as simple as wearing safety goggles [31].

Overall, there are more extensive propellant handling concerns associated with hydrogen peroxide than with most cold gas propellants. However, handling procedures for hydrogen peroxide have been well-documented, and a workable situation could be developed with some additional investments of time, money, equipment, and training.

Obtaining and storing propellant

Obtaining cold gas propellants is relatively straightforward; both MIT and Draper have standing contracts with companies such as Airgas through which cylinders of various compressed gases can be purchased. These cylinders come with protective caps and can be safely stored in many locations, as long as they can be securely attached to a wall or other large solid object like a lab bench with a belt or chain [32].

Hydrogen peroxide at the concentrations needed for use as a rocket propellant is far less readily available. The hydrogen peroxide available in drugstores for cosmetic and antiseptic purposes is generally at only 3% concentration in aqueous solution, hydrogen peroxide for laboratory use is available at 30-35% concentration, and concentrations from 50 to 70% are used for many industrial purposes such as bleaching of textiles and paper, but propellant-grade hydrogen peroxide ranges in concentration from 70 to 98% [33]. This presents two difficulties that were identified during this trade study between propellant system types. Firstly, at the time the work described in this thesis was being performed, few companies offered hydrogen peroxide for sale at propellant-level concentrations, though there was at least one supplier (FMC Industrial Chemicals) located in the United States [33]. Secondly, the concentration of propellant-grade hydrogen peroxide was so much higher than that commonly used in the laboratory that there were no suitable existing storage facilities at MIT, nor any personnel trained to receive and handle the chemical. Again, there is a good deal of literature available describing protocols for safe storage of highly concentrated hydrogen peroxide (see, e.g., [30] and [34]), and several companies that sell propellant-grade hydrogen peroxide or related components also offer training sessions or other consulting services which the TALARIS project could utilize [33,35]. However, this is clearly another area in which considerably more resources would have to be expended to create a safe and working hydrogen peroxide system than for a cold gas system.

Summary

To summarize, a monopropellant hydrogen peroxide propulsion system would almost certainly have a higher performance than a cold gas propulsion system of equivalent mass, given the expected properties of the TALARIS hopper. However, a hydrogen peroxide system would also have more design constraints and be more complex, though not prohibitively so. Furthermore, there are many more serious safety issues related to hydrogen peroxide than to cold gas propellants, and a great deal of preparation and training would be needed to protect personnel. This is an especially large commitment due to the high turnover of students working on TALARIS; each semester, new students join the project, while some experienced students graduate or otherwise move on. None of these drawbacks are insurmountable obstacles on their own. However, when added together, they represent a significantly greater investment of resources in the development of the TALARIS spacecraft emulator propulsion system. Time was deemed to be an especially critical resource; given the competitive nature of the GLXP, the TALARIS vehicle had to demonstrate at least some hopping capability as soon as possible. Thus, it was decided to continue designing a cold gas propulsion system for the TALARIS hopper. Development of the TALARIS spacecraft emulator propulsion system could thus proceed more rapidly,

and if the cold gas system was found to be lacking in performance after initial demonstration, the question of investing more resources into development of a hydrogen peroxide propulsion system might be revisited. (As discussed in section 2.1, this is the path that the NASA Marshall team followed in moving from the CGTA to the WGTA. However, it was anticipated that because the TALARIS hopper had air-breathing EDFs for weight relief, the cold gas propulsion system on TALARIS would be less taxed than the propulsion system of the Marshall CGTA, and therefore flight times for TALARIS would not be limited quite so severely.) A possible framework for the process of upgrading from cold gas to monopropellant hydrogen peroxide is presented in section 7.3 as part of the discussion of future work.

2.4 Selection of Nitrogen Propellant

One final decision was made before proceeding with the detailed design of the TALARIS cold gas spacecraft emulator (CGSE) propulsion system: which particular gas to use as a propellant. This affects component selection in terms of sizing and allowable materials. Many different gases have been used for cold gas propulsion, including nitrogen, helium, carbon dioxide, air, and Freon, among others [24,27]. Selection among the numerous possible gas options was based on several factors. Chief among them were non-reactivity, to minimize materials compatibility issues, and readiness of availability. Eventually, the field was narrowed to four gases that were considered in greater detail, as described below.

Carbon dioxide (CO_2)

Carbon dioxide was considered mainly because it was used effectively for small satellite cold gas propulsion for SPHERES (Synchronized Position Hold Engage Reorient Experimental Satellites), another MIT project with which many TALARIS team members were familiar [36]. In SPHERES, the carbon dioxide is stored in mixed liquid and gas phase. As the gaseous CO_2 is used as propellant, the liquid CO_2 evaporates to replenish it, keeping the pressure inside the propellant tank constant until all the liquid evaporates [37]. This helps keep thruster performance constant, and storage in the high-density liquid phase means that a relatively large mass of propellant can be carried. However, the drawbacks to liquid hydrogen peroxide discussed in section 2.3.2 apply to liquid CO_2 as well, and these were considered serious enough that carbon dioxide was discarded as an option. (Also, modeling of hops as described in section 4.1 revealed that TALARIS uses propellant at a much more rapid rate than SPHERES, raising concerns as to whether carbon dioxide could evaporate rapidly enough to continuously supply gaseous propellant to the TALARIS thrusters.)

Helium (He)

Helium was considered because of its high specific impulse; as previously mentioned in section 2.3.2, it has an I_{sp} of approximately 180 s, which is very high for an inert gas propellant. However, helium also has a very low density, which means that it requires either a large volume or very high pressure for storage of sufficient propellant mass. This often translates to a heavier propellant tank weight, which can reduce some of the gains from the high I_{sp}. Furthermore, helium systems are especially prone to leaking [24]. And finally, helium gas is more expensive than the other propellant options considered. For these reasons, helium was not selected as the primary TALARIS CGSE propellant; however, it was kept in mind as a secondary option, and the MATLAB model described in section 4.1 was written such that helium could be easily substituted in as the modeled propellant if desired.

Nitrogen (N_2)

Nitrogen gas has only a mediocre I_{sp} of 60 to 80 s [27,28]; it is strongly outperformed by helium in terms of specific impulse alone. However, nitrogen is denser and less prone to leaking than helium, and it is also less expensive. It is a common choice for cold gas propulsion systems, as illustrated by the other vehicles described in section 2.1; all of the small robotic testbeds used a cold gas nitrogen system for at least part of their propulsion. Nitrogen gas was found to be a good compromise for the TALARIS hopper as well, and it was chosen as the propellant for which the CGSE was designed.

Air

Because air is about 78% nitrogen, it has a very similar I_{sp} – generally about 2 s lower than that of nitrogen at the same conditions [27,28]. It was thought that air might be obtained for less expense than pure nitrogen. However, there was no equipment readily available to compress air to the high storage pressures desired. Furthermore, the MATLAB model described in section 4.1 indicated that the temperature of the gas in the CGSE would fall well below the freezing point of water. Thus, besides a compressor, a dessicator would also be needed to remove water vapor from the air. Once the cost of this equipment was considered, the potential cost savings of using air instead of nitrogen were negated.

Overall, the TALARIS propulsion system architecture was the result of many decisions made for best possible performance of the system considering many factors beyond the physical characteristics of the vehicle itself, including an aggressive project schedule and a limited budget, as well as especially rigorous safety requirements. These factors continued to influence the decisions made about the TALARIS spacecraft emulator propulsion system through the detailed design phase and into testing.

3 TALARIS CGSE Design Framework

After the major architecture decisions had been made for the TALARIS spacecraft emulator propulsion system, the next step was detailed design. The goal of this development process was not to develop a radically new propulsion system, which would have been extremely difficult given the limited budget and relatively short deadlines of the TALARIS project; cold gas propulsion technology is mature enough that there is little room for drastic improvement. Rather, the aim of the process described in this thesis was to make specific choices that most effectively satisfied the particular needs of the TALARIS project while working within the generally well-established framework of cold gas propulsion system design.

3.1 CGSE Requirements Definition

The architecture definition process had placed some constraints on the design problem, such as the decision that the spacecraft emulator propulsion system would be a cold gas propulsion system, as well as a set of functional requirements. But in order to have definite targets to which to design the TALARIS CGSE, the process of requirements definition had to be carried further forward. The requirements already determined were used to derive quantifiable performance requirements.

3.1.1 Functional Requirements

The decisions to (1) divide the TALARIS propulsion tasks into weight relief and spacecraft emulation, each performed by a separate system, and (2) design for the performance of a hover hop led to three main functional requirements for the TALARIS spacecraft emulator propulsion system. They were:

(1) The CGSE shall lift the TALARIS hopper's lunar weight, defined as 1/6 of its Earth weight.

Though the long-term goals for the TALARIS project include simulation of operations on a range of target bodies, the short deadlines for the GLXP made simulation of lunar operations the top priority. Furthermore, a CGSE capable of lifting the TALARIS hopper under lunar gravity could also function for many other targets with even lower gravities, including Saturn's moon Titan[2] or a variety of asteroids, if EDF output could be increased to provide a higher fraction of weight relief. If later operations on a body with higher gravity than the Moon, such as Mars, were desired, upgrades would be necessary unless the CGSE far exceeded its design goals. However, it was essential to set initial numerical design targets for the CGSE, and designing for lunar gravity was selected for the requirement.

[2] Titan has a surface gravity of $0.138g$, while Earth's Moon has a surface gravity of $0.166g$ [62].

(2) The CGSE shall propel the hopper horizontally.

This is a key difference between TALARIS and the lunar lander testbeds described in section 2.1. Although several of the lander testbeds were capable of traveling horizontally, it was not their primary function. By contrast, horizontal transit over a significant distance is the main goal of hopping, so it was a major design driver for the TALARIS CGSE from the start.

(3) The CGSE shall provide attitude control for the TALARIS hopper.

TALARIS was designed to simulate the functions of a lunar or planetary hopper as completely as possible. Since an actual hopper operating off the Earth would have only its rocket propulsion system, this meant that the TALARIS hopper testbed should ideally rely only on the CGSE for attitude control for maximum similarity, using the EDFs only for passive weight relief. The goal was to design TALARIS such that under nominal operations, where the EDFs were providing pure vertical weight relief, the CGSE would be capable of executing all attitude adjustments necessary to simulate a full hop.

These three functional requirements were the starting point for the requirements flowdown process described in this section.

3.1.2 TALARIS Flight Profile

A more specific definition of the TALARIS flight profile was necessary to proceed with requirements flowdown. As defined in section 2.3.1, a hover hop has three phases: vertical ascent, horizontal transit, and vertical descent. But more precise dimensions had to be assigned to each of these phases.

The TALARIS hopper was primarily designed to simulate the GLXP hopper. However, as discussed in section 2.3.1, it was known that the GLXP hopper would likely have a propulsion system with a higher total impulse capability than the TALARIS hopper, largely because the GLXP hopper would not have to adhere to such strict safety restrictions and could thus use energetic rocket propellants. Thus, the TALARIS hopper was designed to fly a scaled-down version of the planned GLXP hop that still contained all the accelerations that the GLXP hopper would experience in order to retain dynamic similarity. A comparison of the TALARIS and GLXP hops is shown in Figure 3-1.

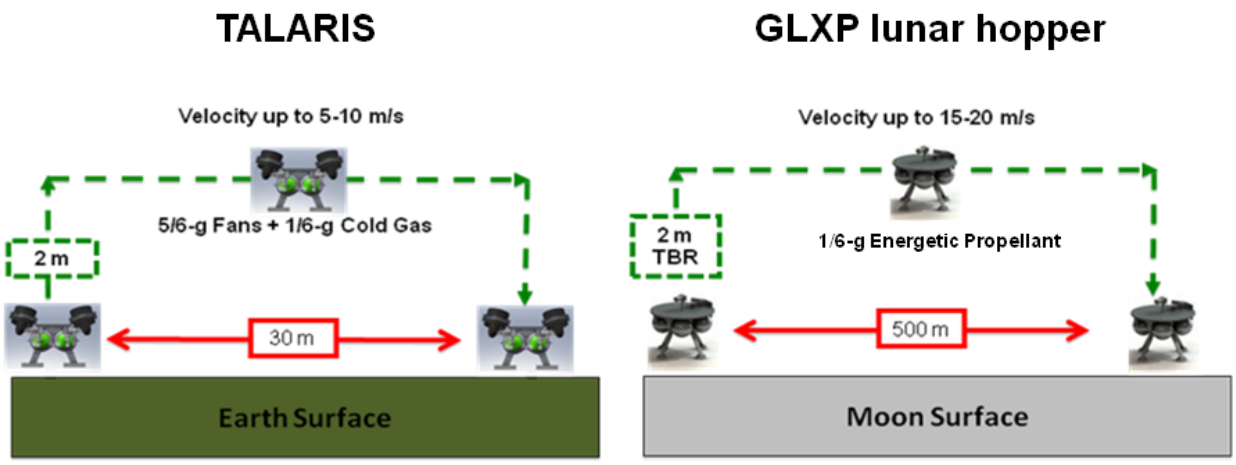

Figure 3-1. Scaling of TALARIS terrestrial hop compared to GLXP lunar hop [38].

As shown in Figure 3-1, the proposed altitude of the GLXP lunar hop was 2 m. This altitude, as indicated in Figure 3-1, was subject to revision, but it was expected that this altitude would allow the GLXP hopper to easily clear most rocks or other obstacles in its path. It was decided to use a 2 m altitude for the TALARIS terrestrial hop as well, since it would be difficult to duplicate the accelerations expected for the GLXP hopper over smaller ascent and descent distances. Furthermore, 2 m was considered to be a good altitude for demonstration purposes, as the TALARIS hopper would then be clearly above the ground and visible at some distance.

Since the vertical dimensions were kept the same for the TALARIS and GLXP hops, the horizontal distance had to be reduced to scale the TALARIS hop down from the planned GLXP lunar hop. The horizontal distance of the lunar hop, 500 m, was set by the GLXP rules as described in Chapter 1, but it was anticipated that the majority of this distance would be a constant-velocity cruise. The 16.898 design class in fall 2008 recommended a horizontal distance of 30 m for the TALARIS hop, and this recommendation was carried forward through the spring 2009 16.83/89 class as well. It was expected that this would be a sufficient distance to allow for acceleration, cruise, and braking phases while still remaining within the impulse capacity of the TALARIS hopper. Later MATLAB modeling, as described in section 4.1, indicated that this target distance was likely achievable, though ambitious.

3.1.3 Requirements Flowdown

With the dimensions of the TALARIS hop defined, each of the three main functional requirements was taken in turn to determine quantitative performance requirements for the TALARIS cold gas propulsion system.

(1) Lifting the hopper's lunar weight

At the conclusion of the spring 2009 16.83/89 class and the start of this requirements definition process, the target mass of the TALARIS hopper was 45 kg, giving it an Earth weight of 441.45 N, or 99 lbs [38]. The EDFs are designed to lift 5/6 of this weight. However, the CGSE must be able to provide a vertical force greater than 1/6 of the hopper's Earth weight in order to accelerate it upward at liftoff. It was decided that the TALARIS hopper should be capable of rising to its operational altitude of 2 m in less than 3 s. (This time was originally chosen arbitrarily; later, results of the computer model discussed in section 4.1 showed that 3 s was approximately 25% of the shortest expected total flight time, which was deemed to be a good fraction since it left the majority of the flight time for the horizontal transit while still being long enough to observe and control the hopper's behavior during ascent.) This ascent can be accomplished with a net upward acceleration of 1 m/s^2, or equivalently a total thrust-to-weight ratio (T/W) of about 1.1, at the moment of takeoff.[3] If the EDFs provide a constant T/W of 5/6 or 0.83, this means that the CGSE must provide vertical thrust equivalent to 0.27 times the Earth weight of the TALARIS hopper. For a 45-kg hopper, this is approximately 120 N.

(2) Propelling the hopper horizontally

The horizontal thrust requirements of the TALARIS hopper are not defined as sharply as the vertical thrust requirements. The distance of the hop is the critical parameter; the speed at which the hopper travels is not important, except in that the hopper must be moving fast enough to cover the required distance before it runs out of propellant to hold itself up. (The velocities indicated in Figure 3-1 are estimates of capabilities, not necessarily design goals.) Furthermore, thrust affects acceleration as opposed to velocity; effectively, any velocity could be provided by any thrust level by simply firing the thrusters for the appropriate amount of time given the acceleration they provided to the vehicle. Therefore, it was decided that the horizontal and vertical thrusters would be made identical. This would allow for greater simplicity, as the interfaces, pressure requirements, etc. would then be the same for all thrusters. Furthermore, fewer different types of spare parts would have to be kept on hand, and replacements and other types of repairs would be easier if necessary.

---

[3] In order to have zero vertical velocity when the hopper reaches its target altitude, it must have a net upward acceleration for the first half of the ascent and a net downward acceleration during the second half of the ascent. If the hopper accelerates upward off the ground at 1 m/s^2, it will reach an altitude of 1 m in $\sqrt{2}$ s, or approximately 1.4 s, with an upward velocity of $\sqrt{2}$ m/s. It can then immediately begin to decelerate its rise at a rate of 1 m/s^2; the second half of the ascent will then be the mirror image of the first half, and the hopper will achieve its target altitude of 2 m with zero vertical velocity at a time approximately 2.8 s after liftoff.

(3) Providing attitude control

There are two main aspects to be considered when providing attitude control: thrust level and thruster geometry. For thrust level, the requirement for the CGSE to lift the hopper's lunar weight led to an estimate of 120 N of maximum vertical force required. But during liftoff, there is a need for attitude control, so there should be additional thrust margin available above the 120 N previously calculated. Furthermore, the CGSE must have sufficient granularity of control to allow for thrust level to be adjusted in small increments throughout a hop. The TALARIS hopper must have a total T/W greater than 1 for liftoff, equal to 1 for level flight, and less than 1 for landing. If the EDFs provide a constant T/W of 5/6 (or the appropriate weight-relief fraction for a target body other than the Moon), the CGSE has to provide a different T/W for every phase of the flight. At the same time, though, the CGSE is expending fuel, consequently decreasing the weight of the hopper. And finally, attitude control may necessitate adjustments of many different magnitudes throughout the flight.

One method of controlling the output of the CGSE would be to use thruster control valves with a variable flow rate. However, this type of valve actuation is complicated, which tends to make the valves massive, complex, and expensive. Instead, most cold gas thrusters use solenoid valves. Most solenoid valves are on/off only, but they have simple electronic actuators. They do not allow for control of thrust level, but by using a method such as pulse-width modulation (PWM), the amount of impulse delivered over a short period of time can be controlled. The faster the actuation of the solenoid valve, the finer the control that can be provided; conversations with controls engineers for the TALARIS project indicated that actuation times in the low tens of ms would be the slowest acceptable.

In terms of thruster geometry, TALARIS would ideally have the same thruster layout as the GLXP lunar hopper for the most accurate possible simulation. Since the GLXP hopper design was not yet finalized, though, there was a great deal more freedom in thruster placement for the TALARIS testbed. As a result, decisions were made to maximize simplicity, both in terms of controllability of the TALARIS vehicle and construction of the CGSE system.

For simplicity of control, it was decided to have separate horizontal and vertical thrusters, as opposed to angled thrusters providing components in each direction, and as already mentioned, these thrusters would be made from identical components and designed to produce nominally identical thrust levels. At least one downward-pointing vertical thruster was required to provide lift. If the thruster could be gimbaled, a single thruster would be sufficient, but this would be too heavy and complex. Without gimbals, at least three thrusters were required for stability, like the legs of a tripod. However, for

simplicity of control, it was decided to use four thrusters, evenly spaced so that they could be fired in pairs to control pitch and yaw of the vehicle (rotation about the Y and Z axes, as defined in Figure 3-2 below). Upward-pointing vertical thrusters were not necessary, since the hopper was designed to operate in a gravity field that would constantly pull it down.

As for horizontal thrusters, at least two were required: one pointing forward to accelerate the hopper in the desired direction of travel, and one pointing backward to decelerate the hopper at the end of the horizontal transit phase of the hop. Again, though, it was decided to use four horizontal thrusters for the purposes of attitude control, with two pointed forward and two pointed backward. They were to be spaced at equal distances from the center of mass such that they could be fired in pairs to roll the vehicle (rotation about the X axis, as shown in Figure 3-2). With this capability, it was decided not to place any horizontal thrusters in the orthogonal direction. This limited the TALARIS hopper to primarily two-dimensional flight profiles, though it did retain some ability to adjust its course similar to the way that a car can change direction by steering. However, a 2D flight profile was deemed sufficient to demonstrate hopping, and it was believed that the reduced mass and simpler plumbing would increase the likelihood of completing a functional cold gas propulsion system within the tight schedule. The idea of mounting the horizontal thrusters at an angle, such that firing an individual horizontal thruster would produce components of thrust both parallel and perpendicular to the intended direction of travel, was briefly considered. However, there were concerns that this would simply reduce the thrust available for the primary direction of travel without providing significant control authority in the orthogonal direction, and also that it would be more difficult to mount and align the thrusters. Thus, the idea of mounting horizontal thrusters at an angle was discarded.

Finally, it was decided to place the horizontal and vertical thrusters near to each other, again to simplify the plumbing as much as possible. This resulted in the thruster geometry shown in Figure 3-2.

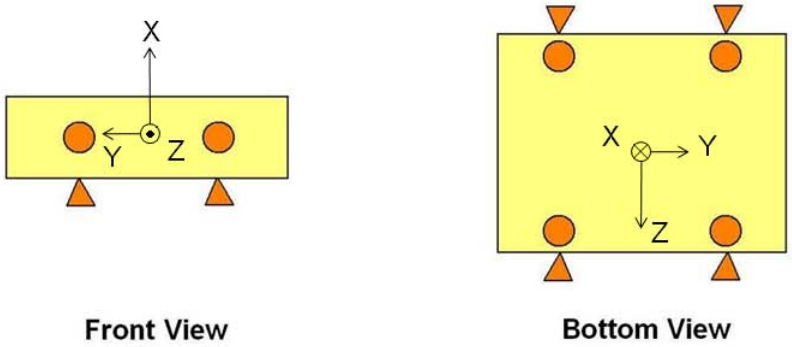

Figure 3-2. TALARIS cold gas thruster geometry.

Figure 3-2 also shows the body coordinate system defined for the TALARIS hopper. The origin is the vehicle's center of mass; it was assumed that the hopper would be balanced to make the center of mass coincident with the geometric center. The primary direction of horizontal travel is defined as the +Z axis; the +X axis points vertically upward; and the +Y axis completes the right-handed coordinate system. This coordinate system was chosen so that the TALARIS GNC algorithms could be more easily integrated with work already being conducted on the ALHAT (Autonomous Landing and Hazard Avoidance Technology) project at Draper.

3.1.4 Derived Requirements

The results of the requirements flowdown process can be summarized in the following derived requirements for the TALARIS CGSE:

(1) The CGSE shall provide at least 120 N of vertical thrust for liftoff.

(2) The CGSE shall have four vertical thrusters, all pointing downward.

(3) The CGSE shall have four horizontal thrusters, two pointing in the primary direction of travel and two pointing in the opposite direction.

(4) The CGSE shall have identical vertical and horizontal thrusters.

(5) The CGSE shall generate at least 30 N thrust per thruster, with a design goal of 35-40 N per thruster.

(6) The CGSE shall have thruster solenoid valves that actuate as rapidly as possible, on the order of tens of ms or faster.

Some of these requirements were additional constraints on the CGSE design. Others were performance requirements, which created specific quantitative goals to which the CGSE could be designed. With these requirements defined, design work for the CGSE could proceed further.

3.2 CGSE System Schematic: Introduction to Components

Once the number of thrusters in the TALARIS CGSE had been set, the diagram of the system shown in Figure 3-3 below could be drawn up.

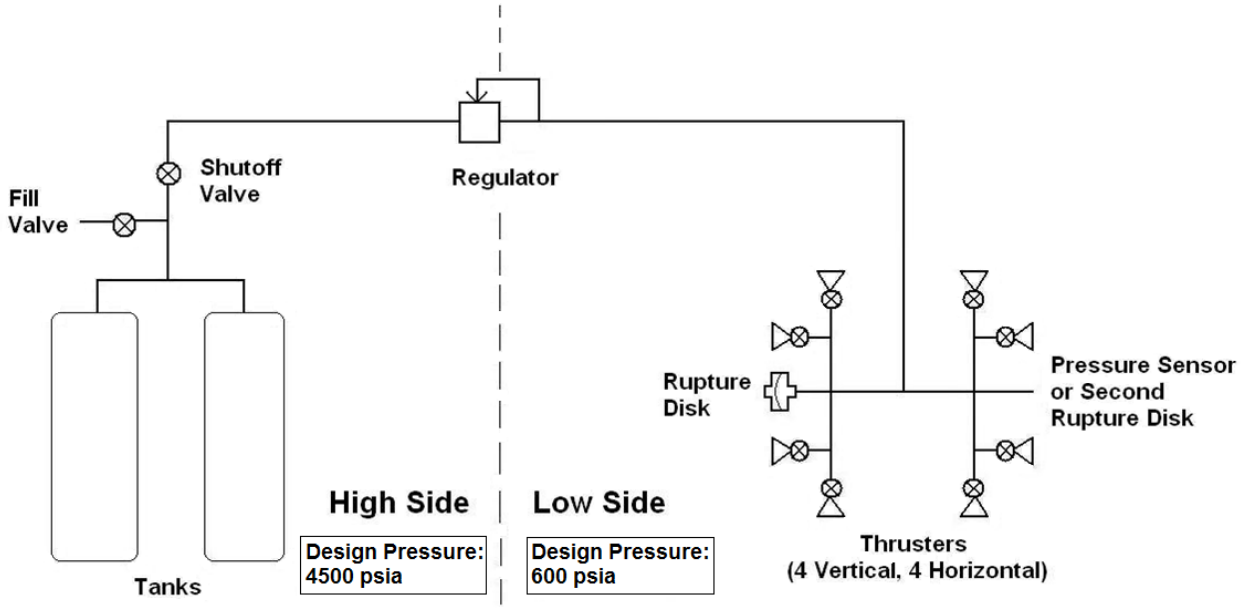

Figure 3-3. CGSE system schematic [38].

The tanks were the first pieces of hardware acquired for the CGSE. They were Luxfer L65G self-contained breathing apparatus (SCBA) tanks, made from aluminum wrapped with carbon fiber [39]. These tanks were inherited from another student project, but they were relatively lightweight and of a suitable form factor to fit with the rest of the TALARIS vehicle. The maximum working pressure rating of the tanks was 4500 psia (31.03 MPa), which set the design pressure for the high side of the CGSE. A quick survey of available solenoid valves suggested that valves able to handle 4500 psia were not readily available in sizes reasonable for a flying vehicle, which reinforced the need for the CGSE to be a regulated system. The low side design pressure of 600 psia (4.14 MPa) indicated in Figure 3-3 was determined by the selection of flow control components, particularly the regulator and the thruster solenoid valves. This selection process was accomplished with the help of a model of the cold gas system written in MATLAB, and it is described in the next chapter.

4 Modeling and Flow Control Components

Once the architecture of the TALARIS CGSE propulsion system had been defined and quantitative performance requirements had been set, detailed design could proceed. Since cold gas propulsion systems are a mature technology, the types of components to be used in the CGSE were known from the start. The design process thus involved sizing these components, particularly the thruster solenoid valves and regulator, as well as the thruster nozzles. In order to accomplish this, a computer model was written in MATLAB. This model was designed with several simplifying assumptions, which are discussed in the following sections. Therefore, the model was not expected to produce highly accurate predictions of the real CGSE's performance. Rather, it was intended to serve as an aid to component selection in the early stages of design, and the results produced by the model were sufficient for this purpose.

4.1 MATLAB Model

The MATLAB model written to assist the CGSE design process was centered on the solution of differential equations tracking the thermodynamic state of the gas in the system. Various hopper flight profiles could be simulated; knowledge of the thrust needed to execute a certain profile was combined with information about the state of the gas to determine the gas flow rate necessary at each point in the flight. From this, the sizes of the thruster solenoid valves and regulator necessary for the system to produce sufficient thrust to execute the intended flight profile could be determined. Digital copies of the model code are held by the TALARIS project and the author, but the derivation, structure, and content of the model are discussed in detail here.

The structure of the model was based on a previous MATLAB model that had been written in the fall 2008 16.898 design class. However, nearly all of the working equations within the model were modified or exchanged for more applicable equations in light of the evolutions of the CGSE design. The method of entering flight profiles was changed to reflect the thruster configuration illustrated in Figure 3-2. A tank-sizing routine that had been included in the 16.898 model was removed, since tanks had already been selected for the CGSE by the time the work described in this thesis began. Most importantly, the 16.898 model used the ideal gas assumption throughout for simplicity. However, the high initial tank pressure as well as the low temperatures that the gas would reach suggested that real gas effects would be non-negligible for the majority of the conditions that the CGSE would experience. Thus, the MATLAB model was modified to use real gas equations. This increased the complexity of the model, but it was believed that it would provide more accurate results for the design process described in this thesis.

4.1.1 Flight Profiles

Hopper flight profiles were entered into in the MATLAB model in terms of varying vertical and horizontal thrust. As discussed in section 3.1.3, the vertical thrust requirements throughout a hop of the desired dimensions were fairly well defined. Because the hopper would constantly lose mass during a hop as it expended nitrogen propellant, the vertical thrust levels for each phase of the hop were defined in terms of T/W, with a new vehicle weight calculated at each timestep of the solution based on previous gas usage. It was assumed that all four vertical thrusters would fire together to provide the total vertical thrust needed from the CGSE.

There was more variation possible in defining the horizontal thrust for the transit phase of the hop. For all flight profiles, it was assumed that horizontal thrusters would fire in pairs, to accelerate or decelerate the hopper in the direction parallel to its Z axis (see Figure 3-2), with no steering or other rotation. However, the hopper could have short periods of acceleration and deceleration with a longer cruise at relatively low constant velocity, or longer periods of acceleration and deceleration resulting in a shorter cruise at higher velocity. In the limit, the hopper would accelerate horizontally for the entire first half of the transit phase and then decelerate over the second half, with no constant-velocity cruise in between. Several different horizontal acceleration profiles were modeled in order to judge their effect on CGSE design requirements.

It should be noted that throughout all phases of the hop, attitude control was known to be necessary but not modeled. Possible sources of disturbances were identified to include gusts of wind (though it was planned to operate the TALARIS hopper indoors if possible to mitigate this), misalignments in the CGSE (i.e. a thruster mounted at a slight angle to its primary direction of force), and torques or lateral forces caused by the EDF weight relief propulsion system. The magnitude of these disturbances was not known at the time the model was written, so it was not possible to make an accurate estimate of the total amount of impulse necessary for attitude control, but it was assumed that it would be much smaller than the impulse required to perform the major planned vehicle maneuvers. Therefore, flight profiles were only considered feasible if the model indicated there was surplus gas available in the tanks at the end of a hop. It was assumed that this additional margin would be used for attitude control during a real hop.

4.1.2 Rocket Propulsion Equations

Like all forms of rocket propulsion, a cold gas thruster produces thrust by converting the internal energy of a gas to kinetic energy in an exhaust flow by means of thermodynamic expansion in a nozzle [28]. As propellant mass is ejected from the thruster at high speeds in the exhaust flow, thrust is produced in the opposite direction to ensure conservation of momentum for the system. Thrust is also produced by any difference between the exhaust pressure and the ambient pressure. In equation form:

$$\boldsymbol{F_{Th} = \dot{m}u_e + (P_e - P_a)A_e} \quad \textbf{(4-1)}$$

where F_{Th} is thrust in N, $\dot{m}$ is mass flow in kg/s, u_e is exhaust velocity in m/s, P_e is exit pressure of the exhaust in Pa, P_a is ambient pressure in Pa, and A_e is cross-sectional exit area of the nozzle in m^2.

It can be seen in equation (4-1) that if P_e is less than P_a, the pressure term will decrease the total rocket thrust. However, if P_e is greater than P_a, the exhaust is not fully expanded, and u_e is not as high as it could be. Due to these opposing effects, rocket thrust is maximized for given chamber conditions and throat area when $P_e = P_a$, a condition known as optimum or ideal expansion [40].

It is convenient to define an equivalent exhaust velocity u_{eq}:

$$\boldsymbol{u_{eq} = u_e + \left(\frac{P_e - P_a}{\dot{m}}\right) A_e} \quad \textbf{(4-2)}$$

such that the thrust equation (4-1) may be written:

$$\boldsymbol{F_{Th} = \dot{m}u_{eq}} \quad \textbf{(4-3)}$$

Thus, for ideal expansion, $u_e = u_{eq}$.

In the MATLAB model, specific impulse was calculated instead of u_{eq}, since propulsion system performance is more commonly expressed in terms of I_{sp}. Specific impulse, defined as the amount of impulse delivered per unit weight of propellant, is proportional to u_{eq} by:

$$\boldsymbol{I_{sp} = \frac{u_{eq}}{g}} \quad \textbf{(4-4)}$$

where g is the acceleration due to gravity at Earth's surface. For u_{eq} in m/s, the value of g used is 9.81 m/s^2, so that the units of I_{sp} are seconds. With this definition of I_{sp}, the rocket thrust equation may be written a third way as:

$$\boldsymbol{F_{Th} = \dot{m} I_{sp} g} \quad \textbf{(4-5)}$$

One final change was made to this expression for thrust. All thrust equations presented so far assume that the exhaust flow is one-dimensional, entirely parallel to the axis of the nozzle and the direction of travel of the rocket. In reality, though, this can never be achieved; there is always some radial component to the exhaust flow, which reduces the available thrust. This may be taken into account with a dimensionless nozzle correction factor λ, which can be calculated if the nozzle geometry is known. For the TALARIS CGSE, it was decided that conical nozzles would be used, as they were easier to machine than bell-shaped nozzles. The nozzle correction factor for a conical nozzle is:

$$\boldsymbol{\lambda = \frac{1 + \cos \alpha}{2}} \quad \textbf{(4-6)}$$

where α is the half-angle of the cone [40]. Thus, for the commonly-used half-angle of 15°, the value of λ is approximately 0.98.

With the addition of the nozzle correction factor, rocket thrust was calculated in the CGSE MATLAB model with the following equation:

$$\boldsymbol{F_{Th} = \lambda \dot{m} I_{sp} g} \quad \textbf{(4-7)}$$

The thrust F_{Th} required at each moment in a simulated hop was known based on the defined flight profile. By definition, g remained constant, and λ also remained constant because the nozzle geometry was fixed, but $\dot{m}$ and I_{sp} both had to be calculated for each moment throughout the hop.

The I_{sp} of a cold gas system depends on the thermodynamic state of the gas, but it is also influenced by nozzle geometry. Under the assumptions of isentropic flow and ideal expansion, these effects combine to form the following equation:

$$\boldsymbol{I_{sp} = \frac{1}{g} \sqrt{\frac{2\gamma}{\gamma - 1} R_{sp} T_c \left[1 - \left(\frac{P_e}{P_c} \right)^{\frac{\gamma - 1}{\gamma}} \right]}} \quad \textbf{(4-8)}$$

where γ is the ratio of specific heats; R_{sp} is the specific gas constant, defined as the ideal gas constant R divided by the molar mass M of the particular gas in use, with units of J/(kg K); T_c is the chamber temperature, i.e. the temperature of the gas immediately before entering the thruster nozzle, in K; and P_c is the chamber pressure [40]. By definition, R_{sp} and g are constant. Since ideal expansion was assumed, P_e was taken to be standard atmospheric pressure of 101,325 Pa (14.7 psia). The remaining

variables in equation (4-8) deal with the thermodynamic state of the gas in the thruster chamber. For P_c, it was assumed that the cold gas system would have a regulator that could deliver a constant chamber pressure to each thruster. Thus, a fixed value of P_c was selected for each run of the model, though many different runs were conducted with a range of settings for P_c. However, T_c was subject to change throughout the hop. Furthermore, although γ is constant for an ideal gas, it varies somewhat with temperature when real gas effects are considered. Therefore, the thermodynamic state of the gas in the CGSE had to be computed throughout the modeled hop.

4.1.3 Thermodynamic Equations

As mentioned in the introduction to section 4.1, the high pressure to which the tanks were initially filled as well as the low temperatures that the model suggested the gas would reach meant that ideal gas assumptions were not valid, so considerations had to be made of real gas behaviors. The simplest way to do this is to use the compressibility factor Z. The ideal gas law can be written:

$$\boldsymbol{P = \rho R_{sp} T} \tag{4-9}$$

where P is pressure, ρ is density, R_{sp} is again the specific gas constant, and T is temperature. The dimensionless compressibility factor is applied according to the following equation:

$$\boldsymbol{P = Z \rho R_{sp} T} \tag{4-10}$$

Comparison of equations (4-9) and (4-10) shows that for an ideal gas, Z is 1 by definition. For real gases, values of Z have been determined experimentally under a range of different conditions. In the CGSE MATLAB model, a lookup table indexed by temperature and pressure was created using Z factors from [41]. Interpolation was used to calculate values of Z that lay between those in the table.

For the initial conditions of the nitrogen gas,[4] it was assumed that the tanks would be filled to their maximum pressure of 4500 psia (31.03 MPa) and that they would be filled slowly so the gas could equalize with the ambient temperature, taken in the model to be 300 K. Using this pressure and temperature, the compressibility factor was obtained from the lookup table; it was found to be 1.15, which is significantly different from the ideal gas value of 1 and thus illustrates the need to use real gas

[4] At these conditions, nitrogen is actually a supercritical fluid (see discussion of the critical point in the main text). However, for most considerations of the TALARIS CGSE, its behavior is not significantly different from that of a gas, especially in terms of flow characteristics. Therefore, the distinction between the supercritical fluid and gaseous phases is generally not made in this thesis.

equations. Equation (4-10) was then used to calculate the initial gas density. However, pressure, temperature, and density were all subject to change as gas flowed out of the CGSE. These changes were modeled with a set of differential equations based on a model originally written by Alessandro Golkar, a student who had worked on TALARIS in the fall 2008 and spring 2009 design classes. The Golkar model was not written for TALARIS, but rather for the pressurant gas tank of a liquid propellant rocket. However, the pressurant tank experienced temperature and pressure ranges very similar to those of the TALARIS CGSE, so the thermodynamics of both cases were comparable in many ways. A full derivation of this model is available in [42], but a condensed outline of it is also presented here.

The Golkar model was based on the Redlich-Kwong equation of state, which is a more complex but often more accurate way of describing real gas behavior than using the compressibility factor Z. The Redlich-Kwong real gas equation of state is:

$$\boldsymbol{P = \frac{RT}{V_m - b} - \frac{a}{\sqrt{T} V_m (V_m + b)}} \quad \textbf{(4-11)}$$

where R is the ideal gas constant; V_m is the molar volume, equal to the molar mass M of the gas divided by its density ρ; and a and b are constants calculated from the critical point data of the particular gas used. The critical point refers to the conditions at which the phase boundary between liquid and gas ceases to exist. At temperatures and pressures above the critical point, a substance becomes a supercritical fluid [43]. Using the critical pressure P_{crit} and the critical temperature T_{crit}, the Redlich-Kwong constant a is defined as:

$$\boldsymbol{a = \frac{0.4275\, R^2\, {T_{crit}}^{5/2}}{P_{crit}}} \quad \textbf{(4-12)}$$

and b is:

$$\boldsymbol{b = \frac{0.08664\, R\, T_{crit}}{P_{crit}}} \quad \textbf{(4-13)}$$

The Golkar model also made use of the principle of conservation of energy, or the first law of thermodynamics, expressed as:

$$\boldsymbol{\dot{Q} = \frac{d}{dt}(mu) + \dot{m}h} \quad \textbf{(4-14)}$$

where $\dot{Q}$ is heat flow (W = J/s), m is mass (kg), u is specific internal energy of the gas (J/kg), and h is specific enthalpy (J/kg). Specific enthalpy and specific internal energy are related as follows:

$$\boldsymbol{h = u + \frac{PV}{m}} \tag{4-15}$$

where V is volume occupied by the gas in m^3. Thus, equation (4-15) can be used to eliminate u from equation (4-14). Furthermore, specific enthalpy may be expressed as a function of pressure and temperature $h(P, T)$ such that:

$$\boldsymbol{\dot{h} = \frac{\partial h}{\partial P}\dot{P} + \frac{\partial h}{\partial T}\dot{T}} \tag{4-16}$$

This allows the first law of thermodynamics to be rewritten as:

$$\boldsymbol{\left(\frac{\partial h}{\partial P} - \frac{V}{m}\right)\dot{P} + \frac{\partial h}{\partial T}\dot{T} = \frac{1}{m}\left[\dot{Q} - \dot{m}\left(2h - \frac{PV}{m}\right)\right] - \frac{PV}{m^2}\dot{m}} \tag{4-17}$$

An expression for $\dot{P}$ was found by differentiating equation (4-11), the Redlich-Kwong equation of state. This, combined with conservation of energy as expressed in equation (4-17), led to the following system of differential equations:

$$\boldsymbol{\dot{P} = \frac{\partial P}{\partial T}\dot{T} + \frac{\partial P}{\partial V_m}\dot{V}_m = A\dot{T} + B} \tag{4-18}$$

$$\boldsymbol{A = \frac{\partial P}{\partial T} = \frac{R}{V_m - b} + \frac{1}{2}\frac{a}{T^{3/2}V_m(V_m + b)}} \tag{4-19}$$

$$\boldsymbol{B = \frac{\partial P}{\partial V_m}\dot{V}_m = \left\{\frac{-RT}{(V_m - b)^2} + \frac{a(2V_m + b)}{\sqrt{T}\,[V_m(V_m + b)]^2}\right\}\left(\frac{-VM}{m^2}\right)\dot{m}} \tag{4-20}$$

$$\boldsymbol{\dot{T} = \frac{1}{\left(\frac{\partial h}{\partial P} - \frac{V}{m}\right)A + \frac{\partial h}{\partial T}}\left\{\frac{1}{m}\left[\dot{Q} - \dot{m}\left(2h - \frac{PV}{m}\right)\right] - \frac{PV}{m^2}\dot{m} - \left(\frac{\partial h}{\partial P} - \frac{V}{m}\right)B\right\}} \tag{4-21}$$

Equation (4-21), the expression for $\dot{T}$, introduces some new variables that have not yet been discussed. One is $\dot{Q}$, the rate of heat transfer. For the TALARIS CGSE, it was known that as gas was expelled from the system through the thrusters, the temperature of the gas remaining in the tanks would decrease, falling below the temperature of the ambient air. Thus, there would be potential for heat flow from the atmosphere into the gas inside the CGSE. However, for simplicity in initial modeling, $\dot{Q}$ was taken to be zero in the CGSE MATLAB model. This represented the worst-case scenario; any heat flow into the system would mitigate the temperature decrease throughout a flight, which would result in higher I_{sp} and thus lower mass flow $\dot{m}$ needed to deliver the required thrust. Consequently, the results generated by the model with $\dot{Q}$ set at zero provided an upper bound on mass flow requirements. The option of later revising the model to include the effects of heat transfer was kept open but never exercised.

The other new variables in equation (4-21) are the partial derivatives of specific enthalpy with respect to pressure and temperature. The Golkar model was written for a pressurant tank using helium gas, for which these derivatives were constant over the range of pressures and temperatures experienced [42]. However, these partial derivatives were not constant for nitrogen over the range of conditions expected in the TALARIS CGSE tanks. This difference is illustrated in Figure 4-1.

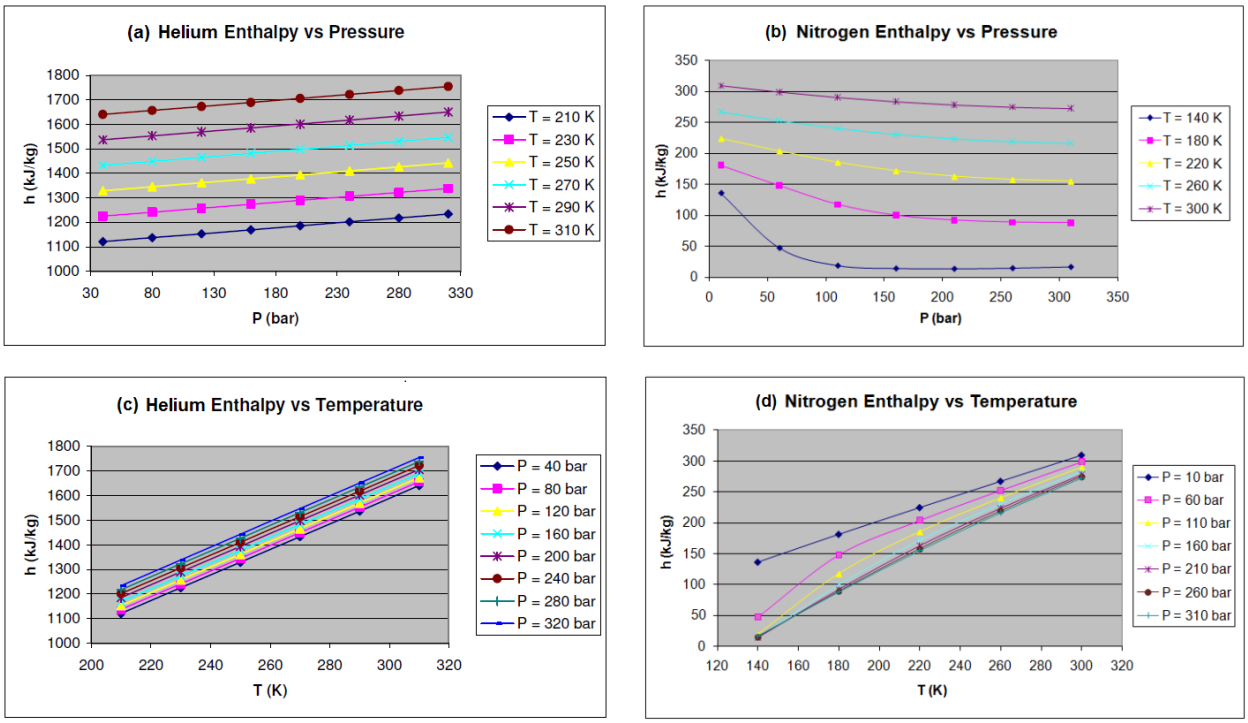

Figure 4-1. Enthalpy relations for helium and nitrogen.
(a) Helium specific enthalpy vs. pressure [42]. (b) Nitrogen specific enthalpy vs. pressure.
(c) Helium specific enthalpy vs. temperature [42]. (d) Nitrogen specific enthalpy vs. temperature.

In Figure 4-1(a), the plots of specific enthalpy vs. pressure for helium are all linear with the same slope regardless of temperature, which shows that $\frac{\partial h}{\partial P}$ is constant for the conditions in the helium pressurant tank. Similarly, Figure 4-1(c) indicates that $\frac{\partial h}{\partial T}$ is also constant for the helium pressurant. However, Figure 4-1(b) and (d) show that the relationships between enthalpy and pressure and enthalpy and temperature are nonlinear for nitrogen in the TALARIS CGSE. Furthermore, the nitrogen enthalpy curves all differ slightly in shape. These effects occur for two reasons. First, the TALARIS CGSE was expected to operate over a broader range of temperatures and pressures than the helium pressurant tank for which the Golkar model was written, reaching lower extremes in both thermodynamic variables. Second, the critical point of nitrogen (3.39 MPa = 492 psi, 126.2 K) occurs at a higher pressure and temperature than

that of helium (0.227 MPa = 32.9 psi, 5.19 K) [43], and the thermodynamic state of the nitrogen in the TALARIS CGSE was found to approach the critical point at the end of a hop. This means that nitrogen in the TALARIS CGSE behaves less like an ideal gas and exhibits real gas behavior more strongly, so $\frac{\partial h}{\partial P}$ and $\frac{\partial h}{\partial T}$ must be calculated as functions of pressure and temperature.

In order to expand the Golkar model for application to the TALARIS CGSE, an additional function was written in MATLAB to calculate variables related to enthalpy. The function included a lookup table of nitrogen specific enthalpy values on which interpolation could be performed to find the specific enthalpy h for any thermodynamic state. These values, some of which were plotted in Figure 4-1(b) and (d), were obtained from [44]. To calculate $\frac{\partial h}{\partial P}$ and $\frac{\partial h}{\partial T}$, curvefit equations were derived from the plots shown in Figure 4-1(b) and (d).

With the addition of the enthalpy function, all of the values needed to calculate the thermodynamic state of the nitrogen in the tanks were known or could be calculated. However, the nitrogen had to flow from the tanks through the regulator to the thrusters, and then through individual thruster solenoid valves before entering the thruster nozzle, and the thermodynamic state of the nitrogen would change along the way. One reason would be losses due to friction in the feed line tubing, especially if the nitrogen had to flow around corners. Furthermore, there would be additional opportunity for heat transfer to the gas through the tube walls as the nitrogen flowed out of the tanks to the thrusters. However, neither the configuration of the plumbing nor the sizes and materials of the tubes to be used for it were known at the time the MATLAB model was written. Therefore, these effects could not be modeled.

The one change in thermodynamic state of the nitrogen between the tanks and the thruster chamber that was modeled was based on the Joule-Thomson effect. The Joule-Thomson effect describes the change in temperature experienced by a fluid as it flows from a region of higher pressure through a valve (or regulator) to expand into a region of lower pressure [45]. This throttling process is assumed to be isenthalpic; that is, the fluid does no work and exchanges no heat with the environment. It was not clear that these conditions would hold true for the TALARIS CGSE; however, it was decided to proceed with the model as if they did. As with the decision to neglect heat transfer to the nitrogen in the tanks, this was done to model the worst-case scenario, with the coldest nitrogen and lowest possible I_{sp}.

The Joule-Thomson coefficient μ_{JT} is defined as the rate of change of temperature with respect to pressure in a throttling process:

$$\boldsymbol{\mu_{JT} = \left(\frac{\partial T}{\partial P}\right)_H} \quad \textbf{(4-22)}$$

Joule-Thomson coefficients for many fluids, including nitrogen, have been determined experimentally and can be found in resources such as [44] and [46]. The coefficient can be either positive or negative, meaning that the Joule-Thomson effect can either heat or cool a gas depending on its initial thermodynamic state. For each real gas, there is an inversion curve in the pressure-temperature plane along which μ_{JT} is zero. However, all modeled states of the TALARIS CGSE were inside the nitrogen inversion curve, so μ_{JT} was always positive and the Joule-Thomson effect always decreased the temperature of the gas [46].

For the TALARIS CGSE model, the Joule-Thomson effect was modeled very simply by making a discrete approximation of equation (4-22), resulting in the following equation:

$$\boldsymbol{T_2 = T_1 - \mu_{JT}(P_1 - P_2)} \quad \textbf{(4-23)}$$

in which P_1 and T_1 are the inlet conditions of the gas and P_2 and T_2 are the outlet conditions. The value of μ_{JT} used was based on the inlet conditions and found with a lookup table and interpolation. It was known that the results provided by this method would not be highly accurate, especially for large pressure differentials. However, a rough first-order approximation of the Joule-Thomson effect was deemed to be sufficient, especially in light of the many other simplifications included in the TALARIS CGSE model.

Equation (4-23) was used to calculate the temperature drop across the CGSE regulator as the pressure dropped from the tank pressure at any given time to the preset thruster chamber pressure P_c. The passage of the gas through the thruster solenoid valve presented a second opportunity for a temperature drop, but it was thought that because the solenoid valve opened almost directly onto the thruster nozzle, isentropic expansion would dominate and the isenthalpic assumption would no longer be reasonable. Furthermore, the pressure drop across the solenoid valve was much smaller than the pressure drop across the regulator for most of the hop, so even if the Joule-Thomson effect could be observed across the solenoid valve, the additional temperature decrease it would provide would be negligible. Therefore, the Joule-Thomson effect was not modeled for passage of the gas through the

thruster solenoid valve, and chamber temperature T_c was taken to be the tank temperature decreased by the Joule-Thomson effect across the regulator.

Once a method for calculating T_c was determined, the set of equations describing the thermodynamic state of the nitrogen in the CGSE was complete. These equations then had to be solved over the course of a simulated hop. This was accomplished numerically with MATLAB's built-in differential equation solver ode45. The total timespan over which the differential equations were solved was predefined by the flight profile programmed into the model; timesteps were set by MATLAB according to internal error tolerance limits and varied for different model runs but were generally on the order of 0.1 ms. At each timestep, the previous thermodynamic state of the nitrogen in the CGSE tanks was used to find T_c by application of the Joule-Thomson effect according to equation (4-23). In turn, this T_c was used to determine of a value for γ by interpolation and then calculate I_{sp} with equation (4-8). Once the available I_{sp} was known, equation (4-7) was used to calculate the mass flow $\dot{m}$ necessary for each thruster to perform as required by the flight profile. The previous thermodynamic state was also used as input for the enthalpy function to calculate h, $\frac{\partial h}{\partial P}$, and $\frac{\partial h}{\partial T}$. Then, equations (4-18) through (4-21) could be used to find $\dot{P}$ and $\dot{T}$, and the thermodynamic state of the nitrogen in the tanks could be propagated forward to the next timestep. This process was repeated to the end of the simulated hop.

In terms of cold gas propulsion system design, the most important outputs of the thermodynamics portion of the MATLAB model were the mass flows needed to deliver the thrust required to execute a hop. Mass flow rates were calculated for individual thrusters as well as the regulator, for which the required mass flow was the sum of the mass flows for all thrusters firing at a given time. These flow rates were used to determine the sizes of the thruster solenoid valves and regulator to be used in the TALARIS CGSE.

4.1.4 Flow Equations

A standard parameter for flow control component sizing is the dimensionless flow coefficient C_V, which relates pressure drop across a valve or orifice to flow rate. It is defined as the number of U.S. gallons of water at 60°F that will flow through the valve or orifice in one minute with a pressure drop of 1 psi [47]. However, water under these conditions is an incompressible fluid, and adjustments must be made to define an expression of C_V for compressible fluids like the nitrogen used in the TALARIS CGSE.

The first step in calculating C_V in the CGSE MATLAB model was to convert all the mass flow rates to volumetric flow rates, which are typically expressed in units of standard cubic feet per minute (SCFM), for which standard conditions are 60°F (289 K) and 14.7 psia. This was accomplished with the following equation:

$$\boldsymbol{q_g = \frac{1763\,\dot{m}}{\sqrt{SG_g}}} \tag{4-24}$$

in which q_g is volumetric flow rate in SCFM and SG_g is specific gravity of a gas relative to air at standard conditions of 60°F and 14.7 psia, which in this case was equal to the density of the nitrogen in the CGSE at its instantaneous conditions divided by the density of air at standard conditions.

Once the volumetric flow rate is known, there are several different equations by which C_V for a gas flow can be calculated, developed by various empirical and theoretical methods. One set of equations commonly provided by valve manufacturers distinguishes between critical, choked, or sonic flow (which is considered to occur when the inlet pressure P_1 is greater than or equal to two times the outlet pressure P_2) and subcritical or subsonic flow. The sonic flow equation is:

$$\boldsymbol{C_V = \frac{2\,q_g\sqrt{SG_g}}{P_1}} \tag{4-25}$$

and the subsonic flow equation is:

$$\boldsymbol{C_V = \frac{q_g\sqrt{SG_g}}{\sqrt{\Delta P \cdot P_2}}} \tag{4-26}$$

where the differential pressure $\Delta P = P_1 - P_2$ [48]. In these equations, the units of P_1 and P_2 are psia, the units of ΔP are psi, and SG_g is taken at the inlet conditions.

Equations (4-25) and (4-26) are fairly simple to implement, but they assume that conditions are close to standard conditions and that the gas behavior can be accurately described by the ideal gas law. As has already been discussed, this is not the case for the TALARIS CGSE for the majority of a hop. A more detailed expression for C_V which takes real gas effects into account and encompasses both sonic and subsonic flows is:

$$\boldsymbol{C_V = \frac{q_g\sqrt{SG_g\,(T_1+460)\,Z}}{22.67\,P_1\,Y\sqrt{\Delta P/P_1}}} \tag{4-27}$$

where T_1 is the inlet temperature in °F, Z is the compressibility factor at the inlet conditions, and Y is a dimensionless expansion factor [49]. (Again, P_1 is in psia, and ΔP is in psi.) The expansion factor Y is the ratio of flow coefficient for a gas to that of a liquid at the same Reynolds number. It has a minimum value of 2/3, which reflects the conditions of sonic flow. For subsonic flow, the expansion factor is calculated by:

$$\boldsymbol{Y = 1 - \frac{\Delta P/P_1}{3\,F_\gamma\,X_T} = 1 - \frac{\Delta P/P_1}{3\left(\frac{\gamma}{1.40}\right)X_T}} \qquad \textbf{(4-28)}$$

where F_γ is the specific heat ratio factor, which as indicated is the ratio of γ of the working fluid to 1.40 (γ of air at standard conditions), and x_T is the terminal pressure drop ratio [50]. This dimensionless factor x_T is highly dependent upon valve geometry, and it may have a value of anywhere from 0.15 to 0.90 depending on a valve's dimensions, flow path, etc. [49,50]. Because no particular valve type had been selected at this stage of CGSE design, it was not possible to define a highly accurate value for x_T . Instead, based on the rule of thumb suggested by equations (4-25) and (4-26), it was assumed that sonic flow conditions would occur for a minimum $\Delta P/P_1$ of 0.5. Thus, in order for the minimum value of Y to be 2/3, equation (4-28) was simplified to:

$$\boldsymbol{Y = 1 - \frac{\Delta P/P_1}{1.5}} \qquad \textbf{(4-29)}$$

Equation (4-29) was applied as follows: for $\Delta P/P_1$ greater than or equal to 0.5, which occurred for instance across the regulator early in a hop when the inlet pressure P_1 was high due to nearly full tanks, flow was assumed sonic and the minimum Y value of 2/3 was used. For $\Delta P/P_1$ less than 0.5, flow was assumed subsonic, and equation (4-29) was used to approximate Y. As $\Delta P/P_1$ became very small, for instance across the regulator late in a hop when the inlet pressure P_1 nearly equalized with the outlet pressure P_2 , Y approached its maximum value of 1.

It should be noted that piping configuration can have an effect on C_V , especially if elements like elbows or reducers are attached directly to the valve's inlet or outlet. Piping configuration can be taken into account in the calculation of C_V in two ways. Firstly, x_T can be replaced by x_{TP} , a terminal pressure drop ratio for the entire valve and fitting assembly. Secondly, the expression for C_V in equation (4-27) can be divided by an additional dimensionless piping geometry correction factor F_P [49,50]. However, as mentioned before, the piping geometry of the TALARIS CGSE was not yet known when the MATLAB model was written. Thus, there was no way to compute x_{TP} and F_P , and equations (4-24), (4-27), and

(4-29) were used as printed to convert the appropriate mass flows to C_V flow coefficients for the individual thruster valves as well as the regulator at each timestep of the MATLAB model.

4.1.5 Summary of the Model

A summary of the CGSE MATLAB model is presented in the form of a flowchart in Figure 4-2 below.

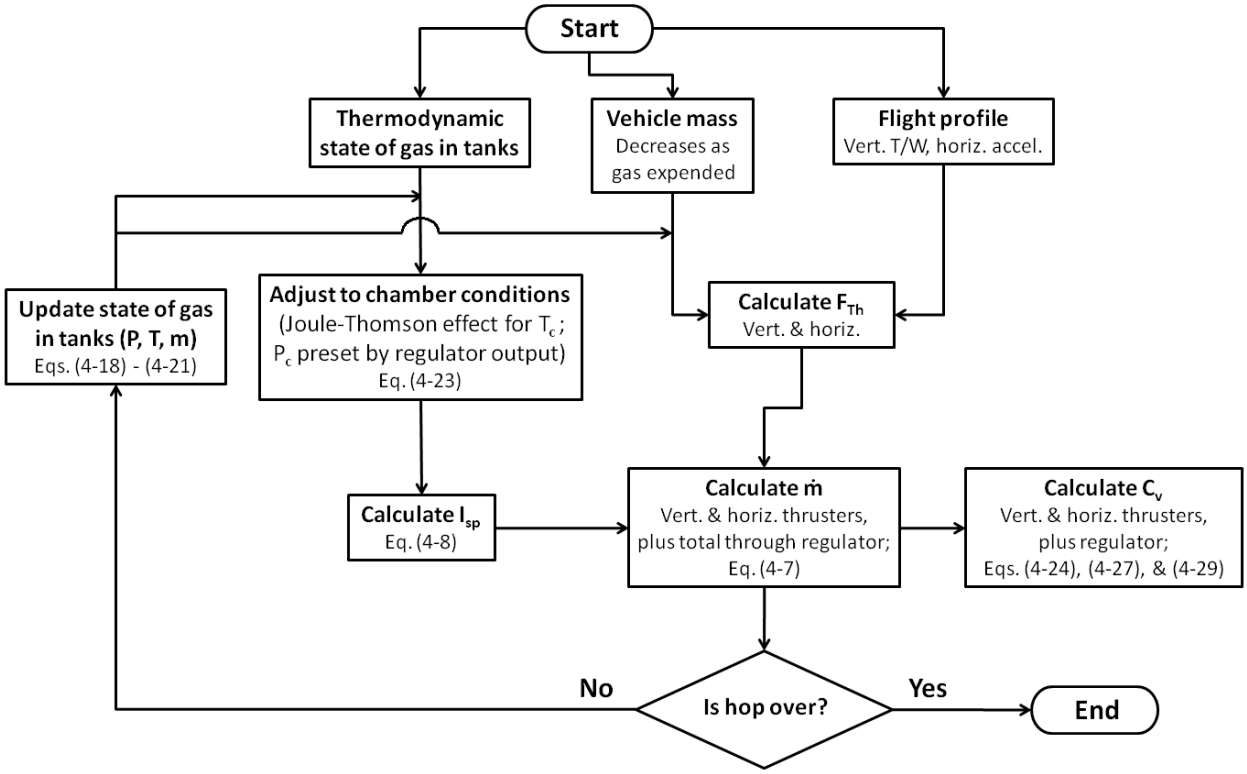

Figure 4-2. CGSE MATLAB model flowchart.

The model illustrated in Figure 4-2 contained a number of simplifications and other sources of uncertainty which were mentioned as they arose in the explanation of the model in the preceding sections. A collected list of these potential sources of error is presented below, along with several additional assumptions that have not yet been explicitly stated.

- The MATLAB model treated thrust as a continuous variable which could be specified to arbitrary precision. In reality, as discussed in section 3.1.3, it would not be possible to control thrust directly in the CGSE. Rather, impulse would be controlled by means of pulse-width modulation, or PWM. Thus, the model contained an implicit assumption that the PWM control period would be small compared to the timescale of the changes in thrust required for a level flight profile. As

discussed later in section 6.3.4, this turned out to be somewhat inaccurate, and the trajectory of actual flights were substantially less smooth than those which were modeled.

- Attitude control was not modeled because the magnitude of disturbances for which corrections would be necessary was not known. Instead, flight profiles were only considered feasible if the model indicated that there would be additional gas remaining in the tanks after the planned maneuvers for the hop, leaving some margin for attitude control.
- The regulator was assumed to be able to provide constant pressure to the low side of the CGSE throughout an entire hop. In fact, pressure regulators are subject to an effect called droop, in which the actual outlet pressure decreases below the set outlet pressure as the flow rate through the regulator increases [51]. Droop can vary greatly for different regulator designs, and it is usually characterized empirically and documented in a regulator's specification sheet with a flow curve. Since a specific regulator had not yet been selected, droop could not be accurately characterized in the MATLAB model. Instead, it was taken into account later in the component selection process.
- Equation (4-8) for I_{sp} involved assumptions of isentropic flow and ideal nozzle expansion. These assumptions became less valid as the behavior of the nitrogen in the CGSE deviated farther from that of an ideal gas.
- Interpolation was used to determine values for a number of variables, including γ, Z, h, and μ_{JT}. Furthermore, the partial derivatives of enthalpy $\frac{\partial h}{\partial P}$ and $\frac{\partial h}{\partial T}$ were determined from cubic spline curvefits. These approximations were based on verified data points from [41] and [44], spaced as closely as feasible, but there was still a chance of error, especially at the extreme ends of the data ranges.
- As mentioned in section 4.1.3, heat transfer from the ambient air to the nitrogen inside the CGSE through the tank walls and plumbing was not modeled.
- The dimensions, materials, and configuration of the tubing to be used to connect the components of the CGSE together were not known at the time of modeling, so piping pressure losses due to friction could not be calculated. Also, it was not possible to compute the factors x_{TP} and F_P for C_V calculations.
- The application of the Joule-Thomson effect assumed that flow across the regulator would be isenthalpic, which may not be accurate. Furthermore, the Joule-Thomson effect was modeled with a highly simplified first-order linear approximation, as expressed in equation (4-23).

- Neither the Joule-Thomson effect nor any other method was used to model temperature drop across the thruster solenoid valves.
- The flow coefficient C_V is defined for incompressible fluids, and all formulas of C_V for compressible fluids involve some degree of estimation. The particular method chosen to calculate C_V for this MATLAB model, using equation (4-27), was especially susceptible to possible errors in calculating Y due to estimating x_T .

With all of these approximations and simplifications, it was known that the MATLAB model would probably not produce highly accurate predictions of CGSE performance. However, that was never meant to be its purpose. Rather, the MATLAB model was intended to provide some approximate baselines to assist in the process of component selection.

4.1.6 Example Model Run

The CGSE MATLAB model was run with a variety of different conditions to characterize a range of possible designs as well as usage plans for the CGSE. The outputs of an example run of the model are presented here, in order to illustrate how conclusions were drawn for the CGSE design process.

The example run took the TALARIS hopper's mass as 45 kg when fully loaded with nitrogen propellant. It was assumed that the EDFs would provide constant 5/6 weight relief, adjusting their force output with the changing mass of the vehicle. A flight profile including a horizontal transit of 30 m with a brief constant-velocity cruise period was programmed into the model. The resulting CGSE thrust profile for the example run is plotted in Figure 4-3.

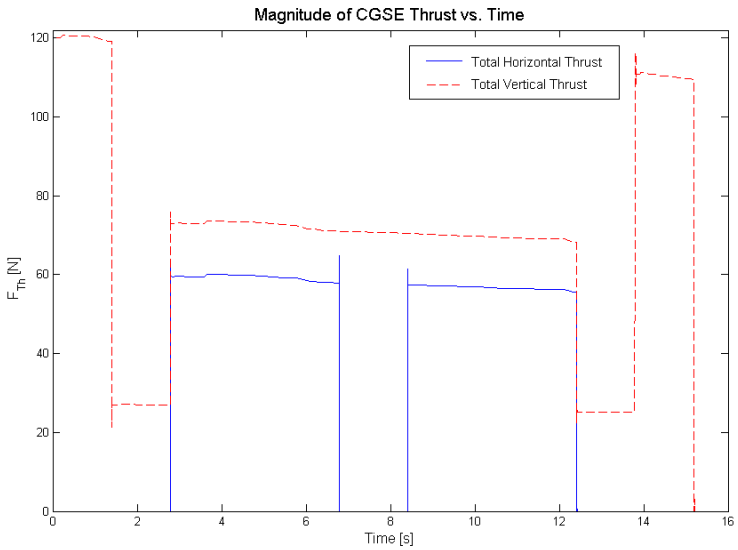

Figure 4-3. CGSE thrust profile from an example run of the MATLAB model.

The flight profile begins with maximum vertical thrust of approximately 120 N, or about 30 N produced by each of four vertical thrusters, as was calculated in section 3.1.3. This period of upward acceleration lasts for about 1.4 s, after which the vertical CGSE thrust drops to a much lower level with less than 30 N produced by the four vertical thrusters together. During this second half of the ascent, the hopper is still moving upwards due to its vertical momentum, but the total T/W is less than 1 even with the 5/6 weight relief provided by the EDFs. This causes the vertical rise of the hopper to decelerate until it reaches its operational altitude of 2 m with zero velocity approximately 2.8 s into the flight.

After the ascent, the horizontal transit phase of the hop begins. Throughout this phase, the CGSE vertical thrusters and EDFs together maintain a constant T/W of 1, but because the mass of the vehicle continually decreases as propellant is expended, the thrust level can be seen to decrease with time in the plot. Meanwhile, the horizontal thrusters fire to translate the hopper. In this particular flight profile, the hopper is first given a constant horizontal acceleration of 1.33 m/s^2 for 4 s. This acceleration is provided by two of the four horizontal thrusters; as with the vertical thrusters, they must decrease their thrust over the firing period in order to maintain constant acceleration as the hopper loses mass.

At about 6.8 s into the flight, the horizontal thrusters shut off, and the constant-velocity cruise begins. At this point, the hopper has translated 10.67 m from its starting point, and it has a horizontal velocity of 5.33 m/s. The hopper cruises for 1.625 s, in which time it covers 8.66 m of additional horizontal distance (assuming drag is negligible).

At the end of the horizontal transit phase, the hopper again fires a pair of horizontal thrusters for 4 s. However, this time it fires the pair opposite to the pair that initially fired, so the hopper decelerates horizontally. (Note that Figure 4-3 plots thrust magnitude, not direction.) The horizontal transit phase ends about 12.4 s into the flight, with the hopper again hovering at 2 m altitude with zero velocity, but now located 30 m from its starting point.

The final phase of the flight profile is the descent. It is essentially the mirror image of the ascent, with the vertical thrust first decreasing so that the hopper begins to drop but then increasing again to decelerate the hopper's fall so that it lands with zero velocity. As illustrated in Figure 4-3, the total flight time for this profile is just over 15 s.

The MATLAB model tracked the remaining nitrogen propellant mass as well as its thermodynamic state throughout this hop, and it also computed the component C_V values needed to produce the required thrust plotted in Figure 4-3 at each moment in time. These results are presented in Figure 4-4 below.

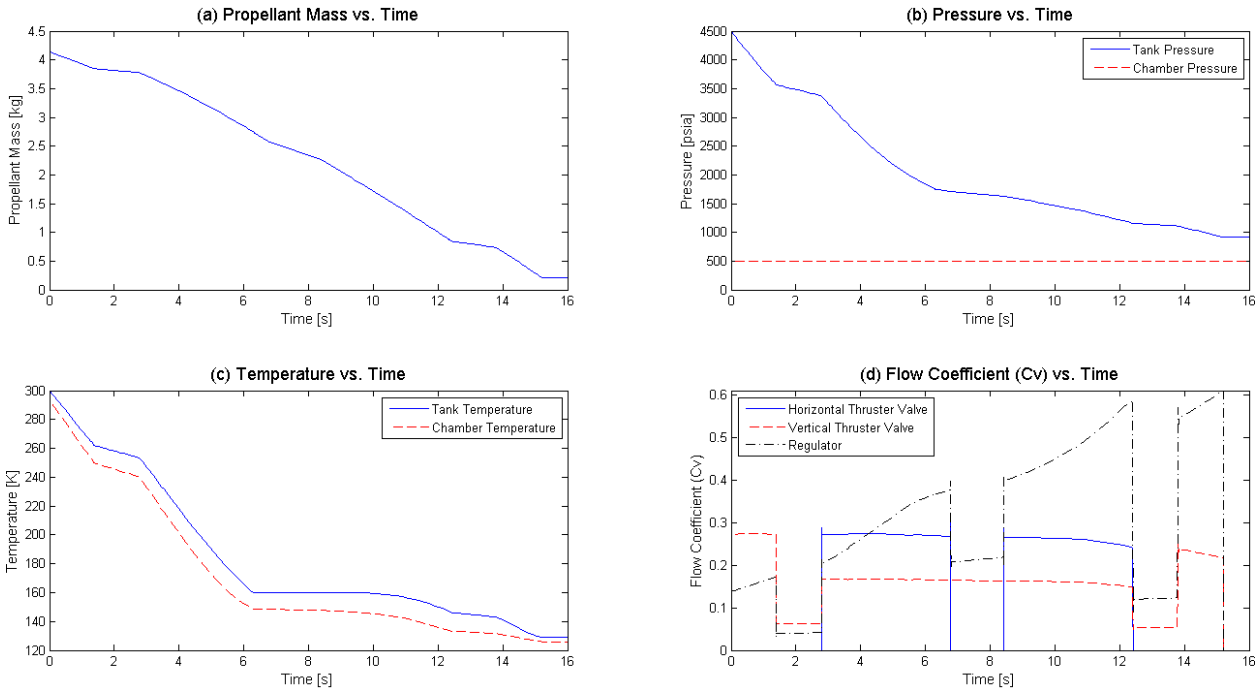

Figure 4-4. Results of the example run of the CGSE MATLAB model.

Figure 4-4(a) shows that when fully fueled to maximum pressure of 4500 psia, the CGSE tanks hold 4.14 kg of nitrogen. By the end of the modeled hop, this has been depleted to 0.21 kg at a pressure of approximately 900 psia. Figure 4-4(b) shows that this is still higher than the chamber pressure, which for this run was set at 500 psia, so there was some additional margin of propellant available for the unmodeled attitude control, and it was concluded that this example flight profile would be feasible. The temperature of the nitrogen in the CGSE declines throughout the hop as illustrated in Figure 4-4(c), with the chamber temperature always somewhat lower than the tank temperature due to the Joule-Thomson effect. According to the model, the final temperature of the nitrogen is about 129 K in the tank and 126 K in the thruster chamber. The critical point of nitrogen is at 492 psi and 126.2 K [43], so the model indicates that at the very end of the hop, the nitrogen could begin to liquefy in the thrusters. However, the model had many known simplifications and was designed to model the worst-case scenario, and conditions only crossed the critical point in the last few timesteps of the model, so this example profile was considered provisionally acceptable. Still, the possible condensation of nitrogen at the end of a hop was a concern kept in mind until testing confirmed that it would not be a problem.

For the purposes of CGSE design, the most important outputs of the MATLAB model were plots such as the one in Figure 4-4(d) showing the required C_V for the horizontal and vertical thruster valves as well as the regulator. Although the C_V values required to produce the thrust for a given flight profile vary over a

hop, any given valve or regulator only has one C_V. Thus, in order for the components to be suitable for an entire flight, they had to be sized based upon the maximum C_V required according to the model. Furthermore, since it had been decided that the horizontal and vertical thrusters would be made identical, a single thruster solenoid valve would be sized based on the highest required C_V among both the vertical and horizontal thrusters if this value differed between the two. Therefore, for the majority of any given hop, full flow would not be required through the solenoid valves, but it could not be prevented. However, it was assumed that PWM would be able to reduce the impulse bits sufficiently to allow for the vehicle to follow the flight profile.

Figure 4-4(d) reveals that the highest required C_V for both the horizontal and vertical thruster valves in the example model run is approximately 0.27. In this case, the maximum valve C_V values are nearly identical because both the horizontal and vertical thrusters are required to provide about 30 N each early in the hop. By contrast, the highest C_V for the regulator comes at the end of the hop, when the pressure differential across the regulator is lowest. For this example hop, the model indicated a maximum required C_V of approximately 0.61 for the regulator.

4.1.7 Major Conclusions Drawn from the Model

As stated before, multiple runs of the MATLAB model were conducted, changing different variables to determine their effects on the design of the CGSE. The main findings of this process are presented in this section.

Effect of changing the horizontal acceleration profile

Regardless of whether the modeled flight profile included high or low horizontal accelerations, the maximum possible flight time did not change greatly. Much more of the total impulse available in the CGSE was required to lift the hopper's lunar weight than to translate it horizontally, and nearly all of the successfully modeled flight profiles had lengths of 15 s or less because the hopper could not hold itself aloft for much longer than that. However, changing the horizontal accelerations did change the distance that could be covered in a hop. Since the time of flight was the limiting factor, the hopper was more likely to reach the target horizontal distance of 30 m with a higher acceleration applied for a shorter time than with a lower acceleration applied for a longer time.

Relationship between P_c and C_V

As the chamber pressure P_c was varied for different runs of the MATLAB model, a pattern became clear. If P_c was set low, higher mass flow rates were needed to achieve the thrust required to complete a given

flight profile. This meant that the propellant mass was depleted more quickly. By contrast, if P_c was set higher, mass flow rates could be lower, but there was more gas left over in the tanks when the tank pressure equalized with P_c and useful thrust production ceased. Thus, there did not seem to be a significant advantage to setting P_c at any particular point from the perspective of propellant usage. However, changing P_c did change the C_V required for the thruster solenoid valves and the regulator.

Maximum pressure rating and C_V were among the few specifications reliably provided by nearly all manufacturers for both valves and regulators, so they were the chief parameters by which comparisons between different models of components were made. Thus, it was essential to understand the relationship between these two variables. For the valves, a lower P_c meant that a higher C_V was required to allow the necessary mass flow for a given flight profile. However, for the regulator, the model suggested that a lower P_c also meant a lower C_V . Apparently, for the regulator, the higher pressure differential resulting from a lower P_c outweighed the effects of the higher required mass flow. An illustration of this relationship is presented in Table 4-1, which shows the maximum required C_V of both the thruster solenoid valves and the regulator for the flight profile plotted in Figure 4-3 run with several different settings of P_c, including the 500 psia setting for which results were described in detail in section 4.1.6.

Table 4-1. Maximum modeled C_V for example flight profile at several different chamber pressures.

P_c	Thruster Valve C_V	Regulator C_V
300 psia	0.48	0.48
400 psia	0.35	0.50
500 psia	0.27	0.61
600 psia	0.23	0.64

Different flight profiles resulted in different values for the C_V of the thruster valves and the regulator, but the basic relationship shown in Table 4-1 remained the same.

4.2 COTS Component Selection

The sense of the relationship between P_c and C_V developed with the MATLAB model was an essential input into the process of selecting thruster solenoid valves and a regulator. However, pressure and C_V were not the only attributes that were considered in component selection. For the solenoid valves,

response time was an important performance characteristic; as stated in section 3.1.4, the opening and closing times of the solenoid valves had to be on the order of tens of ms or better in order for the hopper to be controllable. For both the solenoid valves and the regulator, minimum mass was desired, as is true for most components on flying vehicles. Finally, cost and lead time of the components were also important considerations.

4.2.1 Thruster Solenoid Valves

In surveying available commercial off-the-shelf (COTS) flow control components, it became clear that there were several general classes of solenoid valves, each of which had benefits and drawbacks. One of these classes consisted of small valves marketed for process control in applications such as food or chemical processing, the manufacture of small components, plumbing within dishwashers and other appliances, etc. Most of these valves had fast response times on the order of ms, and the majority were fairly inexpensive and available for immediate shipping. However, the problem with this class of valves was that it was difficult to find any with both pressure and C_V ratings that would work for the TALARIS CGSE according to the results of the MATLAB model. There were many valves that had C_V values of 0.2 to 0.9, and even some with a C_V of 2.0 or higher, but most were only rated for pressures below 200 psia, with many only rated for a few tens of psia. There were also valves rated for higher pressures, up to 500 or even 1000 psia, but the C_V of these valves was very small, often only 0.06. Thus, most of the small process control valves could not handle both the pressure and flow rates required for the TALARIS CGSE.

Another class of solenoid valves was intended for much heavier applications, such as large hydraulic or pneumatic systems. It was possible to find valves in this class with both high C_V (many ranging between 0.4 and 2.0, with some outliers with a C_V up to 10 or higher) and high pressure ratings (from 500 to several thousand psia). However, there were two main problems with this class of valves. One was response time; because of their large orifices, many of these valves had opening and closing times on the order of hundreds of ms, with some as slow as full seconds. Secondly, in order to withstand both high pressures and high flow rates, the valves had to be very strong, so the valve bodies were very large and thick. This made the valves not only heavy (with masses of several kilograms each) but also geometrically large, and the TALARIS hopper would not be able to carry eight valves of the sizes generally found in this class.

A third class of solenoid valves made specifically for spacecraft propulsion systems was also considered. These valves had very good performance specifications: high C_V and high pressure ratings as well as very

fast response times on the order of ms. They were also lightweight, with masses of a few hundred grams. However, because they were space-rated hardware, these valves were prohibitively expensive. While solenoid valves from the other two classes tended to cost a few hundred or even just tens of dollars apiece, a single spacecraft solenoid valve might cost several thousand dollars. Also, there was generally a long lead time associated with the spacecraft valves – at least several weeks, or even longer for custom-made components. Thus, space-rated valves were not a viable option for the TALARIS CGSE.

With all of these tradeoffs, very few COTS solenoid valves were found that would be suitable for the CGSE. The valve finally selected was the Omega SV128, with the optional 24 Vdc coil.

Figure 4-5. Omega SV128 solenoid valve.

The SV128 was essentially a process control valve, although it was slightly larger than most. It was one of the only valves in its class to meet both the pressure and flow rate requirements of the TALARIS CGSE, with a maximum differential pressure of 1500 psi and a C_V of 0.76 [52]. This combination of parameters was higher than necessary for most planned flight profiles according to the MATLAB model (see Table 4-1), but no other candidate valves were found to have acceptable parameters closer to those suggested by the model. Furthermore, although the maximum pressure rating of the SV128 was high, there was no need to operate it at its limits; in fact, with the selection of the regulator described in section 4.2.2, the maximum differential pressure that the SV128 was expected to experience in the CGSE was only 600 psi.

The superior flow performance of the SV128 did come at the cost of a higher mass than most of the valves in its class, but at 0.5 kg, the SV128 was still considered usable. More importantly, to handle the higher pressure and flow rate, the SV128 was pilot-operated, whereas the majority of the small process control valves were direct-operated. In a direct-operated solenoid valve, the action of the solenoid

directly opens and closes the main valve orifice. This allows for a fast response time, but if the size of the orifice is large and the differential pressure across the valve is high, it can become impractical to install and power a solenoid strong enough to actuate the valve directly. By contrast, in a pilot-operated valve, the solenoid opens a smaller pilot orifice which then allows the upstream pressure of the fluid to help actuate the main orifice [53]. This method of actuation has the benefit of allowing a more reasonably sized solenoid to control stronger flows, but the process is more complex and thus takes longer to complete. For this reason, the SV128 had a somewhat slower response time than the other valves in its class. While other valves in the SV120 series which were direct-operated had opening and closing times of 4 to 15 ms, the SV128 was rated at 30 to 60 ms [52]. This was on the boundary of the acceptable range defined in the requirements in section 3.1.4, so it was deemed essential to focus on the time performance of the solenoid valve in component testing. However, the SV128 was relatively inexpensive and available for immediate shipping, and it was considered to be the best choice all around given the constraints of the TALARIS project.

4.2.2 Regulator

In selecting the regulator for the CGSE, the inlet pressure requirement of 4500 psia, as set by the maximum rated pressure of the flight tanks, narrowed the field of COTS components significantly. Among the remaining candidates, there were several models found to have a sufficiently high C_V , and using mass and cost as the chief criteria, the Tescom 44-1363-2122-408 was selected for the CGSE.

Figure 4-6. Tescom 44-1363-2122-408 regulator.

The 44-1363-2122-408 regulator had an inlet pressure rating of 4500 psig, and its outlet pressure range was 0-600 psig [54]. The C_V of the regulator was 2.0, which was substantially higher than any of the C_V values calculated by the MATLAB model, but because the SV128 solenoid valve had a large C_V as well, it was thought that the regulator should have as much flow capacity as possible. The mass of the regulator was slightly less than 3 kg, which was heavier than desired, but the 44-1363-2122-408 was actually one of the lightest options available for its flow characteristics. Its specifications also indicated that it had fairly good droop characteristics compared to similar models. Finally, the 44-1363-2122-408 came with a self-vent option, which meant that if the pressure on the low side of the regulator rose above the output setpoint, the regulator would automatically vent gas in a controlled fashion until the pressure dropped to its intended level. This was considered to be a good safety feature in addition to the other attractive attributes that led to the selection of the 44-1363-2122-408.

4.3 Nozzle Design

One final flow control element of the CGSE was not purchased as a COTS component, but rather designed and fabricated in-house. As mentioned before, a complete cold gas thruster assembly consists of not only a valve but also a nozzle, which expands and accelerates the gas to increase the amount of thrust achieved with it. The nozzles for the CGSE thrusters were designed under the assumptions of 1D isentropic flow, and they were fabricated in the MIT AeroAstro machine shop.

In order to size a nozzle, it is necessary to know the pressures at which the thruster will operate. Since ideal expansion was desired for the CGSE thrusters, and the TALARIS hopper was designed to operate near the ground on Earth, the desired nozzle exit pressure P_e was standard atmospheric pressure of 14.7 psia (0.101 MPa). As for chamber pressure P_c, the selection of the 44-1363-2122-408 regulator meant that it would be no higher than 600 psig, or 614.7 psia (4.24 MPa). The results of the MATLAB modeling, such as those presented in Table 4-1, suggested that since the SV128 solenoid valve had a relatively high C_V of 0.76, the required P_c might be less than 300 psia. However, because of uncertainty in the model, it was decided to perform initial CGSE testing over a range of pressures to determine the actual performance of the CGSE thruster as built. It was considered impractical to machine an individually optimized nozzle for every test pressure, so a single chamber pressure P_c of 425 psia was selected, approximately in the middle of the range of pressures for which testing was planned. This would allow for at least an initial approximation of the thrust levels that could be achieved with the CGSE thruster, and when a definite operational chamber pressure was selected based on these results, a full set of nozzles could be created for ideal expansion at that P_c using this same design and fabrication process.

If 1D isentropic flow is assumed, the pressure and Mach number of the gas at any point in a nozzle can be related to the stagnation or chamber pressure. Therefore:

$$\frac{P_c}{P_e} = \left(1 + \frac{\gamma-1}{2} M_e^2\right)^{\frac{\gamma}{\gamma-1}} \quad \textbf{(4-30)}$$

where M_e is the Mach number of the gas flow at the nozzle exit [27]. In the nozzle sizing calculations, γ was taken to be 1.40, the ideal gas value for nitrogen. With P_e at 14.7 psia and P_c at 425 psia, M_e was calculated to be 2.84.

Once M_e is known, the ratio of the nozzle exit area A_e to throat area A_t, commonly called the expansion ratio ε, can be calculated with the following equation [27]:

$$\varepsilon = \frac{A_e}{A_t} = \frac{1}{M_e}\sqrt{\left[\frac{2}{\gamma+1}\left(1 + \frac{\gamma-1}{2} M_e^2\right)\right]^{\frac{\gamma+1}{\gamma-1}}} \quad \textbf{(4-31)}$$

Using the value of 2.84 for M_e as calculated by equation (4-30), ε was found to be 3.65, but this did not specify actual dimensions for the CGSE nozzle. However, it was known that the nozzle throat should have the smallest diameter in the flow path through the entire CGSE in order for the gas flow to choke there. The smallest diameter upstream of the nozzle was 0.25 in., the diameter of the SV128 orifice. With that in mind, a nozzle throat diameter of 0.154 in. was selected because it was markedly smaller than the next smallest constriction and because it was the diameter of a #23 drill bit, which was readily available for use in machining the nozzle. Therefore, the nozzle exit diameter had to be 0.294 in. For a conical nozzle with a half-angle of 15°, this meant that the length of the diverging section of the nozzle would be 0.261 in. It was believed that these dimensions would result in a machinable nozzle without excessive mass, so they were accepted.

A drawing of the nozzle designed for the initial CGSE tests is shown in Figure 4-7.

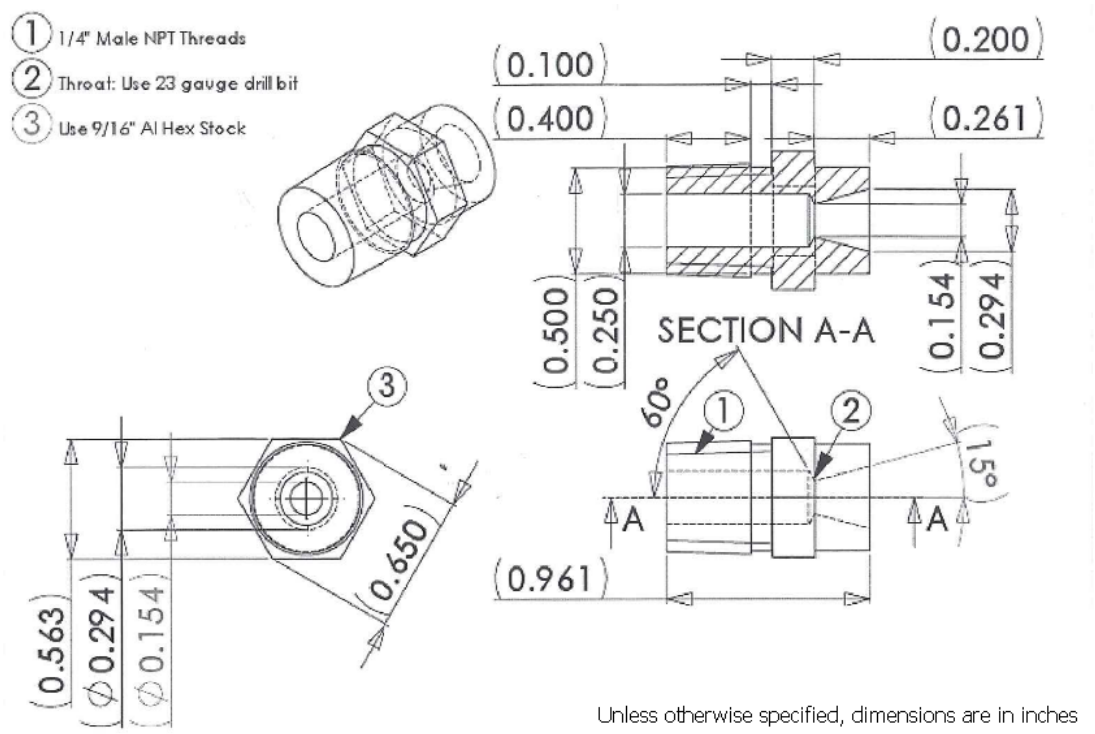

Figure 4-7. Drawing of CGSE nozzle [55].

The nozzle was machined from 9/16 in. aluminum hex stock in the MIT AeroAstro machine shop. The overall external length of the nozzle was 0.961 in.; this included 0.400 in. of ¼ in. male NPT threads[5] cut externally on the inlet end of the nozzle, as well as a hexagonal segment wide enough to be gripped firmly by a wrench, so that the nozzle could be screwed tightly into the outlet of the SV128 solenoid valve. The exact geometry of the converging side of a rocket nozzle is not particularly important, since the flow in this region is subsonic and can be easily turned without much pressure loss [28], so the inlet side of the nozzle was simply drilled out to an internal diameter of 0.25 in., and the angled tip of the drill bit was used to make a short tapering transition to the nozzle throat. (This did create a relatively small chamber-to-throat area ratio, which can cause a small additional pressure drop, but the estimated thrust loss that would result was less than 5% [28].)The diverging section of the nozzle was cut on a CNC lathe, using computer assistance to maintain the 15° half-angle of the cone.

While the nozzle was being designed and machined, the Tescom regulator and an Omega SV128 solenoid valve had been ordered. Once all of these flow control components had been obtained, testing could begin to verify that these components had been appropriately sized for the CGSE.

[5] In NPT sizing, the dimension given is a nominal pipe size, related to the inner diameter (ID) of the fitting.

5 Single-Stream Component Testing

An incremental program of testing for the TALARIS CGSE was designed with three major steps. First, the individual components of the system, which had been selected based on the results of the MATLAB model as well as other considerations, would be tested to verify that their performance met the requirements of the CGSE. Next, a full eight-thruster system would be constructed, and the verification tests would be repeated. The main purpose of this step would be to ensure that components which met requirements on their own would continue to do so even when they had to interact with a greater number of components in a complex system. For instance, the regulator would have to be capable of maintaining pressure on the low side of the CGSE with higher mass flows resulting from multiple thrusters firing at once. Finally, the eight-thruster system would be fully integrated with the rest of the TALARIS hopper and tested under actual flight conditions. In this phase, the idea was to move from verification to validation. It would be necessary to ensure that the CGSE interacted effectively with the other subsystems of the TALARIS hopper in order to produce the desired result: a controllable vehicle capable of completing a demonstration hop. To achieve this goal, it would be necessary to have not only properly functional hardware and software, but also skilled and practiced vehicle operators. Thus, additional goals throughout these three phases of testing were to gain operational experience and to develop procedures and protocols for optimal operation of the CGSE that also ensured the safety of every person involved with TALARIS.

For the first step in the three-step plan, a single Omega SV128 solenoid valve was purchased, in order to verify its suitability before proceeding with the purchase of enough valves to build a full eight-thruster flight system. A single aluminum nozzle was machined, designed for 425 psia chamber pressure as described in section 4.3. The Tescom 44-1363-2122-408 regulator was also purchased. Finally, tubing and fittings were purchased and assembled to connect the components together. Since this setup fed gas to a single thruster, as opposed to the multiple branching flow paths that would be needed in the full eight-thruster system, this first round of component tests was also referred to as single-stream testing.

5.1 Objectives

Several measurable outcomes of the single-stream component tests were defined. The first was to characterize the thrust output of a single CGSE thruster. The maximum amount of force that the thruster could produce when fed through the flight regulator would be determined. It was assumed that

this would be achieved with the regulator set at its maximum outlet pressure of 614.7 psia, and if this maximum thrust level was higher than desired, the optimum pressure level at which to set the regulator output would be determined.

A second characteristic to be measured in the single-stream tests was response time. As mentioned in section 4.2.1, the SV128's rating of 30 to 60 ms was on the borderline of acceptability for the CGSE. It was important to know where in that range the valve actually performed. Thus, measuring the time between the actuation signal and the point in time at which the thrust had reached its target level – full thrust for opening, or zero thrust for closing – was necessary.

The thrust and timing measurements were to be combined to determine impulse characteristics of the thruster, as shown in Figure 5-1 below.

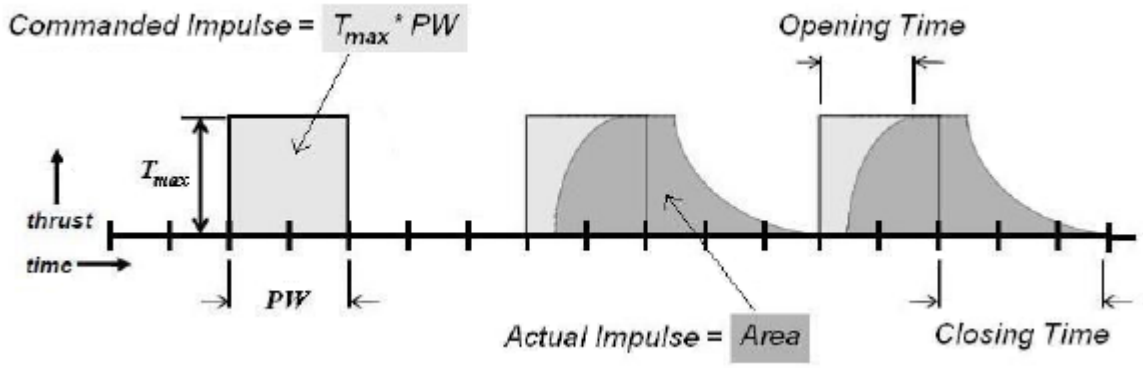

Figure 5-1. Measurements made in single-stream thruster characterization tests [38].

In particular, a major goal of the single-stream tests was to determine the minimum pulse width for which the actual measured impulse equaled the commanded impulse. This minimum pulse width, combined with the thrust level available at the final chosen chamber pressure setting, would thus determine the minimum impulse bit of the CGSE.

5.2 Testing Setup and Procedures

5.2.1 Instrumentation

Instrumentation was of paramount concern in the construction of the single-stream test apparatus; many different sensors were needed to record the data of interest. Pressure was measured immediately upstream of the solenoid valve as well as immediately downstream, before the gas entered the nozzle. To take these measurements, four-way cross fittings were attached to both the inlet and the outlet of

the solenoid valve, and a pressure transducer was placed on one arm of each of the crosses. A thermocouple was placed opposite each pressure transducer, with the goal of collecting temperature data to be used in validating the MATLAB model.

The entire thruster assembly – crosses, solenoid valve, and nozzle – was clamped onto a platform on wheel bearings. One end of the platform was attached to a single-axis load cell, which in turn was bolted onto a heavy stationary frame. Thus, the platform could not actually roll, but the wheel bearings minimized the lateral forces opposing the thruster. To further minimize external forces, the thruster was fed nitrogen through a flexible hose rather than a fixed, rigid line. The platform and thruster assembly are pictured in Figure 5-2 below.

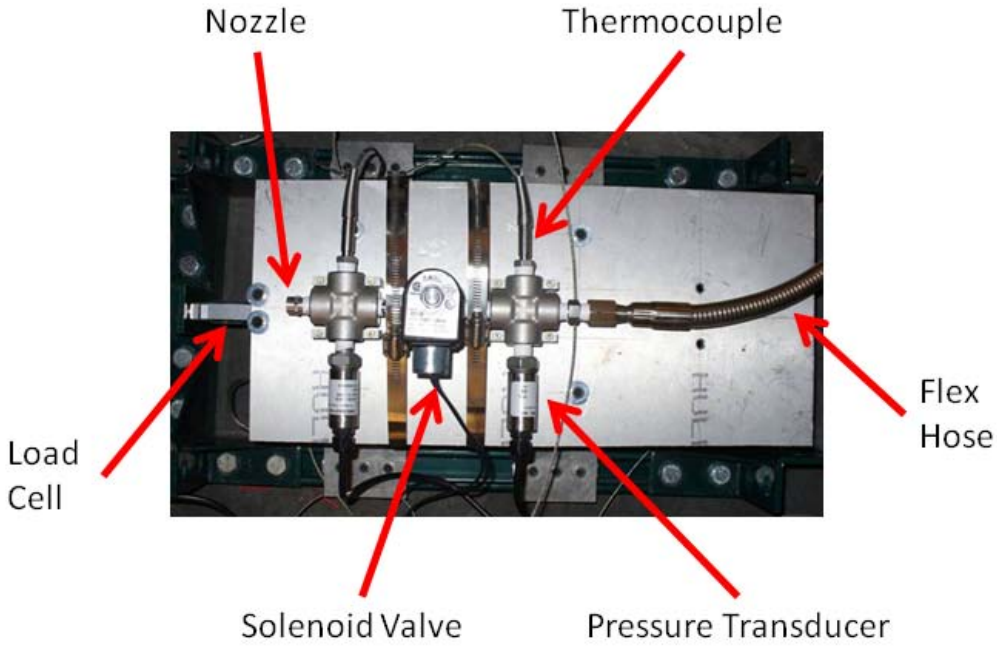

Figure 5-2. Thruster and instrumentation for single-stream characterization tests.

All of the sensors used in the single-stream tests output signals as analog voltages. These signals were collected with a National Instruments (NI) USB-6216 data acquisition device, or DAQ, which was also used to actuate the solenoid valve via a relay.[6] The DAQ was connected by USB cable to a laptop running NI's LabVIEW software, where sensor signals were converted to data in the units of the property being measured before being logged, and control signals were input. At first, opening and closing the valve

[6] The digital output used to control the solenoid valve and the analog input used to collect the sensor signals did not run on the same clock in the DAQ, so an extra wire was run from the digital output to a spare analog input pin in order to have a record of the command signal with the same timestamp as the rest of the sensors.

was controlled manually; later, modules were added to the software to allow for sequences of multiple pulses of predefined pulse width and spacing to be launched with a single command.

5.2.2 Laboratory Nitrogen Cylinders

Some early single-stream characterization tests were performed by feeding the instrumented thruster from a standard laboratory cylinder of compressed nitrogen, with the pressure controlled by the cylinder regulator. This was done for several reasons. First and foremost, the Tescom regulator meant for the flight system could not easily interface with a laboratory cylinder, so using it essentially required constructing the entire high side of the CGSE as shown in Figure 3-3. It was believed that it would be faster and simpler to run off of a laboratory gas cylinder instead of going through the process of filling up the CGSE flight tanks for every test, especially since even though most laboratory cylinders were filled to pressures less than 4500 psia, they could still hold more nitrogen than the flight tanks. Furthermore, it was known that the flow rates required by a single thruster solenoid valve were far below the full capacity of the flight regulator, so it was believed that single-stream testing would provide relatively little useful information about flight regulator performance, and that useful data could be collected about the CGSE thruster without using the flight regulator.

The first setup for collecting single-stream thruster data is shown in Figure 5-3.

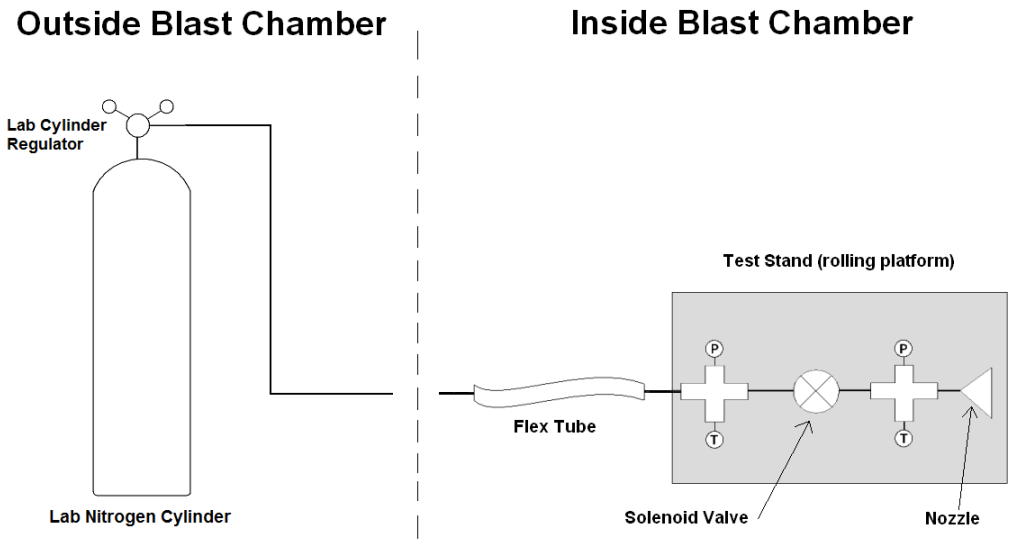

Figure 5-3. First configuration for single-stream characterization tests.

As indicated in Figure 5-3, initial CGSE tests were conducted inside a blast chamber until a better sense of safety around the CGSE was developed. In the first single-stream testing configuration, the laboratory nitrogen cylinder which fed the thruster was located outside the blast chamber, for easy access by operators of the CGSE. However, a very long tube of relatively small diameter (0.375 in. OD, 0.277 in. ID) was used to feed the gas to the thruster, and this made the system prone to choking as described in the next section (see especially Figure 5-7(a)). As a result, the setup was revised to remove the long feed tube. The laboratory nitrogen cylinder was moved inside the blast chamber, near enough to the instrumented thruster that the flex tube could be connected directly to the cylinder regulator as shown in Figure 5-4.

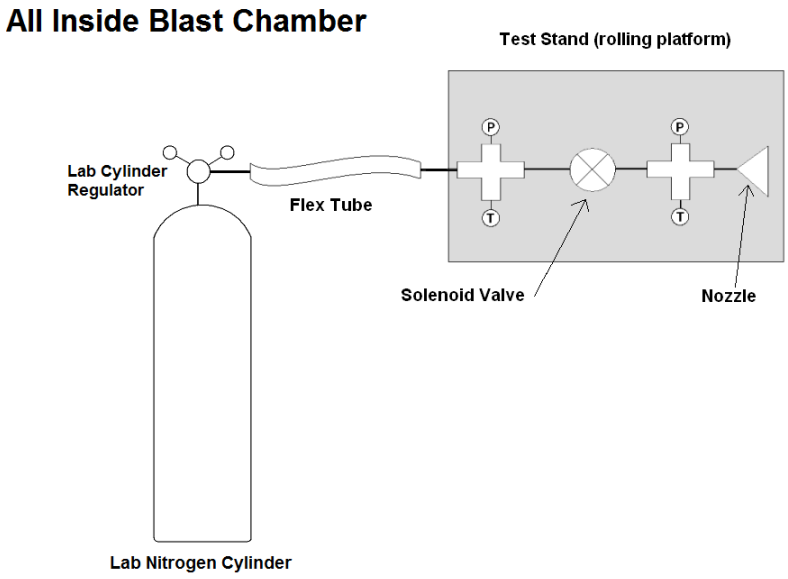

Figure 5-4. Second configuration for single-stream characterization tests.

The setup shown in Figure 5-4 did not produce the dramatic choking effects observed in the first configuration, but the thruster still did not perform as well as anticipated with this setup. The laboratory cylinder regulator had to be set to an output pressure of over 1000 psia to produce the 30 N of thrust required for the CGSE, and the flight regulator was not capable of having an output pressure that high. However, upon investigation, it was discovered that the laboratory cylinder regulator had a C_V of only 0.06, and it was hypothesized that the cylinder regulator could not provide sufficient mass flow for the thruster to perform at its full potential. Thus, the Tescom flight regulator would in fact have to be used to collect accurate data about the CGSE thruster performance.

5.2.3 High Side of CGSE

As mentioned previously, in order to use the flight regulator, it was necessary to construct the entire high side of the CGSE. As shown in Figure 3-3, this required fill and shutoff valves as well as tubing to connect them to the tanks and the flight regulator. Sizing of these valves and the tubing was based largely on practical assembly considerations; flow characteristics were also taken into account but without rigorous analysis. For instance, the tubing used to connect the two flight tanks to a single line to feed into the regulator needed to be rated for at least 4500 psia, but it should also be bendable, since this would allow for less mass and a wider range of possible angles as opposed to using elbow fittings for each turn in the tubing. These criteria led to the selection of 0.5 in. OD (0.334 in. ID) stainless steel tubing, which also interfaced well with the fittings in the necks of the tanks. Two lines of this tubing (one from each tank) came together at a three-way tee fitting, with the third branch leading to the flight regulator. Because this line to the regulator had to carry the flow from both tank lines, it was believed that its internal diameter should be larger than that of the two tank lines. Very few three-way tee fittings satisfied this, but the one selected had a 0.5 in. ID passage leading towards the regulator. This dimension was maintained by using 0.75 in. OD stainless steel tubing with 0.51 in. ID to complete a straight run to the regulator. The regulator had a main valve orifice of 0.375 in. [54], so it was believed that the tubing selections described would not restrict the gas flow more than the regulator itself would.

The selection of high-side tubing helped to guide the selection of the fill and shutoff valves. Both of these valves are manually-actuated ball valves. The flow path through a ball valve is a simple straight line, so when the valve is fully open, it has a high flow capacity with minimal effect on the flow through it [56]. The ball valves selected for the CGSE were manually actuated with a quarter-turn handle, since electric or pneumatic actuators that could be controlled remotely were too large and heavy. Since the shutoff valve was to be placed in line with the single high side feed path to the flight regulator, it was chosen to have an internal diameter of 0.5 in. to match the rest of the line. The fill valve was chosen from the same family of valves as the shutoff valve, but it did not need to be as large since it was not in the main flow path. In fact, it was considered advantageous to have a smaller fill valve, since that would limit the flow rate during filling and allow more time for conditions to settle in the flight tanks, and also provide the opportunity for some mass savings. Thus, the fill valve was selected to have a size of 0.25 in. It was placed on the branch of a three-way tee fitting which had a run of 0.5 in. ID along the main flow path to the regulator.

The high side of the CGSE built for single-stream characterization testing is pictured in Figure 5-5.

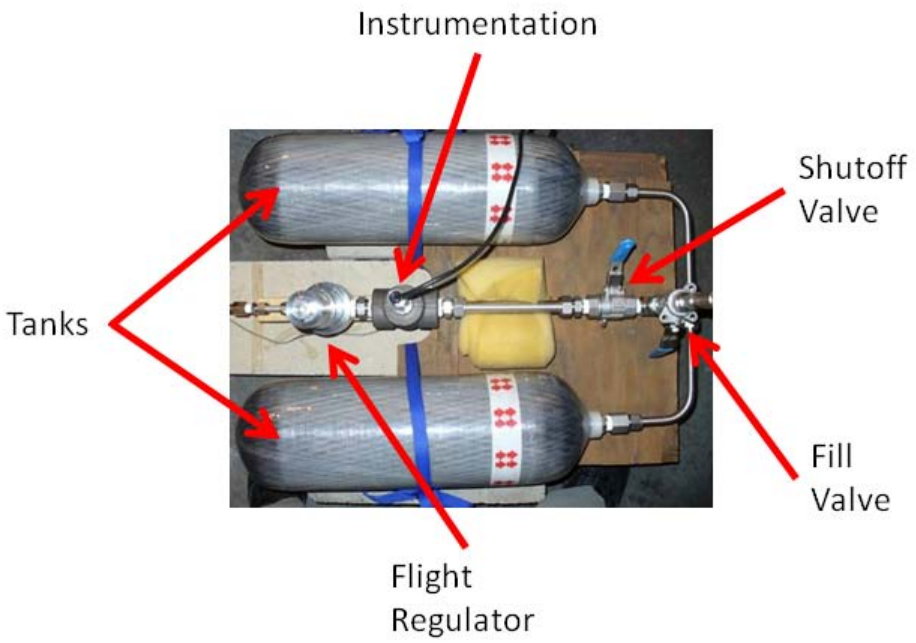

Figure 5-5. CGSE high side as constructed for single-stream characterization tests.

As shown in Figure 5-5, a four-way cross fitting with pressure and temperature sensors similar to those used at the inlet and outlet of the thruster solenoid valve was placed just before the inlet of the regulator to measure conditions on the high side throughout the single-stream tests.

With the construction of the high side, the third and final configuration for the single-stream characterization tests was as illustrated in Figure 5-6.

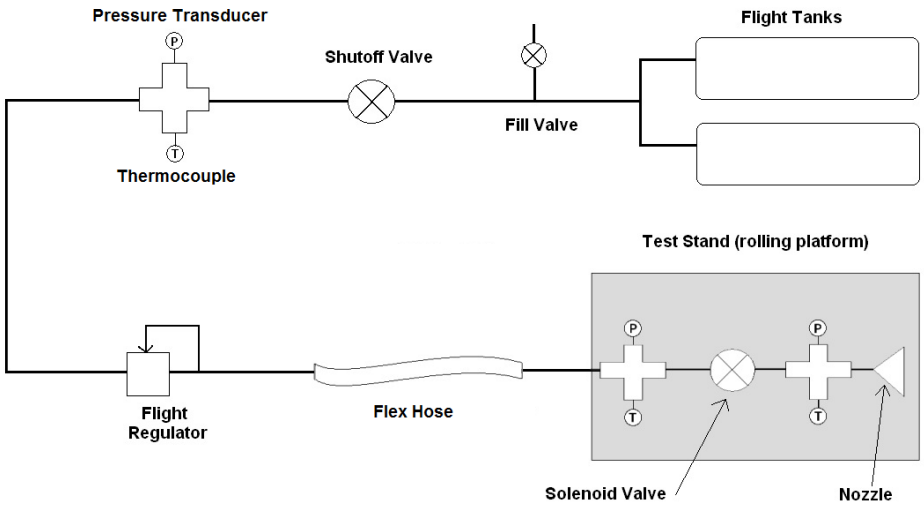

Figure 5-6. Third configuration for single-stream characterization tests [38].

5.3 Results

Originally, it was planned that pressure and temperature data collected in the single-stream tests would be used to validate parts of the MATLAB thermodynamics model. Unfortunately, although pressure data was acquired successfully, the thermocouples used in the single-stream tests were found to have a very slow response time, taking more than a full minute to register a change from 0°C to 100°C when moved from a glass of ice water to a glass of boiling water. This is probably due to the large fittings in which the thermocouples were mounted so that they could be assembled into the high-pressure CGSE, which greatly increased their thermal mass. As a result, accurate measurements of gas temperature could not be obtained, preventing validation of the model. However, sufficient pressure, force, and timing data were collected for full characterization of the single-stream thruster.

In Figure 5-7, thrust is plotted against two different pressure measurements from the single-stream characterization tests.

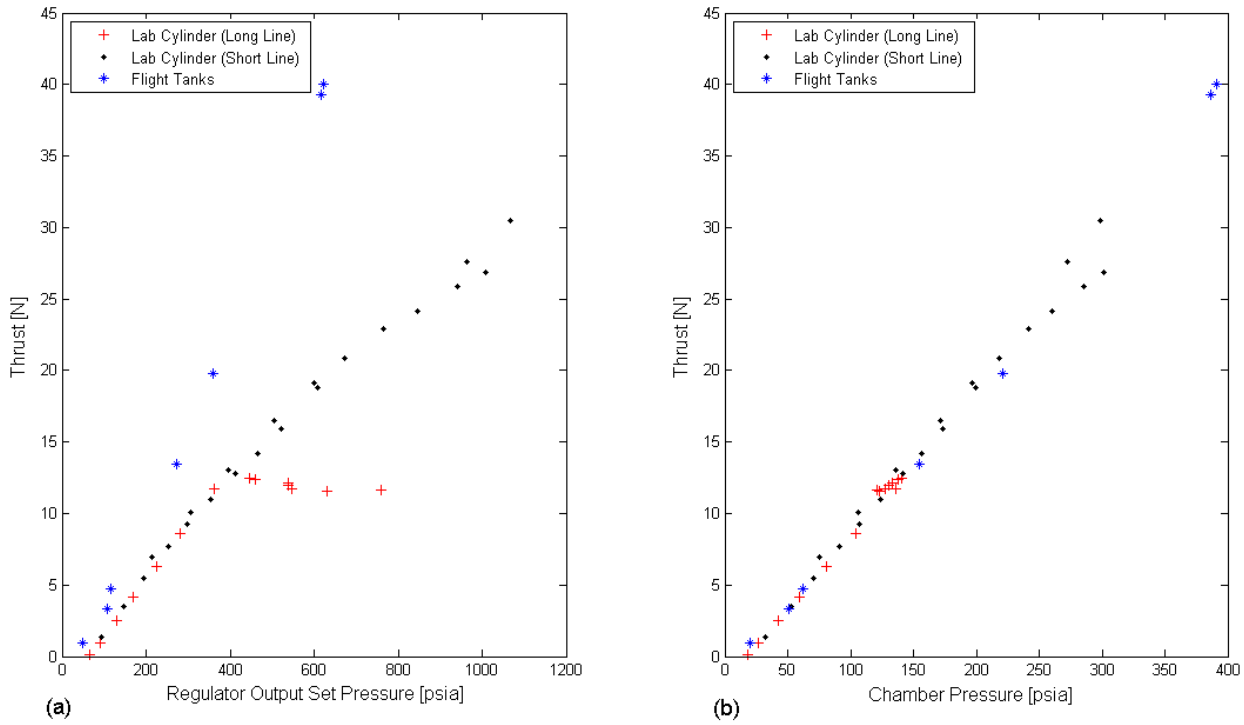

Figure 5-7. Plots of single-stream thruster output vs. pressure [38].
(a) Thrust vs. regulator output set pressure, measured upstream of shut solenoid valve just before thruster firing. (b) Thrust vs. chamber pressure, measured downstream of open solenoid valve but upstream of nozzle during thruster firing.

Figure 5-7 illustrates several aspects of the pressure-thrust relationship that were revealed through single-stream testing. First, there was an approximately linear relationship between thruster output and chamber pressure, as shown in Figure 5-7(b). The maximum thrust attained by the CGSE thruster in the single-stream tests was 40 N, produced with a chamber pressure of 392 psia, and obtained using the flight regulator and flight tanks as shown in the Figure 5-6 configuration. However, comparison between Figure 5-7(a) and Figure 5-7(b) shows that chamber pressure was not the same as the regulator output set pressure, as had been assumed in the MATLAB model. Rather, there were often significant pressure losses incurred, and these losses were strongly affected by feed line geometry. For instance, the choked flow that occurred in the first testing setup (illustrated in Figure 5-3) is clearly visible in Figure 5-7(a), where the Lab Cylinder (Long Line) points level off at approximately 12 N thrust for all regulator output set pressures above 400 psia. This did not occur for either of the other testing configurations. However, the flight tanks and regulator clearly had less pressure loss than the laboratory cylinder and regulator, since the flight setup was able to produce higher levels of thrust at the same regulator output set pressures as the laboratory cylinder setup, even without the long choked feed line. As mentioned before, it was believed that this was due to the low C_V of the laboratory cylinder regulator. This shows that multiple aspects of the feed line configuration including length, diameter, and number and angle of bends could affect the decrease in pressure from the regulator output set point to the pressure actually supplied to the thruster chamber, and thus the thrust that could be produced by the CGSE thruster.

In addition to thrust levels, the thruster solenoid valve response time characteristics were also investigated in the single-stream tests. By measuring the time elapsed between power being sent to the valve and thrust reaching full level, the opening time was determined to be approximately 30 ms. However, commands as short as 10 ms could trigger a thruster pulse. The closing time was also found to be about 30 ms between power to the valve turning off and thrust level falling to zero. These times were at the fast end of the range quoted in the valve specifications. However, the finite opening and closing times did have two major consequences. First, if pulses were commanded too closely together, the trailing tail of one pulse could interfere with the next pulse fired. Second, once the valve was opened, at least a minimum amount of impulse was delivered.

As mentioned in section 5.1, thrust level and timing characteristics for the thruster solenoid valve combined to define the impulse characteristics of the CGSE thruster. The objective was to find the minimum impulse bit. In order to accomplish this goal, a series of tests involving a range of pulse widths

were run with the apparatus set up to produce the maximum single-stream thrust of 40 N. The results of these tests are presented in Figure 5-8.

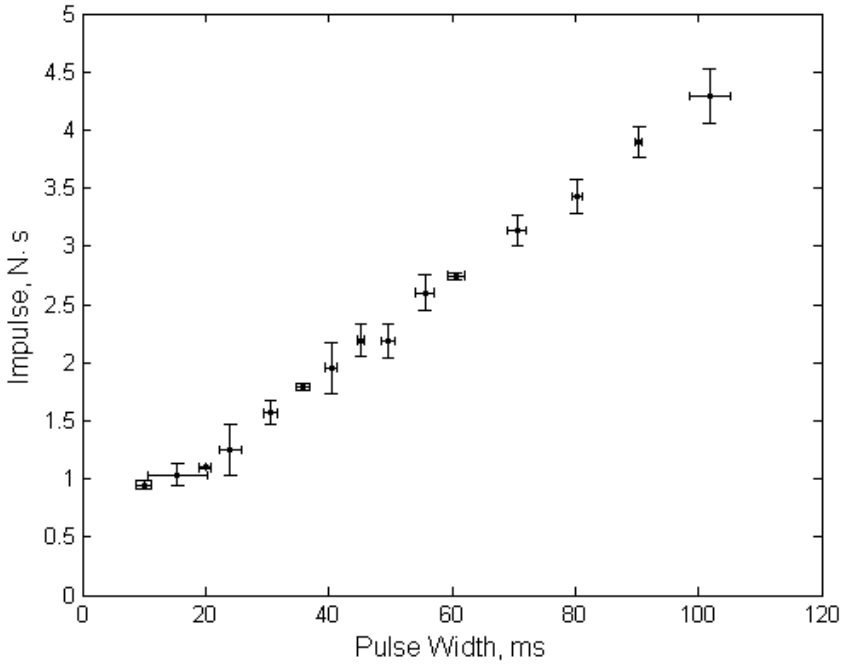

Figure 5-8. Impulse vs. pulse width for single-stream thruster producing 40 N maximum thrust [38].

In Figure 5-8, each point is the average of at least ten measurements, plotted at the commanded pulse width and average impulse measured. The error bars in the x direction represent the range of thruster actuation times actually measured, and the error bars in the y direction are the standard deviation of the impulse measurements. As shown in Figure 5-8, the relationship between impulse and pulse width was linear down to a commanded pulse width of approximately 20 ms, where the impulse bit then leveled off at approximately 1 N·s. However, for consistent control performance, the minimum impulse bit was defined by the minimum pulse width for which the actual measured impulse equaled the commanded impulse. Because of the relatively large uncertainties, the minimum pulse width was taken to be 40 ms, and the minimum impulse bit delivered by the single-stream thruster was 1.6 N·s.

Overall, the results of the single-stream component tests were very positive. The 40 N maximum thrust produced was at the high end of the design goal laid out in section 3.1.4, and it was believed that the 40 ms minimum pulse width and 1.6 N·s minimum impulse bit would allow the CGSE to control the TALARIS hopper. Thus, the flight regulator and thruster solenoid valves appeared to be sized correctly, and the next step was to ensure that they would operate satisfactorily in the full eight-thruster flight system.

6 Full Eight-Thruster Flight System

Due to the strong effect of feed line geometry on thruster performance observed in the single-stream component tests, it was decided to proceed not only to testing all eight CGSE thrusters at once, but to finalizing the configuration of the entire system. The only way to accurately characterize the performance of the CGSE was to test it as it would be flown.

6.1 Hardware Construction

The construction of the full flight configuration of the CGSE coincided with a general upgrade of the TALARIS structure. The first-generation TALARIS hopper constructed by the spring 2009 16.83/89 class (Figure 6-1) had an aluminum frame and a Plexiglas deck which was becoming too crowded as changes and additions were made to the avionics and the other vehicle subsystems.

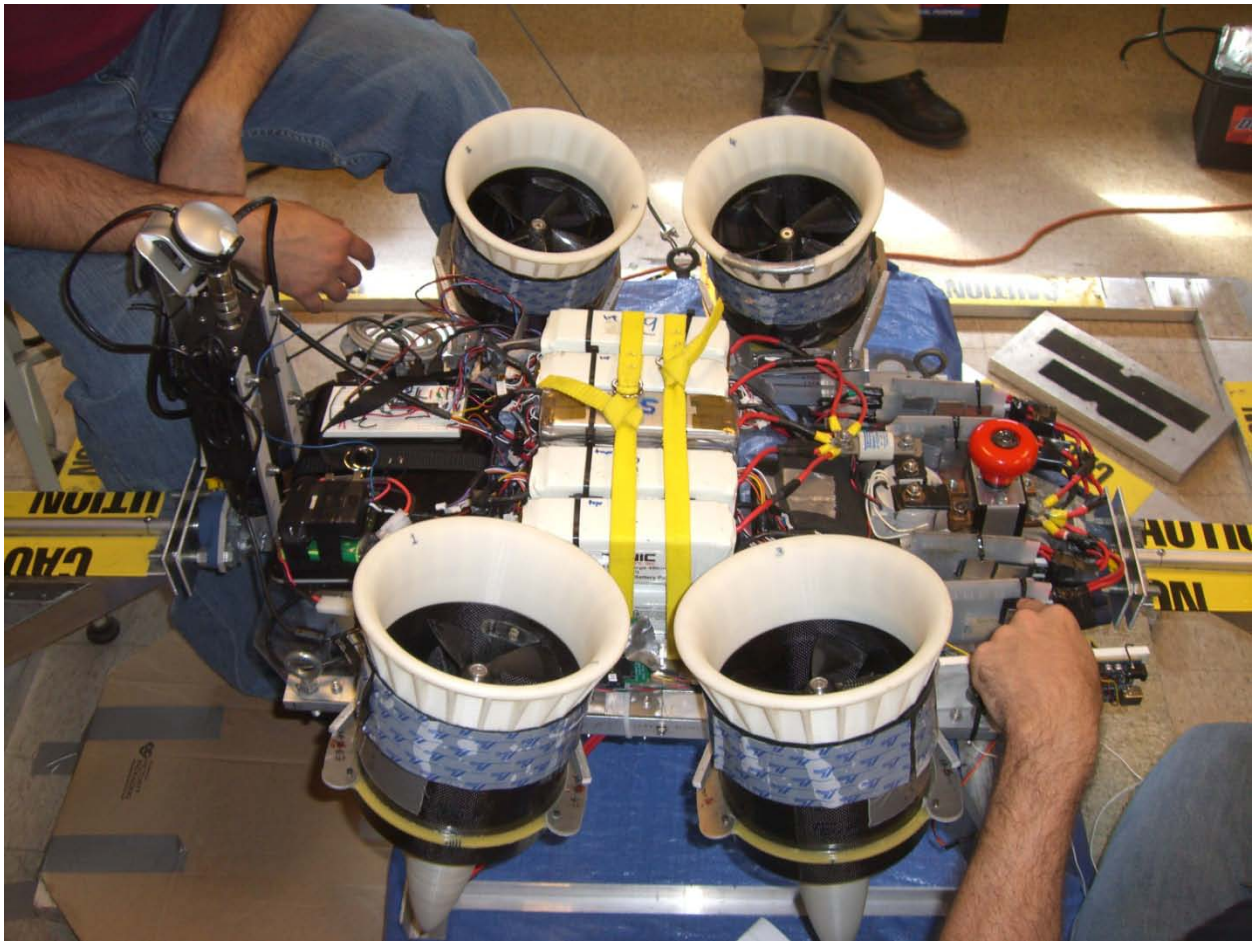

Figure 6-1. First-generation TALARIS vehicle (T-1), which did not include the CGSE.

In order to increase the amount of deck space available, the base structure of the second-generation TALARIS hopper (T-2) was constructed from carbon-fiber composite materials. This allowed for a deck with nearly twice the area at half the mass of the old T-1 structure. To simplify the organization of components on the structure, it was decided that the majority of the CGSE should be located beneath the deck. This left the top of the deck clear for the avionics and the electrical power system, including the large lithium polymer batteries that powered the EDFs, which had to be frequently removed for recharging. By contrast, it was expected that most of the CGSE components would not need frequent adjustments, so they could be placed in less-accessible locations.

The CGSE flight configuration was centered around the Tescom flight regulator. Because the regulator was so large and heavy, it was bolted securely to the underside of the deck near to the geometric center of the vehicle, in order to make it as easy as possible to balance the regulator with other components to keep the center of mass near the geometric center. This also made it possible to have feed line tubes of the same length with bends of the same angle leading to all of the CGSE thrusters, which made thruster performance more uniform. These feed lines were made from 0.5 in. OD (0.43 in. ID) tubing; because they were on the low side of the CGSE, they had a much lower required working pressure than the high side tubing, so it was possible to use aluminum tubing to save mass. Four feed lines were connected to a branching manifold made from brass three-way tee fittings attached to the regulator outlet; at the end of each feed line, one final three-way tee was placed to split the flow to one vertical and one horizontal thruster. These thruster pairs were placed as far apart as possible (approximately ±6.25 in. in the vehicle's Y-axis dimension) to allow for a long torque arm while avoiding interactions between EDF and CGSE exhaust.

The high side of the CGSE was constructed approximately as shown in Figure 5-5, though without the four-way instrumentation cross. Also, the tanks were brought slightly closer together and moved out of the plane of the regulator inlet and the main feed line leading up to it. This made the CGSE slightly more compact so that all components could fit on the new T-2 structure, but it did require that each of the two stainless steel tubes leading out of the tanks be reshaped with two plane-changing bends rather than the single in-plane 90° bend shown in Figure 5-5. Finally, the length of the main high side line to the regulator was adjusted such that with the regulator at its central position, the fill and shutoff valves were beneath the hopper deck but near the edge. This made them accessible for operations such as filling the flight tanks.

The flight configuration of the CGSE is shown in Figure 6-2 below.

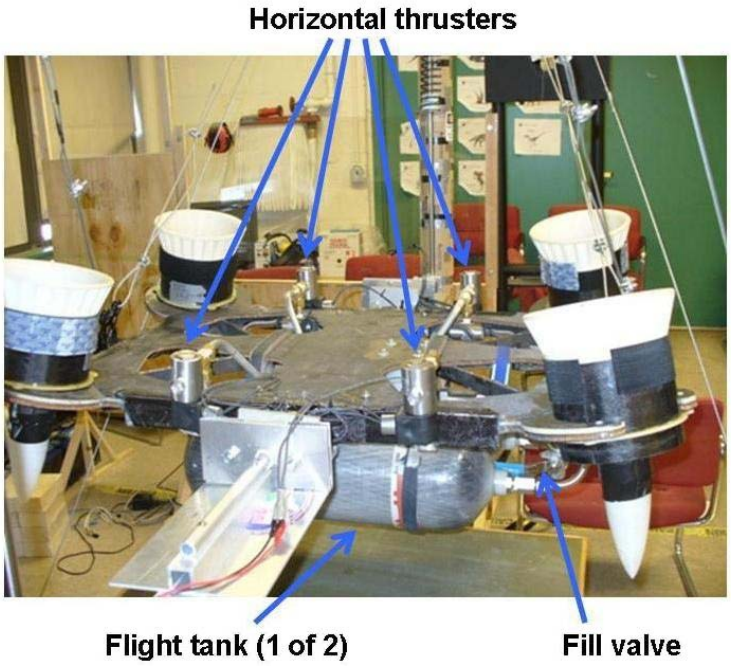

Figure 6-2. TALARIS CGSE assembled in flight configuration on second-generation (T-2) structure [38].

In Figure 6-2, the EDFs are mounted at the corners of the vehicle, but no other electronics are present. Still, most of the CGSE components are not visible because they are located beneath the deck and/or behind other components. They can be seen in Figure 6-3, which shows the T-2 structure upside down with the flight tanks removed.

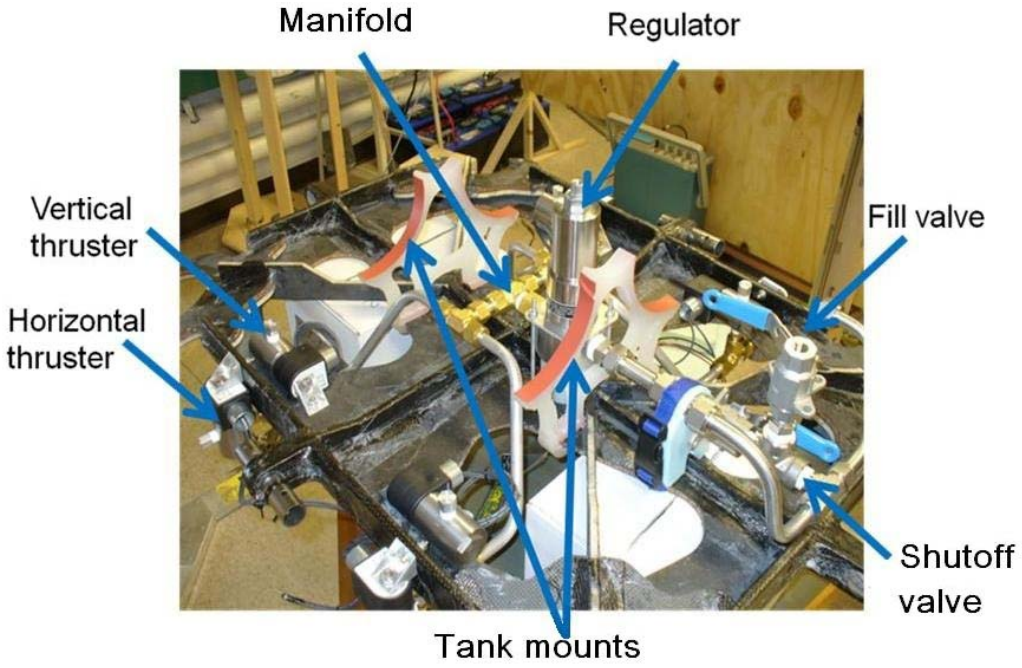

Figure 6-3. Underside of the CGSE assembly [38].

Figure 6-3 shows all three of the major ways in which the CGSE was attached to the TALARIS structure. The first was by the regulator, which was bolted to the underside of the deck as already mentioned. The second was by the tanks, which were positioned by being cradled in the tank mounts but had their weight supported by Kevlar straps encircling the deck. The third was by the thruster valves, which were each bolted through triangular brackets onto the structure to provide a solid path for the force produced by each thruster to transfer to the whole vehicle. All of the CGSE components were connected together rigidly and not able to move significantly relative to each other, so once one part of the CGSE was attached to the structure, the locations of the other components were also fixed.

In Figure 6-3, it can be seen that the thrusters in the full flight CGSE were not built with the instrumentation crosses that were present in the single-stream setup, and as already mentioned, the high side instrumentation cross was also removed. However, a method was developed for measuring the pressure on the high side by attaching a pressure sensor to the fill port and reopening the fill valve after fill operations had concluded. Furthermore, a pressure sensor was eventually added to the low side of the CGSE, opposite a rupture disk as indicated in the schematic in Figure 3-3. The ports for these two components were added by replacing two of the three-way tee fittings in the manifold with four-way crosses, but that change had not yet been made when the picture in Figure 6-3 was taken.

The rupture disk, like the self-vent feature on the Tescom flight regulator, was intended to release gas from the CGSE in the event of overpressurization of the low side. These two measures together provided increased safety through redundancy. However, while the regulator self-vent was adjustable and reusable, the rupture disk had a set burst pressure and was single-use only. For some tests, the rupture disk was replaced with a pop valve, which like the regulator self-vent was adjustable and reusable; however, the pop valve was heavier than the rupture disk, making the rupture disk a better choice for flight. The regulator self-vent was set to engage at a lower pressure than the burst pressure of the rupture disk (or opening pressure of the pop valve), which itself was still lower than the lowest working pressure rating of any of the other low-side components (approximately 1300 psia, set by the 0.5 in. OD aluminum tubing). Thus, the rupture disk or pop valve would only open if the regulator self-vent failed to relieve enough pressure, but if it did, it would still provide a relatively controlled and predictable release of gas well before any of the other components would be in danger of failing.

One final element of the CGSE flight system construction to consider was the thruster nozzles. As mentioned in section 4.3, the nozzle designed for a chamber pressure of 425 psia was originally intended only for temporary use until a final chamber pressure had been selected. However, the single-

stream tests revealed that changes in feed line geometry could make chamber pressure unpredictable, and the exact performance of the CGSE flight system could probably only be determined through testing. Furthermore, the 40 N maximum thrust observed in the single-stream tests was attained with a chamber pressure of 392 psia, which suggested that the optimal design chamber pressure for TALARIS might be near 425 psia. Therefore, the nozzles for the flight system were fabricated to the same specifications as the nozzle used in the single-stream tests, with the idea of revisiting the nozzle dimensions in future if the chamber pressures observed in the flight CGSE were significantly far from 425 psia.

6.2 Interfacing the CGSE to the TALARIS Flight Computer

In the single-stream tests, data collection and thruster control were performed with a USB DAQ, as described in section 5.2.1. For the full CGSE flight system on the TALARIS vehicle, these tasks were performed with an onboard computer which carried out all the tasks required for a hop, including collection of data from navigation sensors, execution of GNC algorithms, and control of the EDFs as well as the CGSE. The computer selected for this purpose was a single-board reconfigurable input/output (RIO) device, the NI sbRIO-9642. The RIO had both analog and digital input and output, as well as a real-time processor that ran the GNC algorithms needed for flight [57]. It communicated with a ground station computer which logged data and accepted commands from a human operator, similar to the way in which the USB DAQ interfaced with a laptop. However, rather than using a USB cable, the RIO was part of a local area network (LAN) that also included the ground station computer, with which it could communicate by means of an Ethernet cable for ground tests or wirelessly for flights.

The RIO had integrated 24 V digital output channels which were used to control the CGSE thruster solenoid valves. Originally, these channels were also used to provide power to the solenoid valves. Each channel could output 0.25 A of steady-state current [57], so four channels were tied together in parallel to deliver up to 1 A for each individual solenoid. The 24 Vdc coil for the SV128 solenoid valve had a rating of 10 W, which meant that it was expected to consume only 0.42 A. However, there were enough digital output channels available to use four for each valve, and providing extra margin for power was considered desirable, especially in case the SV128 solenoid valves might later be exchanged for larger, more powerful models.

The solenoid valves themselves did not require any special control circuitry. The SV128 was a normally-closed valve, so it opened when power was applied to it, and when power was off it was closed.

However, a solenoid is an inductor, which means that it resists changes in its state, and when power to a solenoid is cut, the coil generates a large back voltage. The RIO had no protection against this, so to prevent damage, the RIO manual suggested placing a flyback or snubber diode in parallel with each solenoid [57]. This would allow current flow from the low side of the solenoid back around to the high side in a path external to the RIO, so the induced voltage could dissipate without causing damage. Based on this recommendation, the circuit shown in Figure 6-4 was constructed for each of the eight thruster solenoid valves in the CGSE.

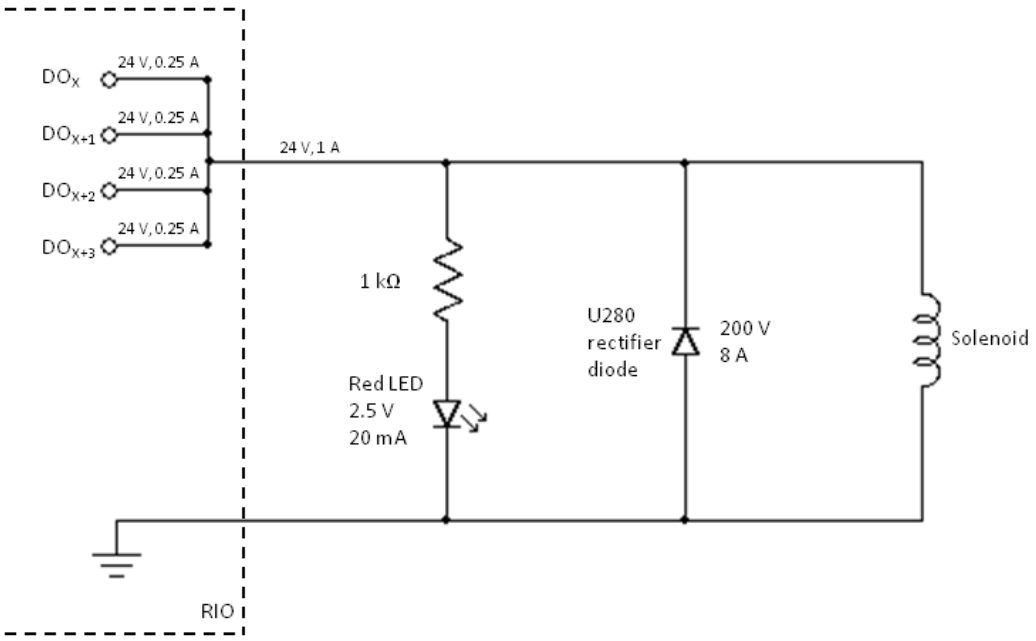

Figure 6-4. Original CGSE control circuit for a single thruster solenoid valve.

Figure 6-4 shows that an LED was also added in parallel with each solenoid such that it would light up to provide visual confirmation when the valve was open. This was an important safety feature which informed people of which direction the thrusters were firing, but it also became a useful tool for debugging.

One solenoid valve had a slight variant of the basic circuit shown in Figure 6-4. For safety reasons, it was considered necessary to have a way to vent gas from the CGSE remotely even if the RIO was not responding to commands. Therefore, an additional line was run from the low power battery (which provided power to all the avionics on the TALARIS hopper but not the EDFs) to one of the solenoid valves, with a switch controlled by a remote. This modification, known as the hardline dump capability, is illustrated in Figure 6-5.

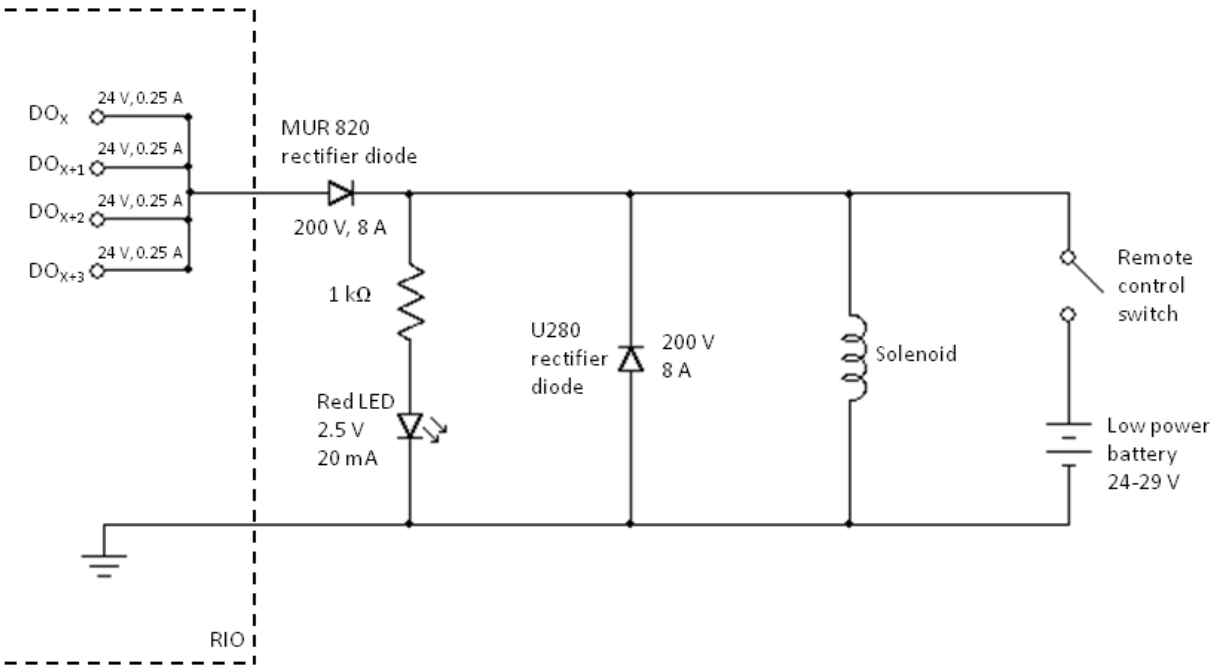

Figure 6-5. Original CGSE control circuit for thruster solenoid valve with hardline dump.

As shown in Figure 6-5, an additional diode was added to the thruster control circuit with the hardline dump. This was done to prevent backcharging of the RIO when the hardline dump was actuated.

The circuits shown in Figure 6-4 and Figure 6-5 were used to control the CGSE for the first few eight-thruster tests, but they were eventually found to have some undesirable attributes. This problem and its resolution are discussed in detail in section 6.3.4.

6.3 Static Characterization Testing

Once the CGSE flight system was fully assembled, characterization testing could begin. The first round of CGSE characterization was conducted on a static test stand. The general goal of this static testing was to verify that the acceptable performance observed in the single-stream tests would still be produced in the full eight-thruster flight system. To this end, two types of tests were performed. One was characterization of the amount of thrust produced by all of the thrusters both individually and in all combinations that might be fired during a hop. The second set of tests focused on pulsed thruster operation, to verify that the thruster valve opening and closing times were the same as those observed in the single-stream tests and to determine the minimum impulse bit provided by each individual thruster.

6.3.1 Thruster Identification

To track the performance of individual thrusters, an identification system involving letters and numbers was developed. The four corners of the TALARIS vehicle were designated as A, B, C, and D, and the thruster pair nearest to each corner was also identified by that letter. These pairs were called station pairs. Each individual thruster was also given an identifying number from 1 to 8. All vertical thrusters had odd numbers, and all horizontal thrusters had even numbers. Numbering proceeded around the vehicle from A to D, so the vertical thruster in station pair A was thruster 1, the horizontal thruster in station pair A was 2, the vertical B thruster was 3, the horizontal B thruster was 4, etc., as shown in Figure 6-6.

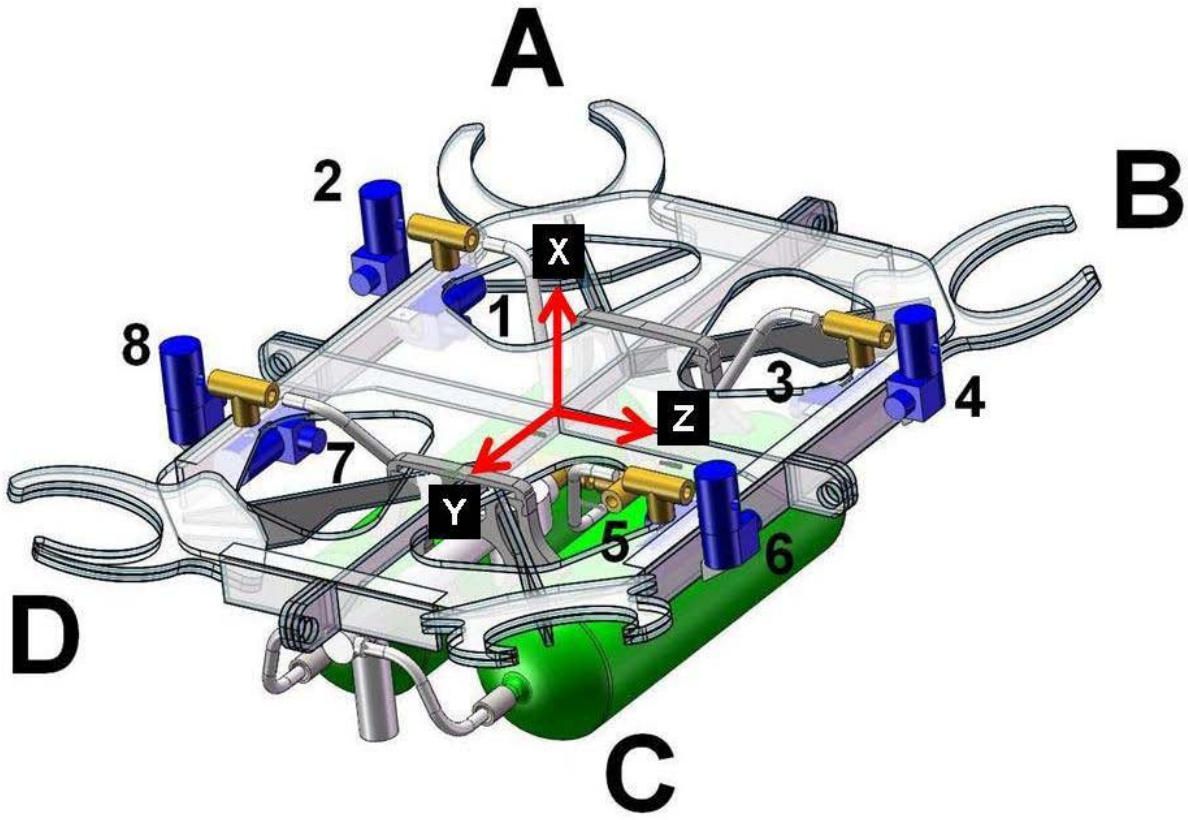

Figure 6-6. Identification of thrusters by number and letter. Body coordinate axes also shown [38].

6.3.2 Static Test Stand

CGSE thruster performance in the full flight system was measured using a 6-axis load cell, which could measure forces along three orthogonal axes as well as moments about those axes. For these measurements to be accurate, the TALARIS vehicle had to be entirely supported by the load cell with no

other constraints. This was difficult because the TALARIS vehicle was irregularly shaped and the load cell was comparatively small. Furthermore, for the easiest interpretation of the data produced, the load cell had to be placed beneath the center of the vehicle with its axes aligned with those of TALARIS. In order to fulfill all these requirements, a two-part static test stand was built from aluminum T-slot framing. One part was a cradle, which firmly supported TALARIS on four posts, each attached to a hard mount at the center of one of the sides of the vehicle. These four posts attached to crossbars which met at a central plate beneath the TALARIS hopper. The second part of the static test stand was a base with widespread legs which were weighted down to hold the stand stationary. These legs also came together at a central plate. Then, the 6-axis load cell was bolted to each of the two central plates, making it the only connection between the cradle and the base as shown in Figure 6-7.

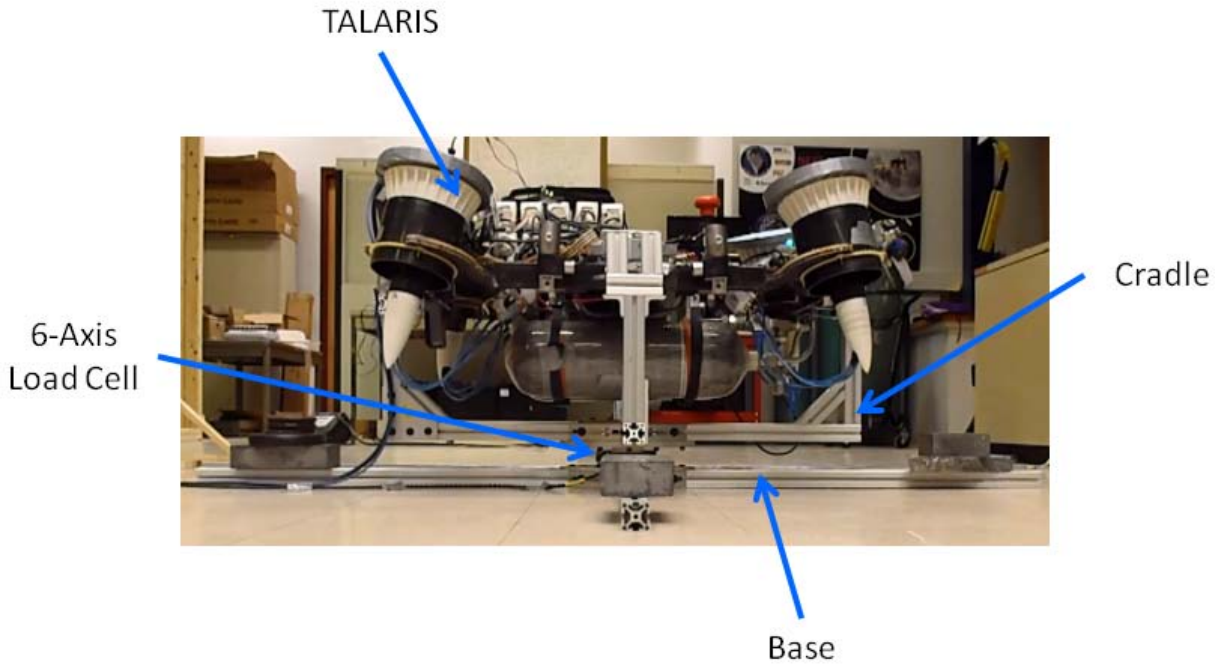

Figure 6-7. Static test stand for CGSE flight system characterization.

The measurement axes of the load cell were aligned with the TALARIS body coordinate axes shown in Figure 3-2 and Figure 6-6. Thus, without having to move or rotate the vehicle in any way, thrust measurements could be taken for all eight CGSE thrusters. Data from the load cell was collected with the RIO, so it had the same timestamps as the thruster commands, which was especially important in the analysis of the results of the pulsed operation tests.

6.3.3 Thrust Output Characterization

To make measurements of static thrust production, thrusters were fired for at least 1 s, with at least 2 s of space between successive firings. This allowed time for transient effects to damp out. The following thruster combinations were fired:

- Each individual thruster
- Each pair of vertical thrusters
- Each station pair
- Each set of three vertical thrusters
- All four vertical thrusters together
- All four vertical thrusters plus each individual horizontal thruster
- All four vertical thrusters plus a pair of horizontal thrusters firing to provide translational force (e.g. thrusters 2 and 8)
- All four vertical thrusters plus a pair of horizontal thrusters firing to provide a torque to roll the vehicle about its X axis (e.g. thrusters 2 and 6)

This set of combinations (31 in total) was chosen for several reasons. First, the single thruster firings allowed for the easiest comparison to the results of the single-stream tests. Second, the wide range of combinations tested allowed for some characterization of the effects on an individual thruster's performance depending on how many other thrusters fired with it. This was useful in planning future changes to the CGSE; for instance, it gave some sense of how performance might change if horizontal thrusters were added in the Y direction. Finally, the combinations most likely to be used in flight were tested. During a hop, the four vertical thrusters would essentially be firing constantly (though not at 100% duty cycle); the horizontal thrusters would only fire some of the time, and then most likely in pairs to translate or rotate the vehicle, although under certain conditions a single horizontal thruster might be fired to make a small attitude correction. All of these situations were included in the static testing plan.

As testing of the various planned combinations began, it became clear that one effect that had not been fully considered was the state of gas in the CGSE when a given thruster was fired. The starting pressure of the flight tanks did not seem to matter, as long as it was high enough for the regulator to maintain a given chamber pressure; if thruster 1 was the first thruster fired in a test, it produced approximately the same thrust level whether the tanks started at 4500 psia or 1500 psia. However, as a given test progressed and gas was depleted from the flight tanks, thruster output decreased even if no other

variables (such as number of thrusters firing) were changed. This effect is illustrated in Figure 6-8, for both a single horizontal thruster and the set of all four vertical thrusters.

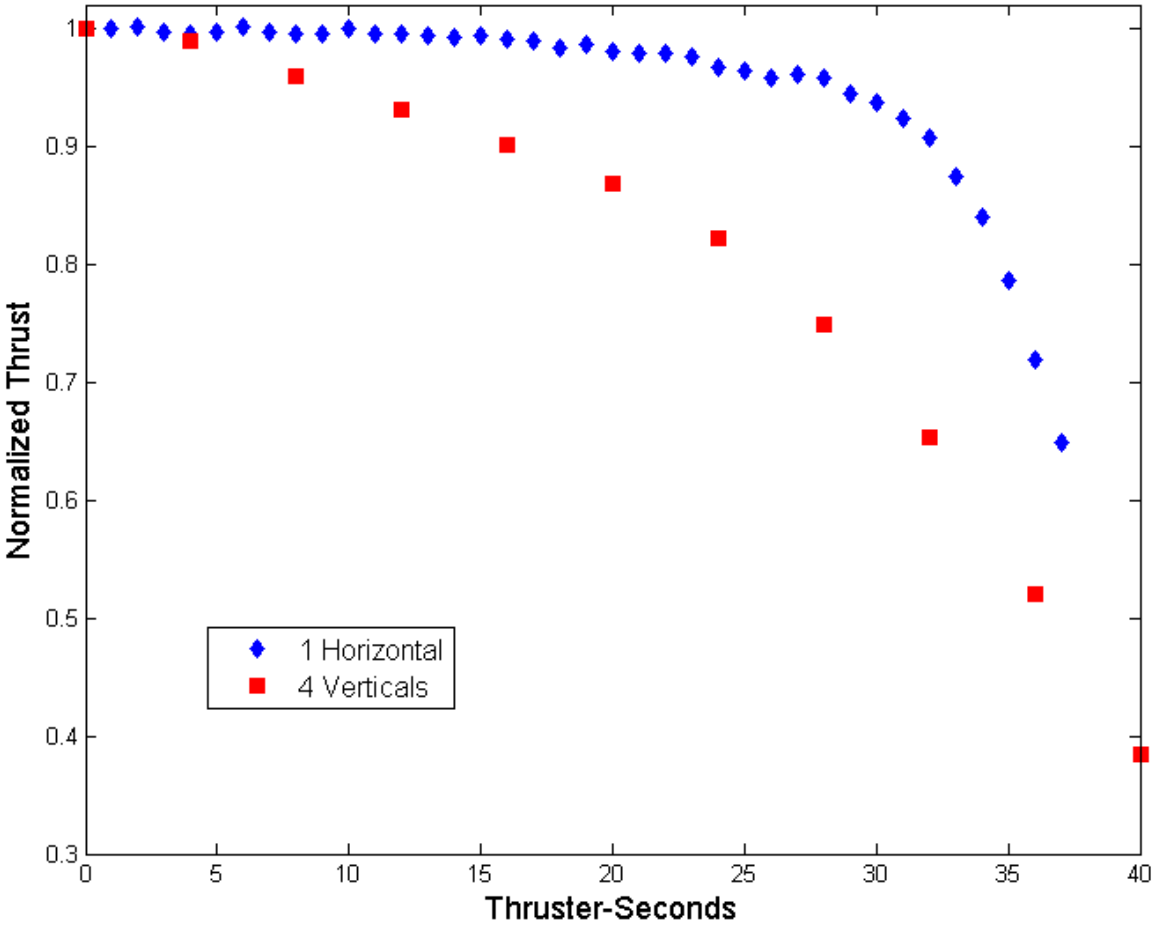

Figure 6-8. CGSE thrust decrease with gas usage.

In the tests from which this data was collected, the flight tanks were filled to approximately 4500 psia, and the thruster(s) were fired for 1 s pulses at 2 s intervals until the pressure across the flight regulator equalized at the output set pressure of approximately 600 psia. On the y axis, thrust is normalized against the thrust measured for the first firing in a given test. On the x axis, gas usage is tracked with the unit of thruster-seconds. One thruster firing for one second consumes one thruster-second of gas, one thruster firing for two seconds and two thrusters firing for one second both consume two thruster-seconds of gas, etc. Figure 6-8 shows that there is a general decrease in thrust level as gas is consumed from the tanks. This decrease appears to be more severe at an earlier stage for the four thrusters firing together; the single thruster firing alone maintained a higher percentage of its initial thrust for a longer period, although it did drop off sharply at the end of the test.

Thruster-seconds are something of a placeholder variable against which to plot this thrust loss; there are no thruster-second terms in the thrust equations (4-1), (4-3), (4-5) or (4-7). At first, it was thought that the observed thrust loss might be a temperature effect; the temperature of the nitrogen in the CGSE was known to decrease as the flight tanks were drained, since condensation and frost were observed to form on the outside of various CGSE pipes and fittings (although no direct measurements of nitrogen temperature were taken), and equation (4-8) does show that I_{sp} decreases with temperature. However, as equations (4-5) and (4-7) indicate, thrust is determined not only by I_{sp} but also by mass flow $\dot{m}$. As the temperature of the gas decreases, its density increases, so $\dot{m}$ increases (assuming that volumetric flow rate remains constant). Thus, the effects of temperature changes are canceled out, and thrust remains dependent on pressure. The low side pressure of the CGSE had been expected to remain constant throughout a test, as determined by the regulator output set point, and by extension thruster chamber pressure P_c would then remain constant (though lower than the regulator output set pressure due to losses in plumbing and pressure drop across the thruster valve, as illustrated by Figure 5-7). However, pressure measurements taken during the tests indicated that the CGSE low side pressure did in fact decrease over the course of a test, following trends nearly identical to those of the thrust decreases plotted in Figure 6-8. It was hypothesized that this might be a consequence of regulator droop; that is, as gas temperature decreased and $\dot{m}$ increased over the course of a test, the flight regulator was less able to maintain its output set pressure, so P_c decreased, and thrust output also decreased. This possibility is further discussed in section 7.2.

The phenomenon illustrated in Figure 6-8 had not been observed in the single-stream tests, in which the thrust (as well as the chamber pressure P_c) had always remained approximately constant for a given regulator output set pressure and plumbing configuration. Most likely, this happened because the single-stream tests all involved relatively low gas usage, so the thrust measurements were all taken in the regime where normalized thrust was nearly one for the single thruster. This was definitely not the case for full flight system testing, though, and it made it difficult to decouple the various effects that decreased thrust output. If vertical thrusters were first fired in pairs, and then later in the same test all fired together, the thrust levels would be higher for two separate pair firings added together than for all four vertical thrusters at once. However, it was not clear how much of the loss was due to increasing the number of thrusters firing simultaneously and how much was due to the decrease of thrust with gas usage.

One solution to this problem would have been to run a very extensive test battery so that a large number of data points could be grouped in different ways to isolate particular effects. For example, the type of test for which results were plotted in Figure 6-8 could be performed for each of the 31 thruster combinations of interest, to obtain initial thrust levels and individualized profiles of thrust decrease with gas usage for each combination. However, this would have been very resource-intensive in a number of ways. Each characterization test involved a range of tasks including preparing the TALARIS vehicle, filling the flight tanks, and making safety checks before thruster firing and data collection could occur; the process took two to four people at least one to two hours to complete. Then, the data had to be analyzed, which took additional people and time. The cost of propellant was also a concern. The nitrogen used in the CGSE was ordered in cylinders pressurized to 6000 psig at 70°F [58]; in terms of moles of gas, each cylinder held slightly more nitrogen than necessary to fill the flight tanks three times. However, a cylinder could only be used for filling if its pressure was higher than that of the flight tanks, and as the pressure of a cylinder was depleted it became more and more difficult to use the gas inside it. In order to mitigate this issue, several nitrogen cylinders were kept on hand and used for staged filling; the cylinder at lowest pressure would be used to fill the flight tanks as full as possible, after which the cylinder at next lowest pressure would be used to increase the flight tank pressure further, and so on until the fullest cylinder simply topped the flight tanks off. This practice enabled more efficient use of the nitrogen, but it also increased the amount of time needed for fill operations, and it was still never possible to use all of the nitrogen in a cylinder. With all these considerations, it was simply not practical to run 31 separate tests; even 8 to 10 tests required several weeks of work, which was a considerable amount of time given the accelerated schedule of the TALARIS project. Thus, each of the 31 combinations was fired at least once, but only a few representative selections of the combinations were repeated in a different order over several tests to try to identify the envelope within which the CGSE thrust levels varied.

Maximum thrust levels

Data from single-thruster firings at the very beginning of test sequences was used to determine the maximum thrust of each CGSE thruster, as presented in the following Table 6-1.

Table 6-1. Maximum thrust levels for individual CGSE thrusters.

Vertical Thruster #	Maximum Thrust [N]	Horizontal Thruster #	Maximum Thrust [N]
1	51.5 ± 2.5	2	57.9 ± 0.2
3	51.7 ± 3.2	4	56.7 ± 0.5
5	53.4 ± 2.0	6	57.4 ± 1.3
7	52.5 ± 2.2	8	57.0 ± 1.7

Each of the thrust values listed in Table 6-1 is an average of three tests, except for thruster 1, which had a clearly anomalous measurement in one of the tests and is therefore the average of only two tests. The uncertainty is the difference between the average and the actual thrust measurement furthest from it.

Table 6-1 shows that the CGSE thrusters in the full flight system significantly outperformed the single-stream thruster. This was unexpected; it had been anticipated that the branches and bends in the feed lines in the low side of the CGSE would result in greater pressure losses and thus lower thrust levels. However, there was actually much less pressure loss during single thruster firings in the flight system; with the flight regulator set at maximum output of approximately 620 psia, the low side pressure of the CGSE was measured at about 590 psia while firing single thrusters, much higher than the chamber pressure of 392 psia that had been attained with maximum regulator output in the single-stream tests. The reason for the higher pressure loss in the single-stream setup is unknown, but one possible cause was the flexible hose used between the regulator output and the thruster assembly. The hose had an inner diameter of 0.25 in., which was the same size as the thruster valve orifice, but the hose was relatively long with several bends which may have cumulatively created high pressure losses. Alternatively, the four-way instrumentation crosses on the thruster may have adversely affected the gas flow in the single-stream tests.

Table 6-1 also indicates that the horizontal thrusters outperformed the vertical thrusters by approximately 4 to 6 N. All thrusters were built with the same components, but because of the three-way tee fitting used to make the final split in the feed line to the two thrusters at a station pair, the gas flowing to the vertical thrusters had to make one more 90° turn than the gas flowing to the horizontal thrusters. It is believed that this caused enough additional loss to account for the lower performance of the vertical thrusters.

One of the characterization tests was run with the static test stand elevated so that the thrusters were at the operational altitude of the hopper, about 2 m above the ground. This was done to check for ground effect, which had been observed in EDF testing. However, the elevated CGSE test was inconclusive. Thrusters 5 and 7 produced about 2 or 3 N less thrust at the 2 m altitude than they had in the weaker of their two ground tests, but that was also the approximate spread between the weaker and stronger ground tests. Thruster 3 produced a thrust level at the 2 m altitude that fell between its two ground test results. And thruster 1 produced its anomalous thrust reading during the elevated test. The measured thrust from thruster 1 in the elevated test was 10 N less than any other single thruster output measurement in the averages presented in Table 6-1, which was a decrease of about 20%; nothing of that magnitude was seen in any other thruster firings during this set of tests. Therefore, that measurement was considered invalid and not used in the analysis of thruster performance. All of the horizontal thrusters produced very similar amounts of thrust at both altitudes. Time and other resources did not permit a repeat of the elevated test, so all non-anomalous test results were averaged together regardless of altitude, resulting in the larger uncertainty for the vertical thrusters shown in Table 6-1.

The maximum thrust levels presented in Table 6-1 were substantially higher than the original design goal of 35 to 40 N. These thrust levels could have been decreased by setting the flight regulator output to a lower pressure. However, the expected total mass of the TALARIS hopper had risen to 51 kg by the time characterization of the CGSE flight system was underway, and it was anticipated that the mass might increase even further.[7] Furthermore, as shown in Figure 6-8, a very large decrease from the initial thrust levels was expected by the end of a hop. Therefore, additional thrust margin was considered desirable, and the flight regulator was left at its maximum output set pressure of 620 psia.

Thruster directions

Single-thruster firings were also used to make a better determination of the direction in which each of the CGSE thrusters were pointing. Although each thruster was supposed to be parallel to one of the vehicle axes, the construction of the CGSE was imprecise, and each thruster had some degree of misalignment, as shown in Table 6-2.

[7] The mass of the TALARIS hopper did continue to rise, largely due to changes in the EDF system which required heavier wires and the addition of more lithium polymer batteries for power. At the time of writing this thesis, the estimated mass of the entire vehicle was approximately 60 kg.

Table 6-2. Thruster directions as unit vectors in TALARIS body coordinates.

Thruster	Intended Direction	Actual Direction
1	[1, 0, 0]	[0.9948, -0.0735, -0.0693]
2	[0, 0, 1]	[-0.0224, -0.0167, 0.9996]
3	[1, 0, 0]	[0.9921, -0.0508, 0.1146]
4	[0, 0, -1]	[0.0554, -0.0071, -0.9984]
5	[1, 0, 0]	[0.9936, 0.0093, 0.1128]
6	[0, 0, -1]	[0.0565, -0.0900, -0.9943]
7	[1, 0, 0]	[0.9917, 0.0766, -0.1035]
8	[0, 0, 1]	[-0.0276, -0.0040, 0.9996]

The actual thruster directions in Table 6-2 represent deviations of 1.6 to 7.4° from the nominal directions. In one sense, these were relatively small misalignments; although the maximum thrust levels in Table 6-1 were based on total thrust magnitude, the thrust levels in the primary intended thruster direction were less than 0.5 N lower. However, the effects of the misalignments were not quite negligible; some of the thrusters had components of thrust as high as 7 N orthogonal to the primary intended direction when producing maximum thrust. Thus, the actual thruster directions presented in Table 6-2 were taken into account in the GNC algorithms to ensure better control of TALARIS.

Characterizing decrease in thrust

As mentioned previously, it was difficult to fully decouple the various factors that decreased CGSE thrust from the maximum levels presented in Table 6-1. However, even with only a limited number of tests, a few major trends became clear. The gas usage effect illustrated in Figure 6-8 seemed to cause the largest overall decrease in thrust by the end of a test, but it had less of an impact early in tests, and to some extent it could be predicted with the curves plotted in Figure 6-8. Using these ideas to compare thrust levels with the gas usage effect minimized, the next greatest decrease in thrust was found to occur when station pairs fired. There was also some thrust loss when multiple thrusters that were not station pairs fired, and the amount of loss increased with the number of thrusters firing simultaneously, but this effect was generally outweighed by the other two reasons for decreasing thrust. Furthermore, the maximum number of non-station-pair CGSE thrusters that could fire simultaneously was four; if five

or more thrusters were firing together, at least two of them had to be part of a station pair, and those effects then coupled.

With the observations made in the characterization tests, a method was developed for estimating the thrust produced at any given point in a hop. The basic idea was to take the maximum thrust values in Table 6-1 as nominal thrust values and then adjust them with a set of correction factors based on what was going on in the hop. First, the thrust loss due to gas usage was estimated, generally by means of a curvefit. (The GNC algorithms were already modeling gas usage anyway to track mass loss of the vehicle and estimate time of flight remaining.) Then, this adjusted thrust was multiplied by a correction factor based on how many non-station-pair thrusters were firing: 0.99 for 2, 0.98 for 3, or 0.95 for 4. Finally, if a station pair of thrusters was firing, the adjusted thrust levels of those two thrusters were multiplied by a final correction factor of 0.94.

The method described above produced only very rough estimates of thrust, but it was difficult to be more precise given the restricted resources of the TALARIS project. It was hoped that this initial effort would be sufficient to allow for testing of some basic GNC algorithms and preliminary demonstrations of the capabilities of the TALARIS CGSE. At the time of writing this thesis, improving CGSE thrust characterization is an ongoing effort being pursued as scheduling permits, discussed in more detail in section 7.2.

6.3.4 Pulse Testing and CGSE Control Circuit Improvement

Based on the results of the single-stream tests (section 5.3), the controls engineers for the TALARIS project had proposed a 5 Hz control cycle for the CGSE. This meant that PWM would be performed on a 200 ms period, with pulses of thrust ranging in width from 40 to 160 ms, except for certain flight modes in which continuous thruster firing was enabled. The start time of a pulse could coincide with the start of a period, or it could be delayed to position the pulse later in the period, but there would always be a minimum off time of 40 ms between pulses from an individual thruster. Before this control scheme was used in flight, though, tests were performed on the static test stand to verify that the full CGSE flight system was capable of implementing it successfully. These tests involved commanded pulse widths ranging from 40 to 160 ms in 20 ms increments, each repeated for 10 PWM cycles for each individual thruster.

As the pulse tests began, it became clear that most of the CGSE thrusters were not able to perform the 5 Hz control cycle as desired. All of the measured pulse widths were longer than commanded, and several

of the thruster valves never shut completely for the longer pulses, so the 10 individual commanded pulses effectively ran together into one long pulse. Only one of the thrusters even came close to meeting the requirements of the 5 Hz control cycle, and it still produced a minimum pulse width of only about 60 ms reliably [59]. This performance was far worse than that observed for the single-stream thruster (as illustrated in Figure 5-8), so an investigation of the possible reasons for this was conducted.

At first, it was thought that the thruster valve used in the single-stream tests might have been unusually fast, and the results obtained with CGSE flight system simply represented a more typical distribution of valve timing performance. However, the response times observed in the first round of pulse testing of the CGSE flight system were far slower than the 30 to 60 ms range quoted in the SV128 specifications [52], so it was suspected that some external influence might be slowing the valves down. To examine this possibility in more detail, the valve response time was broken down into four timing metrics, as illustrated in Figure 6-9.

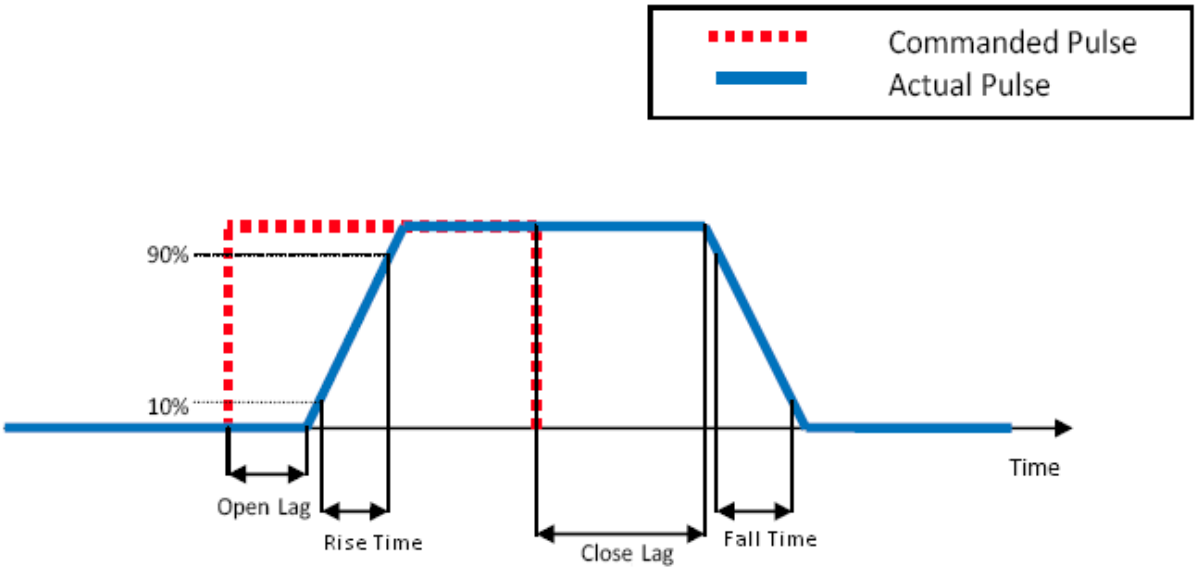

Figure 6-9. Valve timing metrics [59].

As shown in Figure 6-9, the opening time of the valve was separated into two parts: open lag, which was the time between the command to open the valve and the point at which the load cell began to measure an increase in thruster force, and rise time, which was defined as the time between measuring 10% and 90% of the steady-state force. Similarly, closing time was broken into close lag and 90-10% fall time. Measurements for these four timing metrics for each thruster valve as taken in the first round of CGSE flight system pulse testing are presented in Table 6-3.

Table 6-3. Valve timing metrics during first CGSE flight system pulse tests [59].

Valve Timing Metrics [ms]									
Thruster	**1**	**2**	**3**	**4**	**5**	**6**	**7**	**8**	**Avg.**
Open Lag	12	18	13	21	13	20	12	22	**16**
Rise Time	15	20	16	18	17	19	15	19	**17**
Close Lag	19	43	72	56	66	79	62	39	**54**
Fall Time	16	23	16	25	16	24	16	17	**19**

Table 6-3 reveals that the Close Lag time had by far the largest magnitude compared to all of the other valve timing metrics. Furthermore, thruster 1 was the one thruster performing close to acceptably, and it had a Close Lag time shorter than that of any of the other thrusters.[8] This suggested that most of the CGSE thrusters were staying open for an extended length of time after the closing signal had been sent. After conversations with Draper electrical engineers and re-examination of the CGSE control circuits depicted in Figure 6-4 and Figure 6-5, the flyback diode was targeted as the cause of this issue. In essence, the original control circuit allowed induced voltage to continue cycling power through the solenoid, holding the valve open for a significant length of time after the power/signal from the RIO was shut off. To eliminate this problem, a new CGSE control circuit was designed to quickly dissipate the induced voltage while still protecting the RIO.

In the new CGSE circuit, the 24 V output from the RIO was used as a control signal only, providing the gate voltage to a MOSFET. The thruster solenoids drew their power from the low power battery via a newly designed low power distribution board, and the MOSFET acted as a switch to close and open the circuit. Because the MOSFET could withstand large voltage spikes, it was possible to place a resistor in series with the flyback diode to cut down the current more rapidly when the solenoid was switched off.

The modified CGSE control circuit is shown in Figure 6-10.

[8] The reason for this was not fully understood. Thruster 1 had the hardline dump circuit variant, but there was no apparent reason why that would have improved the Close Lag time. It is possible that there was a poor electrical connection to the flyback diode, either increasing the resistance of that path or failing to close it at all. If so, the RIO might have been exposed to back voltage if not for the additional diode in series with the solenoid, in which case it was quite fortunate that this anomaly did occur in the circuit with the hardline dump modification.

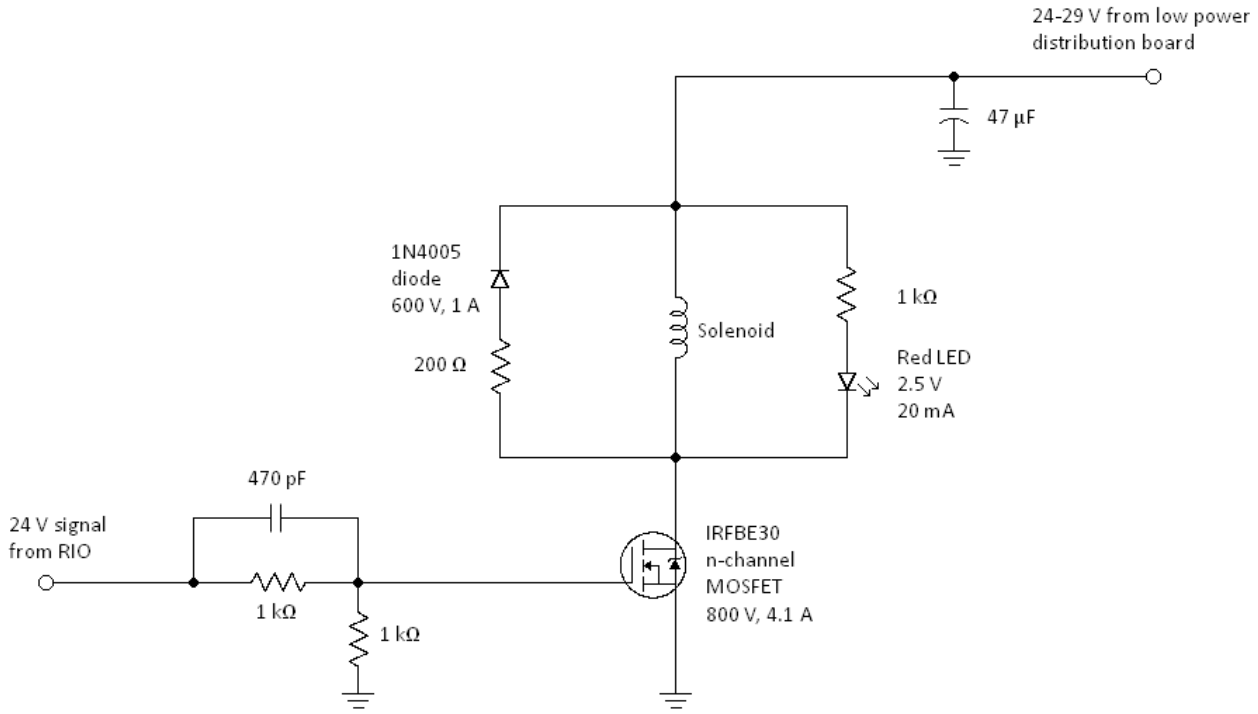

Figure 6-10. Redesigned CGSE control circuit for a single thruster solenoid valve.

The resistors and capacitor at the lower left of Figure 6-10 form a voltage divider; the MOSFET had a gate voltage input limit of 20 V, and the voltage divider cut the 24 V signal from the RIO down to 12 V so it would come in under this limit. The polarized capacitor at the upper right was put in the circuit to help smooth out transient effects in the power supply.

A hardline dump variant was also made for the new CGSE control circuit, as it was considered important to retain the ability to vent gas in the event of RIO failure. However, in the new circuit, the hardline dump closed an alternate path to ground, rather than closing a circuit with an alternate power supply as it had in the first CGSE control circuit. This is illustrated in Figure 6-11 below.

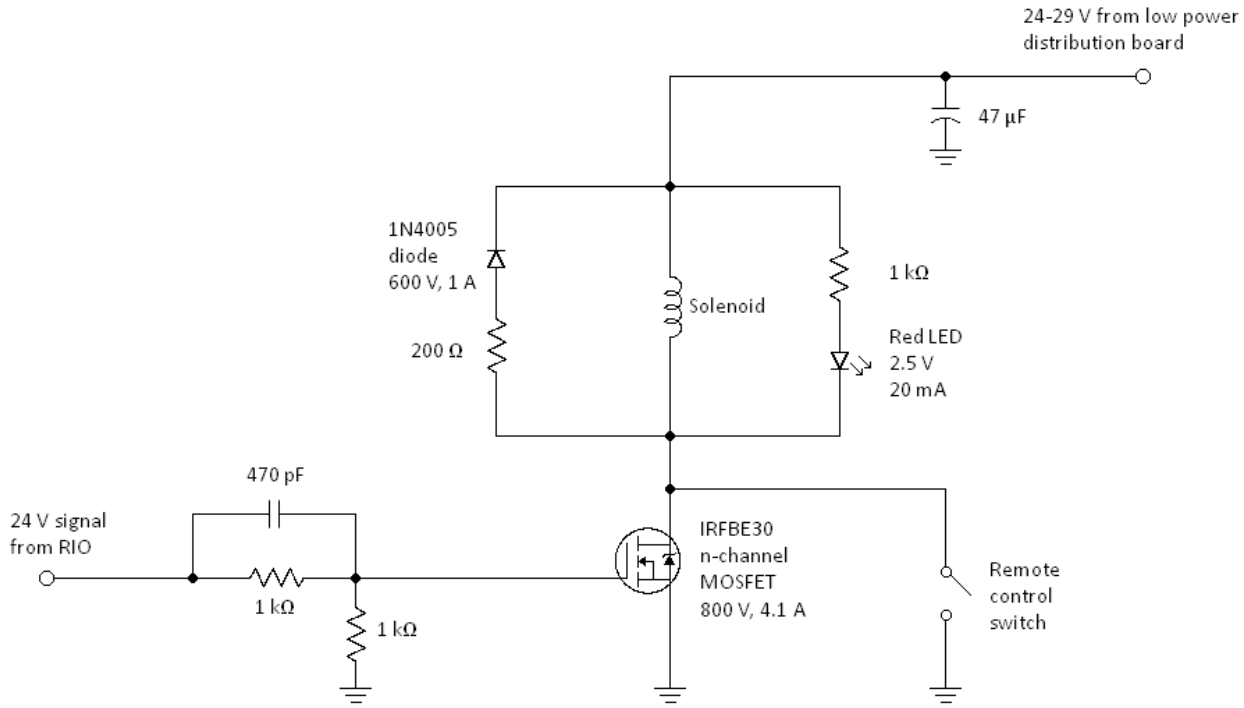

Figure 6-11. Redesigned CGSE control circuit for thruster solenoid valve with hardline dump.

The redesigned CGSE control circuit illustrated in Figure 6-10 and Figure 6-11 allowed for a great improvement in valve response time compared to the original circuit illustrated in Figure 6-4 and Figure 6-5. Table 6-4 demonstrates this with a comparison of the performance of several thruster valves controlled via the original and redesigned circuits.

Table 6-4. Comparison of valve timing metrics for original and redesigned CGSE control circuits.

Valve Timing Metrics [ms]						
Thruster	3 (old circuit)	3 (new circuit)	7 (old)	7 (new)	8 (old)	8 (new)
Open Lag	13	**11.2**	12	**12.5**	22	**11.2**
Rise Time	16	**8.4**	15	**9.3**	19	**9.6**
Close Lag	72	**26.0**	62	**25.2**	39	**26.0**
Fall Time	16	**10.8**	16	**9.9**	17	**14.3**

Table 6-4 shows that not only did the new CGSE control circuit shorten nearly all of the valve timing metrics, especially Close Lag, it also made them more consistent for different thrusters. With the redesigned control circuit, all eight CGSE thrusters had an opening time (sum of Open Lag and Rise Time) of about 20 ms and a closing time (sum of Close Lag and Fall Time) of about 35 ms, which was much

closer to the valve timing performance observed in the single-stream tests than anything that had been attained with the original CGSE control circuit in the flight system.

6.4 Controller Implementation

With the new CGSE control circuit, valve response times were fast enough to enable the proposed 5 Hz control cycle. However, commanded pulse widths had to be scaled down from the actual desired pulse width, and there was also an impulse centroid shift that had to be taken into account. These ideas are illustrated with the simplified example that follows.

Assume that there is a thruster valve with Open Lag of 10 ms and Close Lag of 25 ms. Assume further that when the valve is opened, thrust rises linearly from 0% to 100% over 10 ms, and when the valve is closed, thrust falls linearly from 100% to 0% over 10 ms. Thus, these transient rise and fall periods together produce impulse equivalent to that produced by the thruster at 100% for 10 ms, and the overall shape of a thruster pulse is a trapezoid.

If this imaginary simplified thruster were commanded on at 0 ms and off at 40 ms, it would actually produce a pulse longer than 40 ms. In fact, it would produce impulse equivalent to a 55 ms square pulse. Furthermore, while the ideal centroid for a 40 ms pulse started at 0 ms would be located at 20 ms, the centroid for the actual pulse produced by the thruster would be located at 42.5 ms. Figure 6-12 illustrates these differences between the commanded and actual thruster pulses.

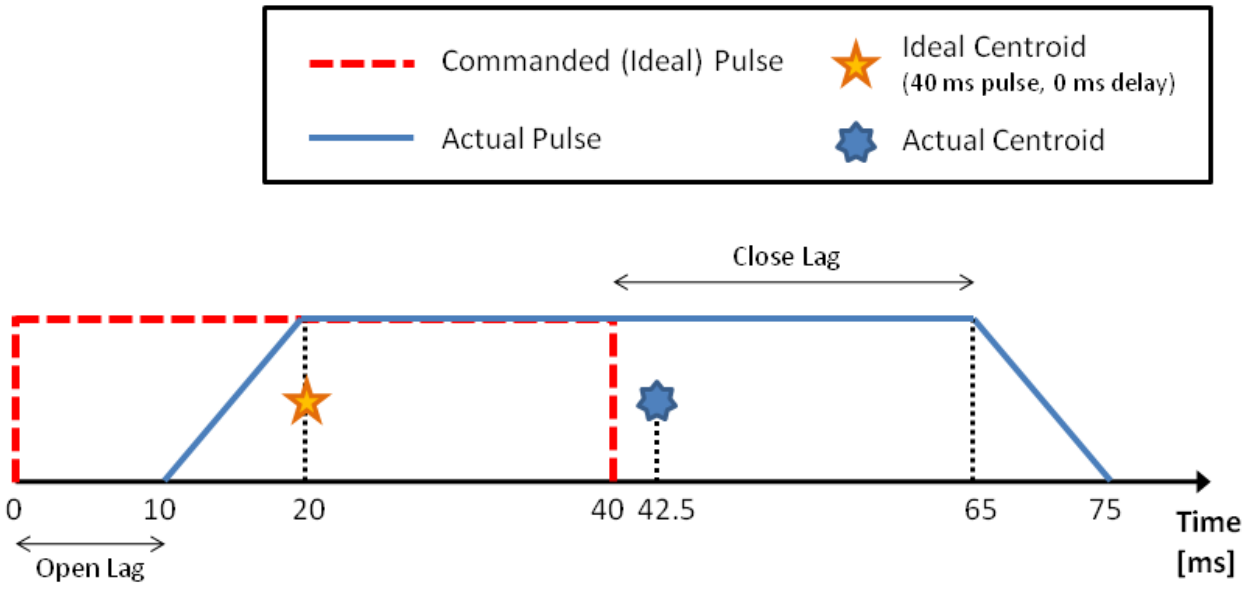

Figure 6-12. Simplified diagram of a commanded 40 ms thruster pulse and its actual results.

The imaginary simplified thruster can actually produce the amount of impulse equivalent to a 40 ms square pulse if it is given a commanded pulse of only 25 ms. However, as shown in Figure 6-13, the centroid of the actual pulse is still shifted, although now it is only located 15 ms later than the ideal centroid. It is not possible to remove this centroid shift, but with sufficient knowledge of the thruster timing characteristics, the location of the shifted centroid can be predicted.

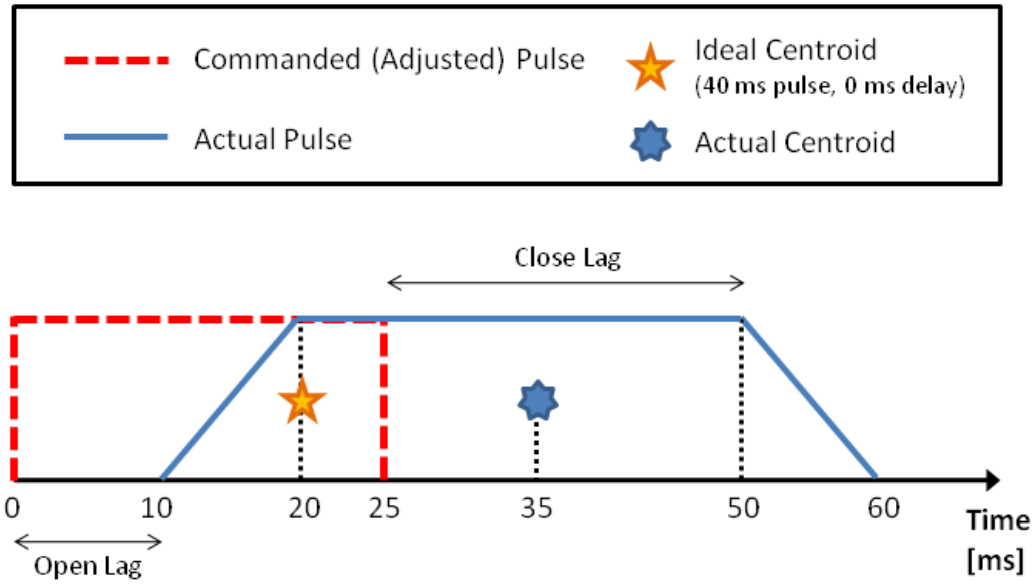

Figure 6-13. Simplified diagram of adjusted command to produce impulse of a 40 ms square pulse.

Although the actual CGSE thrusters did not have linear rise and fall characteristics, and their timing metrics all varied slightly from those assumed for the simplified thruster, the basic ideas illustrated in Figure 6-12 and Figure 6-13 still applied. By scaling down commanded pulses and predicting centroid shifts, impulse bits equivalent to 40 to 160 ms square pulses could be delivered on a period of 200 ms, and the 5 Hz control cycle was considered to be feasible. However, this was not a very fast control cycle; at 5 pulses per second and an estimated flight time of 15 s, each thruster could only produce 75 pulses during a hop, which suggested that flight profiles would not be very smooth. Also, there were additional difficulties created by the decrease in thrust magnitude with gas usage. If this decrease could be predicted, pulse width commands could be gradually increased to keep the produced impulse bits constant. The decrease was only roughly characterized, though, and there was a chance that by the end of a hop, the thrust would fall so low that the controller would saturate. Thus, as flight testing and the validation of the CGSE system began, the possibility of having to perform further verification testing was also kept in mind.

7 Ongoing and Future Work

There are three main thrusts of ongoing and future work for the TALARIS CGSE. The first is validation testing of the CGSE, which couples further hardware testing with tests of GNC algorithms. The second is more complete characterization of the existing CGSE system's capabilities as well as the development of best practices for its operation. The third is making changes to improve the TALARIS spacecraft emulator propulsion system. This work could range in scope from relatively small changes, like swapping out parts in the CGSE, to a full redesign of the system to utilize hydrogen peroxide as a monopropellant.

7.1 Validation Testing

The single-stream component tests as well as the static characterization tests of the CGSE flight system had all been performed for verification; that is, to ensure that the CGSE met the derived technical performance requirements laid out in section 3.1.4. The next step was to check that these requirements added up to a system that performed the original top-level goals for which it was designed, and the way to accomplish this was through validation testing. As the NASA Systems Engineering Handbook says, "Validation testing is conducted under realistic conditions (or simulated conditions) on any end product to determine the effectiveness and suitability of the product for use in mission operations by typical users and to evaluate the results of such tests" [60].

For the TALARIS CGSE, validation means proving that it can propel and control the vehicle through all phases of a hover hop. However, it would be a very large leap to go directly from static characterization testing to unrestrained free flight, and due to its limited budget and rigorous safety constraints, the TALARIS project cannot tolerate a crash or other destructive failure. Thus, an incremental validation testing program was developed. It was planned that in the first few tests, the hopper would have some of its degrees of freedom (DOFs) restricted so that it could only move in certain ways. Closed-loop CGSE control could progressively be applied to more and more degrees of freedom, with a greater chance of catching any major problems early in a more controlled environment, until enough confidence had been developed in both the hardware and the software to permit 6-DOF free flight hopping. The execution of this plan is in progress at the time of writing this thesis.

7.1.1 Horizontal Traverse and Roll Testing

When validation testing for the TALARIS CGSE began, the EDF weight-relief propulsion system was being upgraded and was not available for flight. Thus, the first CGSE validation tests focused on the horizontal

traverse phase of a hop and involved only the horizontal thrusters. For the very earliest tests, the two parts of the static test stand shown in Figure 6-7 were separated from the load cell, and wheels were bolted onto the bottom of the cradle. This formed a sort of cart into which the TALARIS hopper could be locked for 1-DOF horizontal testing, as shown in Figure 7-1.

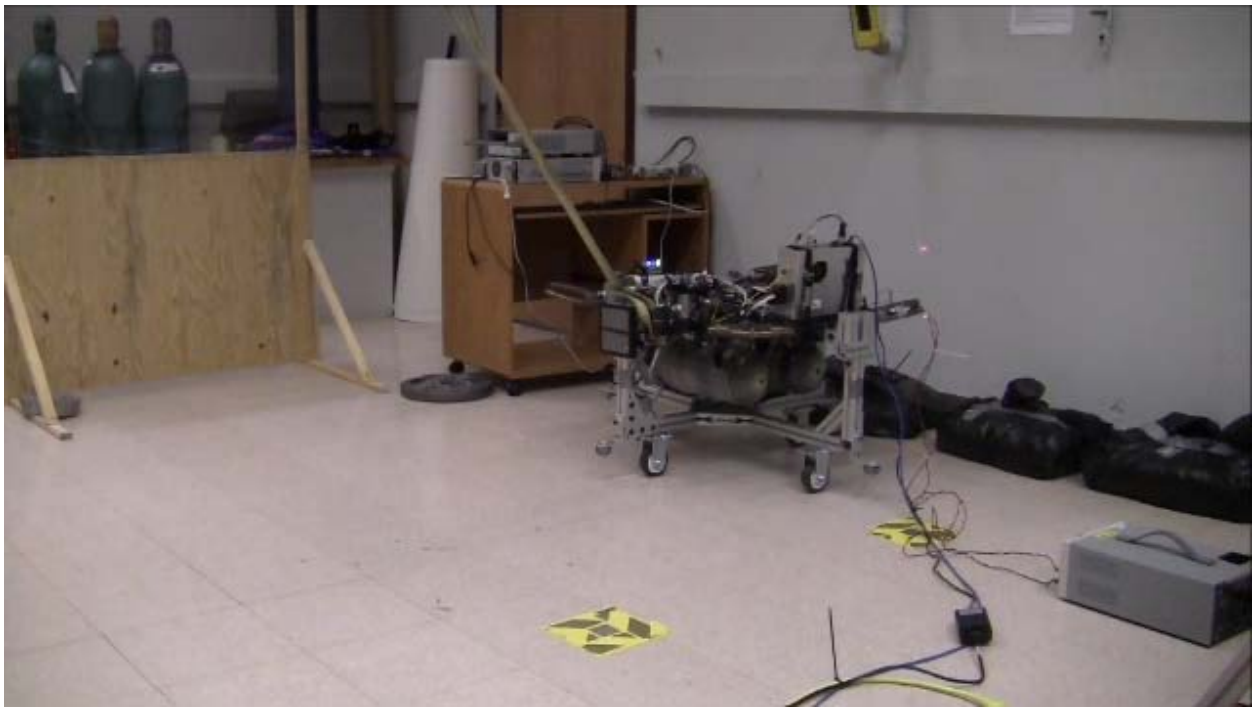

Figure 7-1. CGSE 1-DOF horizontal traverse testing on wheels.

By firing its horizontal thrusters, the TALARIS hopper was free to roll back and forth across the floor parallel to the hopper's Z axis, but it could not move in any other dimensions. However, it was soon found that there was a great deal of friction in the wheels, so the cart was not providing an accurate simulation of the transit phase of a hop. To reduce friction with the floor, the wheels were replaced with an air bearing of the sort used to help move vending machines or large pieces of furniture. This improved apparatus is pictured in Figure 7-2.

Figure 7-2. CGSE 3-DOF horizontal traverse and roll testing on air bearing.

With the air bearing shown in Figure 7-2, the TALARIS hopper hovered about an inch off the floor on a cushion of air, so friction was greatly reduced. The air bearing also freed two degrees of freedom which had been constrained by the wheels, allowing the hopper to roll about its X axis and travel across the entire 2D plane of the floor. Furthermore, although the TALARIS hopper did not have any thrusters aligned with its Y axis, the air bearing did not prevent it from drifting in that direction, so it provided an opportunity to test software compensation for thruster misalignment. Thus, the air bearing allowed for 3-DOF testing, such as the roll and traverse test illustrated in Figure 7-3 below.

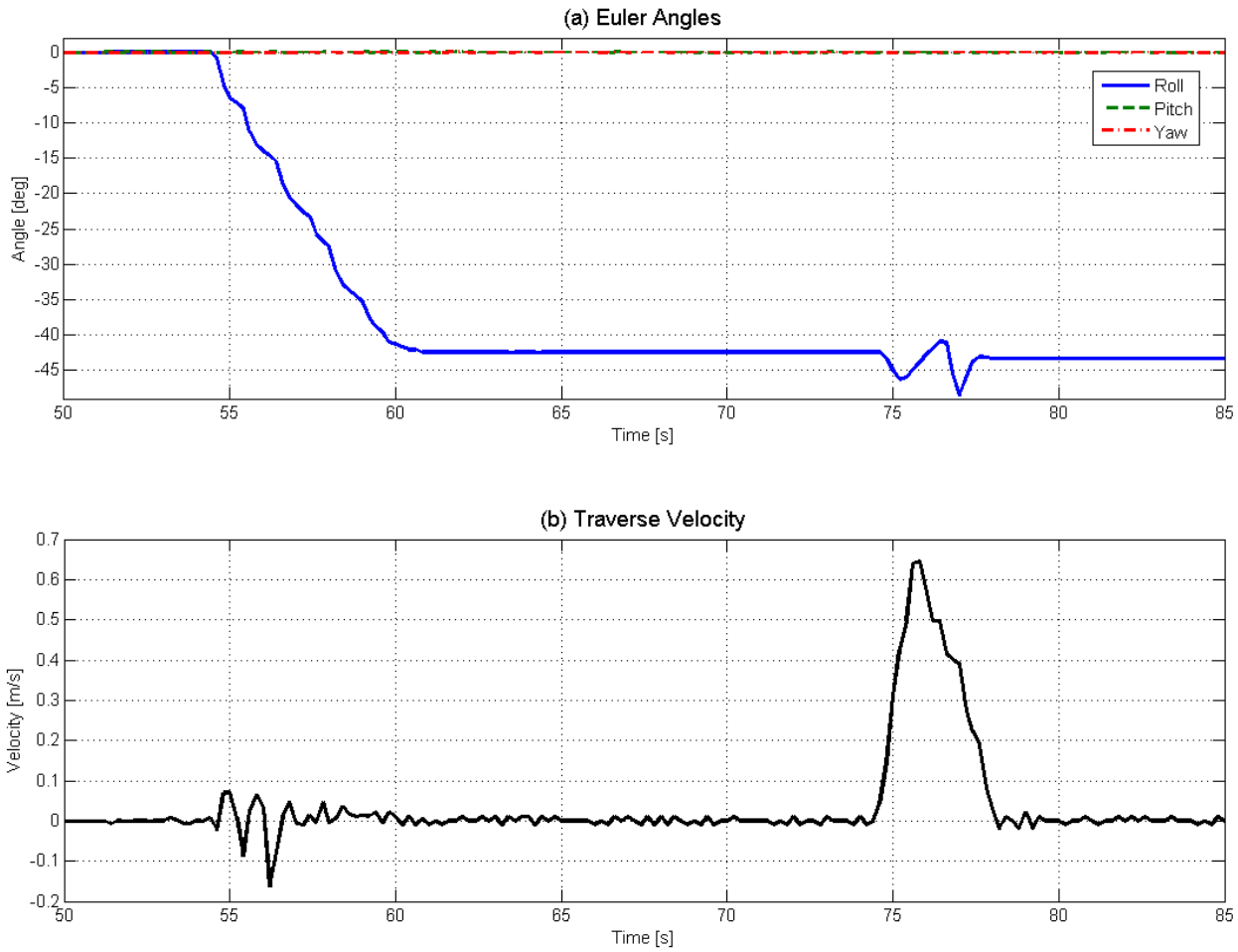

Figure 7-3. GNC data from 3-DOF test of TALARIS hopper, with 45° roll and horizontal traverse. (a) Angular position. (b) Linear traverse velocity.

Figure 7-3 was created with data collected from the hopper's inertial measurement unit, or IMU. Before the depicted test began, the hopper was placed on the air bearing and set at about a 45° angle to the intended direction of travel. Then during the test, after a calibration period, the vehicle fired its horizontal thrusters in pairs to roll to the desired heading. This maneuver can be seen from about 54 to 61 s in Figure 7-3(a). The hopper then held its new position briefly before performing a horizontal traverse, as shown from about 74 to 78 s in Figure 7-3(b). During the traverse, the hopper drifted slightly off course, probably due to thruster misalignments; however, as shown in Figure 7-3(a), the GNC algorithm executed small roll maneuvers to correct the heading.

With a series of tests such as the one illustrated in Figure 7-3, TALARIS horizontal thruster control was successfully validated. The next step was to continue on to validation testing involving the vertical CGSE thrusters.

7.1.2 Vertical Test Stand

For initial validation tests with the CGSE vertical thrusters, a test stand was built as an evolution of the one that had been used for 1-DOF vertical testing of the EDFs. In that original stand, the TALARIS hopper had been suspended between two arms which slid up and down on two tall posts but prevented the vehicle from rotating about any of its axes [17]. The new vertical test stand could be used in this way as well. However, in addition to having sliders, it also had rotational bearings at the points where it attached to the TALARIS hopper. Either the sliders or the bearings could be locked if desired to constrain particular degrees of freedom. Furthermore, the spacing of the vertical posts could be changed to allow TALARIS to be mounted in the stand such that the bearings could allow for rotation about either the Y or Z axes. Thus, the following degrees of freedom could all be tested in the new vertical stand:

- 1-DOF altitude (travel parallel to X axis)
- 1-DOF attitude (either pitch about the Y axis or yaw about the Z axis)
- 2-DOF altitude plus attitude (travel parallel to X plus either pitch about Y or yaw about Z)

Figure 7-4 shows the TALARIS hopper in the new vertical test stand.

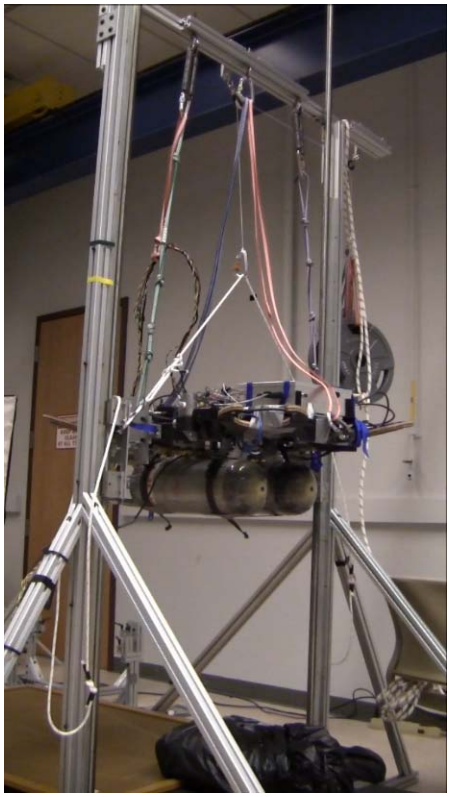

Figure 7-4. TALARIS hopper in vertical test stand, allowing both altitude and attitude control testing.

Tests on this vertical stand demonstrated 1-DOF attitude control, as shown in Figure 7-5.

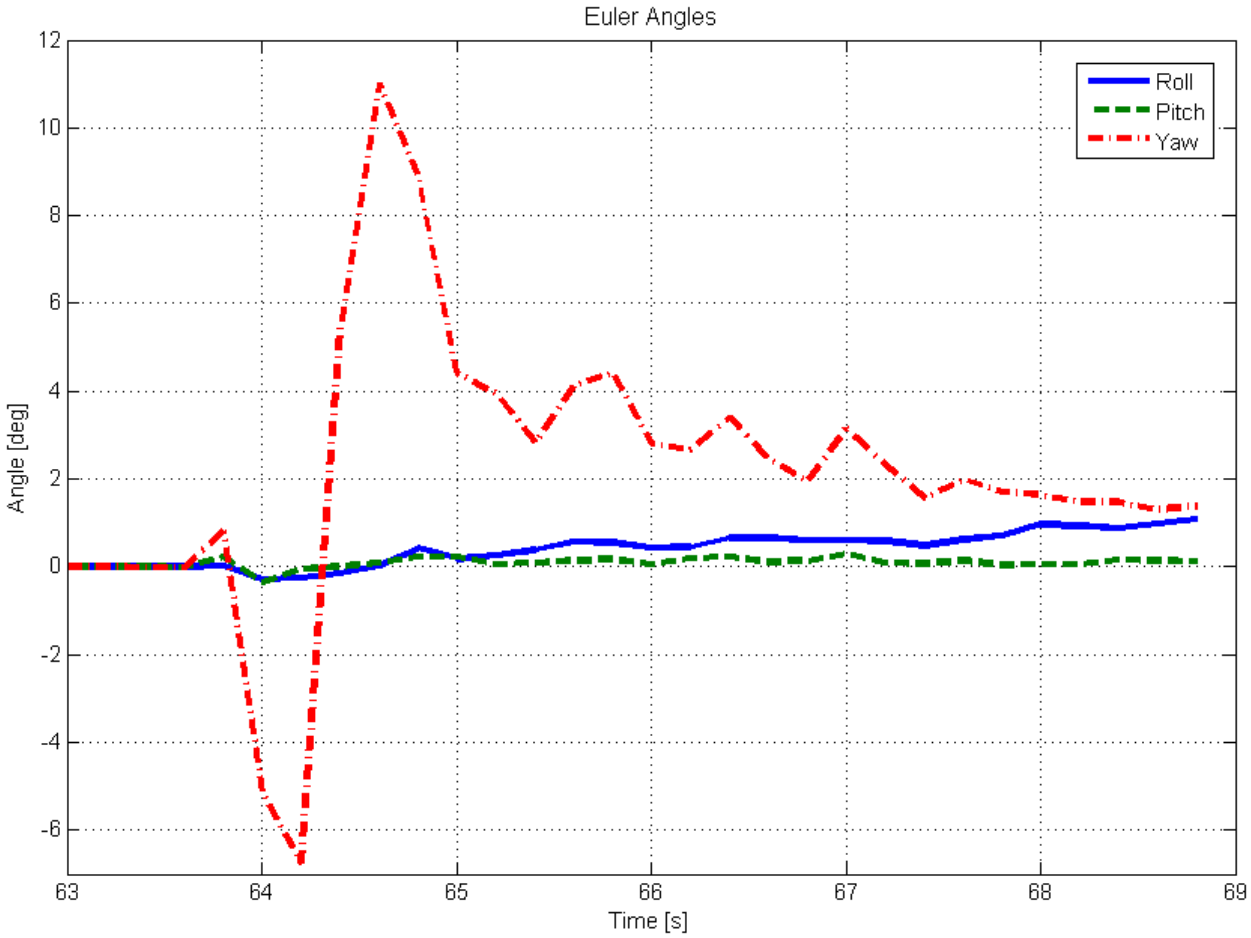

Figure 7-5. Yaw disturbance rejection demonstrating 1-DOF attitude control of TALARIS hopper.

In the test shown in Figure 7-5, the sliders on the vertical test stand were locked, and the hopper was only free to yaw about its Z axis. (Although the test stand prevented the hopper from rolling or pitching, the plot shows some IMU drift, particularly in roll.) The attitude of the hopper was disturbed, but the vertical CGSE thrusters were able to return it to stability.

Although 1-DOF attitude control was verified on the vertical test stand, the tests involving altitude were inconclusive. The EDFs still were not ready when vertical validation testing began, so a temporary weight-relief system was devised, utilizing a counterweight which is visible behind the vertical stand at the center right of Figure 7-4. Unfortunately, this applied undesirable dynamics to the vehicle during altitude tests. Furthermore, although the vertical stand was designed to allow only one degree of rotational freedom, when the sliders were unlocked they could travel at slightly different rates, and this meant that there was some degree of both pitch and yaw possible in altitude-plus-attitude testing.

Therefore, the vertical test stand did not provide as constrained a testing environment as had been desired. If time had permitted, adjustments probably could have been worked out to mitigate these problems to at least some extent. However, because of schedule pressure, the vertical test stand was abandoned slightly earlier than had been planned. Instead, as work on the EDFs was completed and all of the subsystems were integrated together on the TALARIS vehicle, validation testing moved on to 6-DOF free flight.

7.1.3 6-DOF Flight Testing

Full 6-DOF flight testing of the TALARIS hopper is currently ongoing at the time of writing this thesis. For these tests, the hopper is hung beneath a pyramid-shaped frame that connects to four hard points on the structure. The hopper is then belayed by a single rope attached to the tip of the pyramid, as shown in Figure 7-6.

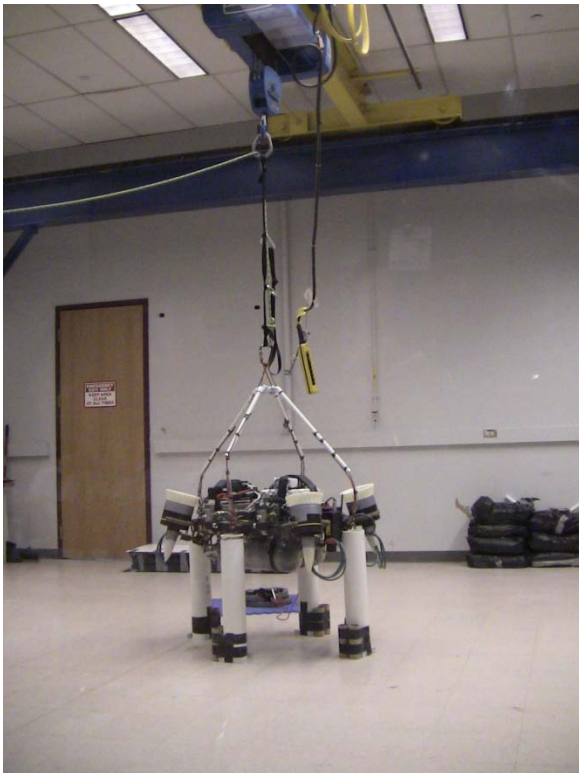

Figure 7-6. Full 6-DOF flight testing of TALARIS hopper.

As shown in Figure 7-6, the hopper sits elevated on four pylons before the start of a flight test, which then fall away as the propulsion systems engage and the hopper begins to rise. The belay line is usually kept slack, so the hopper is free to rotate and translate in all dimensions, but if it begins to go out of

control the belay line can be put under tension to arrest the hopper's motion. Various tethers attach the TALARIS hopper to weights on the ground; these lines are long enough to allow the hopper to move freely within a restricted area, but if it gets too far out of range, the tethers catch and prevent the hopper from moving further. These precautions both help to prevent crashes and to protect hopper operators and test observers.

Initial plans are for the TALARIS vehicle to first demonstrate an ascent, hover, and controlled descent. Once control is demonstrated for this primarily vertical maneuver, flights can expand to include significant attitude changes and horizontal motion. Eventually, the goal is to perform a demonstration hop at 2 m altitude with a 30 m horizontal traverse, as illustrated at left in Figure 3-1.

7.1.4 Summary of Validation Testing Efforts

Although the flight tests had not yet led to full validation of the CGSE at the time of writing this thesis, they had revealed some important aspects of CGSE operation. The CGSE in general was found to be quite reliable; in nearly all tests where the CGSE did not perform as expected, the problem was traced back to another subsystem such as avionics or software, although in one case CGSE performance was reduced because the cable carrying the signals from the RIO to the CGSE control circuit was not plugged in tightly and the connection was intermittent. Furthermore, the majority of the CGSE components were found to hold up well over the intensive testing schedule. The one hardware element found to be subject to wear and tear was the seat of the valve in the main orifice of the Tescom flight regulator; however, this seat is simply a small plastic gasket, and it is inexpensive and easily replaced when it becomes too worn down to function properly.

The flight tests, in combination with the static characterization tests, also provided some points of comparison to the flight times predicted by the MATLAB model. As mentioned in section 4.1.7, the MATLAB model predicted maximum flight times of approximately 15 s. During the static characterization tests, the CGSE was found to hold about 36 to 40 thruster-seconds of gas, as indicated by Figure 6-8. If all four vertical thrusters had an average duty cycle of 50% (an approximate percentage based on the total thrust available from all four vertical thrusters, the anticipated total vehicle mass, and the changing thrust-to-weight ratios required during a hop), this would allow them to fire for 18 to 20 s. However, a hop also includes horizontal maneuvers and attitude control; once these are taken into account, estimated flight times decrease toward 15 s and below. The flight tests that were run generally supported these estimates, although a full hop had not yet been flown at the time of writing this thesis,

and adjustments made to account for decreasing thrust levels throughout a hop as discussed in section 6.4 might shorten the actual flight time slightly. But a 15 s flight time would be a 50% increase over the 10 s limit on flight time reported by the NASA Marshall CGTA [14], showing that the TALARIS propulsion architecture could indeed achieve the goal of longer flight times with a cold gas system without loss of simulation fidelity that was described in chapter 2.

As mentioned previously, the TALARIS vehicle had not yet performed a full demonstration hop at the time of writing this thesis. Although the CGSE horizontal thrusters appeared to provide sufficient control of horizontal motion and roll about the hopper X axis as reported in section 7.1.1, vertical motion of the hopper had not yet been fully controlled, and the ascent phase of a hop was proving particularly difficult to perform. There were two main possible reasons for this: either the GNC algorithms had simply not been tuned correctly yet, or the vehicle hardware was deficient in some way that precluded the development of a successful GNC algorithm. For the CGSE hardware, the issue of thrust decrease with gas usage and the borderline acceptability of the 5 Hz control cycle have already been discussed. However, in integrated flight tests, the EDFs might also be a source of problems. Like the CGSE, the EDFs were only partially characterized, but there were indications from RPM sensors that they might not be producing enough thrust for full 5/6 weight relief, and also that individual fans might be producing different thrust levels, which could contribute to vehicle instability.

If further flight tests are unsuccessful, and it is too difficult to isolate the GNC algorithms, CGSE hardware, and/or EDF hardware as the cause, it may become necessary to perform additional static characterization tests of both the CGSE and the EDFs. In addition to running more tests of each propulsion subsystem individually (such as the CGSE thrust loss characterization plans discussed in the following section 7.2), it would also be worthwhile to test them together, to attempt to determine the degree and consequences of interaction between the two. In this way, it might be possible to identify hardware deficiencies, hopefully correctible by small changes rather than a major redesign causing one or both of the propulsion systems to be rebuilt. Alternatively, the tests might simply provide a clearer picture of the propulsion systems' performance, leading to the development of better GNC algorithms.

7.2 Improved Characterization of Thrust Levels Throughout a Hop

As mentioned in section 6.3.3, characterization of thrust levels for the CGSE flight system was limited due to the aggressive schedule of the TALARIS project. However, work is ongoing to provide both a more detailed theoretical understanding of the factors affecting thrust level and improved methods of

accounting for changes in thrust levels over the course of a hop, particularly the decrease in thrust with gas usage that is illustrated in Figure 6-8.

The characterization tests that were performed did indicate a clear correlation between CGSE low side pressure and thrust output. One way to account for thrust loss would be to measure the low side pressure throughout a hop and use it as an input to the controller. However, the TALARIS flight software is not currently set up to support this sort of feedback, and adding it might be too intensive in terms of data rates or computation time. Instead, current efforts are focused on predicting the pressure and corresponding thrust losses ahead of time.

As suggested in section 6.3.3, regulator droop has been proposed as the main effect driving the thrust loss over the course of a hop. However, without direct measurements of mass flow, it is difficult to verify this. Furthermore, there are difficulties in using droop as a framework to predict thrust loss even if it is in fact the main cause. Tescom provides droop curves for its regulator [54], but each curve assumes constant input pressure, while the tank pressure in the CGSE decreases continuously throughout a hop. Also, using the droop curves to predict actual regulator output pressure requires knowledge of mass flow, which as stated before has not been directly measured. Some estimates of mass flow have been made by comparing the weight of the hopper before and after thruster pulses of known duration; these estimates do not show any clear trends in mass flow over the course of a hop, but they are also not very precise. There is ongoing investigation into ways of resolving these problems, including possibly developing a method of measuring gas temperature and correlating that with mass flow or pressure loss, but this work must be balanced with the need to continue flight testing.

Further discussion of these efforts to improve characterization of CGSE thrust levels can be found in greater detail in [61].

7.3 Possible Upgrades

With additional resources, it would be possible to make some upgrades to the TALARIS CGSE. For instance, with a very large increase in budget, it might be possible to purchase some of the space-rated solenoid valves mentioned in section 4.2.1. Using them instead of the SV128 solenoid valves would decrease the system mass slightly, but more importantly, the faster response time might allow for a faster control cycle and improved controllability of the vehicle. A less expensive upgrade would be to purchase larger flight tanks, although it would be important to weigh any increase in tank mass against

the gains in propellant carrying capacity, and the method of mounting the flight tanks to the vehicle would most likely have to be revised.

Other possible upgrades might be identified with more in-depth analysis of the pressure and mass flow characteristics of the CGSE. For instance, it might be worthwhile to use larger-diameter tubing on the low side, even if it had a low working pressure rating preventing the regulator output pressure from being set to maximum, if the larger diameter resulted in less pressure loss on the way to the thruster chamber. More efficient sizes, combinations, and/or configurations of fittings, such as those forming the low side manifold, might also be identified with future trade studies.

While there might be some performance gains to be made by upgrading the CGSE, they would likely be relatively small, since cold gas is simply not a particularly efficient form of propulsion. To make any significant improvements, particularly in terms of longer flight times, it would likely be necessary to convert the TALARIS spacecraft emulator propulsion system from cold gas to an energetic propellant. As discussed in section 2.3.2, the most likely candidate for this upgrade would be monopropellant hydrogen peroxide. However, an upgrade of this scale would require a significant investment of time and money, and development would have to proceed extremely carefully, due to the more extensive hazards inherent in working with energetic propellants.

Unless a large source of funding could be procured specifically for the development of a hydrogen peroxide propulsion system, it would be prudent to commit resources gradually, carefully assessing the feasibility of ideas before investing large amounts of time and money in system development. For example, the initial team working on the upgrade should be small – possibly only a single person. Development of a hydrogen peroxide propulsion system might proceed in similar fashion to that of the CGSE, by starting with a review of existing technology, developing appropriate requirements, and producing an initial system design. Then, testing of individual components and eventually small subassemblies of the propulsion system could be performed to assess feasibility of the design and also to gain expertise in working with hydrogen peroxide. For this stage, it would be good to identify another program or organization already working with high-concentration hydrogen peroxide or possibly with chemicals of a similar nature, in order to investigate the possibility of taking advantage of their facilities and expertise. If no suitable opportunities were found at MIT or Draper, it could be worthwhile to look into collaboration with another Boston-area university or company, or even any of the military facilities in Massachusetts, such as Hanscom Air Force Base. It might even be possible for a student to apply for summer research fellowships that could allow them to work on hydrogen peroxide thruster

development under the supervision of a mentor at another university, a NASA center, or some similar facility even if it were far from the Boston area. However, the idea would be to keep the project and the number of people involved in it as small as possible until a better sense of the feasibility of the design and the challenges associated with implementing it had been developed. If that were achieved, the TALARIS team could then begin to think about expending significant resources on purchasing and storing hydrogen peroxide, identifying and outfitting a location in which to safely test hydrogen peroxide rockets, and training enough team members in hydrogen peroxide safety to allow for operation of the full TALARIS vehicle with its new, more dangerous spacecraft emulator propulsion system.

Although converting to a hydrogen peroxide propulsion system would probably result in a significant increase in performance as compared to the CGSE, it is important to consider all the consequences of such a change and how they would affect the overall goals of the TALARIS project. While the hydrogen peroxide system would probably make TALARIS a more capable testbed, with the ability to produce higher thrust levels and to fly for longer periods of time, it might negatively impact its function as a demonstrator, since the increased safety concerns would limit the number of places it could operate and also make it difficult for audiences to observe the vehicle at close range. It is important to consider the relative emphasis of these two roles for the hopper and also to be aware of any other opportunities that might develop as the TALARIS project moves forward, in order to determine the best course of action for future work.

8 Conclusion

The TALARIS CGSE is an application of mature technology to a very specific purpose. While cold gas propulsion has been used for decades, and several small robotic lunar lander testbeds have recently been designed and flown with cold gas propulsion systems, the requirements and constraints of the TALARIS program made the CGSE unique. Hopping as a mode of transportation for lunar or planetary surface exploration is a relatively new and untried idea, and the hover hop in particular is a maneuver which few if any space exploration vehicles have been purposely designed and built to perform. In addition, the dual role of TALARIS as testbed and demonstrator drove a unique design philosophy for the CGSE. Finally, the limited budget, aggressive schedule, core of student participation, and exceptional focus on safety all contributed to setting TALARIS and the CGSE apart from similar projects.

Development of the CGSE to fit the unique conditions of TALARIS was a process that required the application of many tools and techniques. Familiarization with existing technologies was necessary to understand the baselines from which to create a design. Modeling was an essential tool for applying science to designing the CGSE, but it was important to understand the model's limitations and to analyze its results in the context of real-world considerations and imperfections. Testing was critical for characterizing the performance of the CGSE but also for pointing out ways to iterate on the original design and improve the functioning of the system. And throughout the entire development process, it was necessary to keep track of requirements, to ensure not only that the CGSE could perform to meet set standards, but also that it was able to fulfill the overarching objectives for which it was originally designed.

In the process of completing the work documented in this thesis, several lessons were learned which seemed to have broader significance beyond the development of the CGSE. They are presented briefly here, in hopes of positively influencing work on other parts of TALARIS or perhaps any project involving the design of a subsystem to be integrated into a larger system.

Documentation is important.

Many parts of the process of developing the CGSE, such as selecting the basic system architecture and writing the MATLAB model to name just two, were built on work started by previous students, and it was invaluable to have a record of not only the results of their work but the thought processes and assumptions that went into it. Documentation can help prevent the duplication of previous efforts, troubleshoot problems, and suggest (even through omission) possible new directions of work. Properly

documenting progress takes time which could be spent doing other kinds of work, but it is an investment which can pay off well in future.

Safety is essential.

Safety was a central consideration in all phases of CGSE development. Sometimes actions taken for safety reasons came at the cost of performance, such as the overall decision to develop a cold gas system rather than a monopropellant hydrogen peroxide system. Often, extra time had to be taken to ensure safety, as with the effort put in to developing, following, and updating checklists for CGSE operation. However, safety is another area in which effort put in up front pays off later. For example, at one point during CGSE flight system testing, the low side became overpressurized enough to vent the two rupture disks in the system. The root cause of the overpressurization was eventually traced to a leak in the main orifice of the flight regulator due to wear and tear on the seat in the valve, as mentioned in section 7.1.4. This specific problem had not been anticipated, but the possibility of overpressurizing the low side had been considered, and measures had been put in place to handle that situation as safely as possible. The rupture disks functioned as expected and released the pressure in a relatively controlled and predictable way; they were simply replaced after the incident, and it was possible to return to testing very quickly. Had the rupture disks not been in the system, the overpressurization might have been severe enough to cause a component to fail in an unpredictable way and to cause damage that might have been more difficult to repair. More importantly, no one was injured when the rupture disks vented, partly because everyone present at the test was following established safety procedures and staying in shielded zones. Because time and effort had been invested in safety beforehand, the rupture disk incident was a small hiccup rather than a major roadblock, and progress in the development of the CGSE was able to continue on smoothly.

There is a balance to be struck between modeling/simulation and hardware testing.

Modeling and testing were both important elements of the CGSE development process. However, limited resources meant that neither activity could be pursued in as much depth as might be desired, and compromises had to be made. For instance, the MATLAB model had many inherent simplifications and sources of error, as listed in section 4.1.5. For some of these, such as the lack of a heat transfer model, a method of addressing them was known but would take time to implement. Instead, it was decided to use the model as it was, make component purchasing decisions with the help of its results, and spend the time on testing instead. This turned out to be the right decision; the components selected proved to be acceptable in the single-stream tests, and CGSE development proceeded. However, testing

would not have been sufficient on its own; there were far too many flow control components available to purchase one of each and try them out to see which one worked best, and the MATLAB model played an essential role in narrowing the field. The CGSE development process illustrates that modeling and testing both have their uses, and it is important to think about when each can be employed most effectively and when it might be necessary to neglect one in favor of the other if resources are scarce.

Unexpected things can happen at interfaces.

In the CGSE, this is perhaps best illustrated by the issue of the solenoid valve response times. The SV128 was sufficiently fast in the single-stream tests, when the CGSE parts were being tested all on their own. However, when the CGSE was integrated onto the TALARIS vehicle and had to interface with the avionics subsystem, the need to protect the RIO led to the development of control circuitry which slowed the solenoid valve response times to unacceptable levels. Then, additional time had to be spent to investigate the problem and then to design and construct new control circuits. This was not something that had been anticipated in the original design of the CGSE; the solenoid valves seemed quite simple, opening with power on and closing with power off, and they did not in themselves require any special control circuitry. It was only in considering the interface with the RIO that new concerns arose to be addressed. The takeaway lesson is that integration of subsystems should not be taken lightly, and it should instead be recognized as a prime source of emergent behavior.

Incremental development takes time, but it does produce solid results.

The majority of the CGSE development process was a gradual progression, and the success of this approach was particularly evident in early verification testing. The results of the MATLAB model were used to select CGSE components which were tested individually before being assembled into a full system. Had the components been found to be unacceptable, this single-stream testing step would have saved money, since a full set of components for the entire system had not yet been purchased. And even when the components performed suitably in the single-stream test setup, the knowledge gained helped to direct full flight system testing. When flight system performance was found to be suboptimal in terms of valve response time as mentioned above, it was possible to identify the problem as a difference from the single-stream setup rather than an inherent characteristic of the valve and to trace the source to the interface with the flight computer so that the problem could be resolved. This situation can be contrasted with the validation flight testing, in which schedule pressure led to the abandonment of incremental progression in favor of attempting to advance with larger leaps. If each leap had been successful, it would indeed have resulted in faster progress. However, when difficulties

were encountered, it was harder to determine exactly where the problem had been introduced. For instance, when ascent in the 6-DOF setup was found to be difficult, the vertical 1-DOF CGSE altitude tests might have provided a baseline comparison to aid troubleshooting if they had been completed. But because the vertical stand tests had been stopped early, it was much harder to ascertain whether the problems originated in the CGSE, the EDFs, the GNC algorithms, or a combination of some or all of the above. If ongoing flight tests cannot resolve the ascent issue, it may be necessary to return to an earlier stage of testing for more in-depth investigation. Trying to take larger steps forward can mean having to take larger steps backward, and this risk must be kept in mind when planning the development of a system.

The ability to identify such universal lessons learned indicates that the development of the CGSE was something of a prototypical engineering problem. However, it was a particular problem that had not been previously addressed. Its solution required the synthesis of several different areas of knowledge and the application of a variety of tools. The end result of this process was a cold gas propulsion system developed specifically to meet the needs of the TALARIS project. Testing of the system is ongoing, and several ways in which it might be improved have already been identified, but so far the CGSE has met all the goals that have been set for it. It is a reliable part of the TALARIS testbed, helping to advance the development of hoppers for lunar and planetary exploration.

Works Cited

[1] National Aeronautics and Space Administration, "Surveyor Program Results," NASA SP-184, Washington, DC, 1969.

[2] Lanford, E. R., "Unique Abilities of Hopper Spacecraft to Enable National Objectives for Solar System Exploration," S.M. Thesis, Engineering Systems Division & Department of Aeronautics and Astronautics, Massachusetts Institute of Technology, Cambridge, MA, 2011.

[3] Cunio, P. M., et al., "Options in the Solar System for Planetary Surface Exploration via Hopping," *2011 IEEE Aerospace Conference*, Big Sky, MT, 2011.

[4] Cohanim, B. E., et al., "Small Lunar Exploration and Delivery System Concept," *AIAA SPACE 2009 Conference & Exposition*, Pasadena, CA, 2009.

[5] X PRIZE Foundation, "About the Google Lunar X PRIZE," *Google Lunar X PRIZE*, 2011, URL: http://www.googlelunarxprize.org/lunar/about-the-prize [cited 15 Feb. 2011].

[6] "Armadillo Aerospace Qualifies For Lunar Prize," *AviationWeek.com*, 16 Sep. 2009, URL: http://www.aviationweek.com/aw/generic/story_channel.jsp?channel=space&id=news/SCORPIUS091609.xml [cited 15 Feb. 2011].

[7] "Masten and Armadillo Claim Lunar Lander Prizes," *NASA Office of the Chief Technologist*, 2 Nov. 2009, URL: http://www.nasa.gov/offices/oct/early_stage_innovation/centennial_challenges/cc_ll_feature_lvl2.html [cited 28 Mar. 2011].

[8] National Aeronautics and Space Administration, "GPN-2000-000215 - Lunar Landing Research Vehicle in Flight," *GRIN: Great Images in NASA*, 1964, URL: http://grin.hq.nasa.gov/ABSTRACTS/GPN-2000-000215.html [cited 15 Feb. 2011].

[9] Matranga, G. J., Ottinger, C. W., Jarvis, C. R., and Gelzer, D. C., "Unconventional, Contrary, and Ugly: The Lunar Landing Research Vehicle," Monographs in Aerospace History #35, National Aeronautics and Space Administration, NASA SP-2004-4535, Washington, DC, 2005.

[10] Bryant, K. M., Knight, C. J., and Hurtz, R. J., "Planetary Lander Vehicles Utilizing LEAP Technology," *30th AIAA/ASME/SAE/ASEE Joint Propulsion Conference*, Indianapolis, 1994.

[11] Nishioka, O., "NASA Ames Hover Test Vehicle Flight Test," *NASA Ames Images and Video*, 12 Nov. 2008, URL: http://www.nasa.gov/centers/ames/multimedia/images/2008/nasa-ames-lunar-lander-flighttest.html [cited 15 Feb. 2011].

[12] Coulter, D., "Lunar Lander Floats on Electric-blue Jets," *Science@NASA Headline News*, 15 Oct. 2009, URL: http://science.nasa.gov/science-news/science-at-nasa/2009/15oct_lunarlander/ [cited 15 Feb. 2011].

[13] Gundy-Burlet, K., Schumann, J., Menzies, T., and Barrett, T., "Parametric Analysis of a Hover Test Vehicle using Advanced Test Generation and Data Analysis," *AIAA Infotech@Aerospace Conference and AIAA Unmanned.Unlimited Conference*, Seattle, 2009.

[14] Chavers, D.G., et al., "Robotic Lunar Landers for Science and Exploration," *7th International Planetary Probe Workshop (IPPW-7)*, Barcelona, 2010.

[15] Morring Jr., F., "Peroxide Phase," *Aviation Week & Space Technology*, Vol. 173, No. 2, 10 Jan. 2011, p. 21.

[16] Hendry IV, M. L., et al., "LEAPFROG: Lunar Entry and Approach Platform For Research On Ground," *AIAA Infotech@Aerospace 2007 Conference and Exhibit*, Rohnert Park, CA, 2007.

[17] Cunio, P. M., et al., "Initial Development of an Earth-Based Prototype for a Lunar Hopper Autonomous Exploration System," *AIAA SPACE 2009 Conference & Exposition*, Pasadena, CA, 2009.

[18] Middleton, A. J., "Modeling and Vehicle Performance Analysis of Earth and Lunar Hoppers," S.M. Thesis, Department of Aeronautics and Astronautics, Massachusetts Institute of Technology, Cambridge, MA, 2010.

[19] Meetin, R. J. and Seifert, H. S., "Propulsion Dynamics of Lunar Hoppers," *Journal of Spacecraft and Rockets*, Vol. 11, No. 12, 1974, pp. 852-856.

[20] Fiorini, P., Hayati, S., Heverly, M., and Gensler, J., "A Hopping Robot for Planetary Exploration," *Proceedings of 1999 IEEE Aerospace Conference*, Vol. 2, Snowmass, CO, 1999, pp. 153-158.

[21] Yoshimitsu, T., Kubota, T., Nakatani, I., Adachi, T., and Saito, H., "Micro-hopping robot for asteroid exploration," *Acta Astronautica*, Vol. 52, No. 2-6, Jan.-Mar. 2003, pp. 441-446.

[22] Montminy, S., Dupuis, E., and Champliand, H., "Mechanical design of a hopper robot for planetary exploration using SMA as a unique source of power," *Acta Astronautica*, Vol. 62, No. 6-7, Mar.-Apr. 2008, pp. 438-452.

[23] Chiaverini, M. J. and Kuo, K. K. (eds.), *Fundamentals of Hybrid Rocket Combustion and Propulsion*, American Institute of Aeronautics and Astronautics, Reston, VA, 2007.

[24] Brown, C. D., *Spacecraft Propulsion*, American Institute of Aeronautics and Astronautics, Washington, DC, 1996.

[25] "16.898 Critical Design Review: Earth-Based Prototype of a Lunar Hopper," Class Report, Department of Aeronautics and Astronautics, Massachusetts Institute of Technology, Cambridge, MA, 2008 (unpublished; archived in TALARIS SVN file repository).

[26] Golkar, A., et al., "TALARIS 1g Hopper Demonstrator Design Document," 16.83/89 Class Final Report, Department of Aeronautics and Astronautics, Massachusetts Institute of Technology, Cambridge, MA, 2009 (unpublished; archived in TALARIS SVN file repository).

[27] Humble, R. W., Henry, G. N., and Larson, W. J. (eds.), *Space Propulsion Analysis and Design*, Revised ed., McGraw-Hill, New York, 1995.

[28] Sutton, G. P. and Biblarz, O., *Rocket Propulsion Elements*, 7th ed., John Wiley & Sons, New York, 2001.

[29] Wernimont, E. J. and Mullens, P., "Capabilities of Hydrogen Peroxide Catalyst Beds," *36th AIAA/ASME/SAE/ASEE Joint Propulsion Conference & Exhibit*, Huntsville, AL, 2000.

[30] Solvay Chemicals, "Safety and Handling of Hydrogen Peroxide," *Solvay Chemicals, Inc.*, 2006, URL: http://www.solvaychemicals.us/static/wma/pdf/6/6/0/4/HH-2323.pdf [cited 7 Mar. 2011].

[31] Canadian Centre for Occupational Heath and Safety, "How Do I Work Safely with Compressed Gases?," *CCOHS: Canada's National Centre for Occupational Health and Safety Information*, 8 Jul. 2008, URL: http://www.ccohs.ca/oshanswers/prevention/comp_gas.html [cited 7 Mar. 2011].

[32] Massachusetts Institute of Technology Environment Health & Safety Office, "Compressed Gas Cylinder Safety," *MIT EHS: Environment Health & Safety*, 2 Mar. 2011, URL: https://ehs.mit.edu/site/content/compressed-gas-cylinder-safety [cited 7 Mar. 2011].

[33] FMC Corporation, "Hydrogen Peroxide," *FMC Industrial Chemicals*, 2010, URL: http://www.fmcchemicals.com/Products/HydrogenPeroxide.aspx [cited 7 Mar. 2011].

[34] Ventura, M., Wernimont, E., Heister, S., and Yuan, S., "Rocket Grade Hydrogen Peroxide (RGHP) for use in Propulsion and Power Devices - Historical Discussion of Hazards," *43rd AIAA/ASME/SAE/ASEE Joint Propulsion Conference & Exhibit*, Cincinnati, 2007.

[35] General Kinetics Inc., "Products," *General Kinetics Inc.: Hydrogen Peroxide for Propulsion and Power*, 2010, URL: http://www.gkllc.com/products.html [cited 7 Mar. 2011].

[36] Saenz-Otero, A., "Design Principles for the Development of Space Technology Maturation Laboratories Aboard the International Space Station," Ph.D. Thesis, Department of Aeronautics and Astronautics, Massachusetts Institute of Technology, Cambridge, MA, 2005.

[37] Berkovitz, D. S., "System Characterization and Online Mass Property Identification of the SPHERES Formation Flight Testbed," S.M. Thesis, Department of Aeronautics and Astronautics, Massachusetts Institute of Technology, Cambridge, MA, 2008.

[38] Nothnagel, S. L., et al., "Development of a Cold Gas Spacecraft Emulator System for the TALARIS Hopper," *AIAA SPACE 2010 Conference & Exposition*, Anaheim, CA, 2010.

[39] Luxfer Gas Cylinders, "LCX® composite cylinder specifications," *Luxfer Gas Cylinders*, 2011, URL: http://www.luxfercylinders.com/products/scba-and-life-support-cylinders/187-lcx-composite-cylinder-specifications [cited 14 Apr. 2011].

[40] Hill, P. G. and Peterson, C. R., *Mechanics and Thermodynamics of Propulsion*, 2nd ed., Addison-Wesley, Reading, MA, 1992.

[41] Perry, R. H. and Green, D. W. (eds.), "Table 2-179: Compressibility Factors for Nitrogen," *Perry's Chemical Engineers' Handbook*, 7th ed., McGraw-Hill, New York, 1997, Ch. 2, p. 2−145.

[42] Golkar, A. A., "Thermodynamics and Heat Transfer Analysis of the Pressurant Gas Tank for a Liquid Propulsion System," L. Thesis, School of Aerospace Engineering, Università di Roma "La Sapienza", Rome, 2006.

[43] Sonntag, R. E., Borgnakke, C., and Van Wylen, G. J., *Fundamentals of Thermodynamics*, 6th ed., Wiley, Hoboken, NJ, 2003.

[44] Lemmon, E. W., McLinden, M. O., and Friend, D. G., "Thermophysical Properties of Fluid Systems," *NIST Chemistry WebBook*, Linstrom, P. J. and Mallard, W. G. (eds.), NIST Standard Reference Database No. 69, National Institute of Standards and Technology, 2011, URL: http://webbook.nist.gov/chemistry/fluid/ [cited 30 Mar. 2011].

[45] Sprackling, M. T., *Thermal Physics*, American Institute of Physics, New York, 1991.

[46] Hendricks, R. C., Peller, I. C., and Baron, A. K., "Joule-Thomson Inversion Curves and Related Coefficients for Several Simple Fluids," National Aeronautics and Space Administration, NASA TN-D-6807, Washington, DC, 1972.

[47] Hott Jr., M. W., "Control Valve Components, Definitions, Terminology, and Specifications," *ISA Handbook of Control Valves*, Hutchison, J. W. (ed.), Instrument Society of America, Pittsburgh, 1971, pp. 3-12.

[48] Tescom Corporation, "Flow Formulas for Computing Gas and Liquid Flow through Regulators and Valves," *Tescom Technical Support*, Aug. 2001, URL: http://www.tescom-europe.com/fileadmin/user_upload/Tescom_UK/Tescom_Common_Flow_Formulas.pdf [cited 4 Apr. 2011].

[49] Driskell, L. R., "Sizing Theory and Applications," *ISA Handbook of Control Valves*, Hutchison, J. W. (ed.), Instrument Society of America, Pittsburgh, 1971, pp. 125-140.

[50] ISA - The Instrumentation, Systems, and Automation Society, "Flow Equations for Sizing Control Valves," ANSI/ISA-75.01.01-2002 (IEC 60534-2-1 Mod), Research Triangle Park, NC, 2002.

[51] Arcuri, L. J., "Droop and accumulation, they go with the flow!," *Pressure Controls Express: An informative newsletter for Tescom distributors & representatives*, Vol. 4, No. 10, Oct. 2005, pp. 1,3-4, URL: http://www.shavogroup.com/pdf/newsletter/2005-10news.pdf [cited 6 Apr. 2011].

[52] Omega Engineering, Inc., "2-Way General Purpose Solenoid Valves: SV120 Series," *Omega.com*, 2010, URL: http://www.omega.com/Pressure/pdf/SV120_Series.pdf [cited 9 Apr. 2011].

[53] Omega Engineering, Inc., "Solenoid Valves for Process Applications," *Omega.com*, 2010, URL: http://www.omega.com/techref/pdf/Solenoid_Valve_Select.pdf [cited 9 Apr. 2011].

[54] Tescom Corporation, "44-1300 Series," *Emerson Process Management*, Jun. 2006, URL: http://www.documentation.emersonprocess.com/groups/public/documents/data_sheets/d44130549x012.pdf [cited 9 Apr. 2011].

[55] Drawing from SolidWorks model by Zach Bailey.

[56] Weil, R. B., "Ball Valves," *ISA Handbook of Control Valves*, Hutchison, J. W. (ed.), Pittsburgh, 1971, pp. 21-25.

[57] National Instruments Corporation, "NI sbRIO-961x/963x/964x and NI sbRIO-9612XT/9632XT/9642XT User Guide," *National Instruments*, Jun. 2010, URL: http://www.ni.com/pdf/manuals/375052c.pdf [cited 18 Apr. 2011].

[58] Airgas, Inc., "Airgas 2011 Product Catalog," *Airgas.com*, 2011, URL: http://www.airgassgcatalog.com/catalog/ [cited 19 Apr. 2011].

[59] Morrow, J., "Evaluation of Valve Timing Characteristics for All Thrusters," TALARIS Internal Report, Massachusetts Institute of Technology, Cambridge, MA, 14 Nov. 2010 (unpublished; archived in TALARIS SVN file repository).

[60] National Aeronautics and Space Administration, "NASA Systems Engineering Handbook," NASA/SP-2007-6015 Rev1, Washington, DC, 2007.

[61] Morrow, J., Nothnagel, S. L., Cunio, P. M., Cohanim, B. E., and Hoffman, J. A., "Characterization of a Cold Gas Propulsion System for the TALARIS Hopper Testbed," *AIAA SPACE 2011 Conference & Exposition*, Long Beach, CA, 2011 (abstract accepted).

[62] NASA Jet Propulsion Laboratory, "Planetary Satellite Physical Parameters," *JPL Solar System Dynamics*, 18 Oct. 2010, URL: http://ssd.jpl.nasa.gov/?sat_phys_par [cited 28 Mar. 2011].